DEVELOPMENT OF SSZ-54 ZEOLITE FOR CATALYTIC CRACKING OF ALKANES FOR PRODUCTION OF LIGHT OLEFINS

BY

SAHEED ADEWALE LATEEF

A Thesis Presented to the
DEANSHIP OF GRADUATE STUDIES

KING FAHD UNIVERSITY OF PETROLEUM & MINERALS

DHAHRAN, SAUDI ARABIA

In Partial Fulfillment of the
Requirements for the Degree of

MASTER OF SCIENCE

In

CHEMICAL ENGINEERING

MAY, 2017

KING FAHD UNIVERSITY OF PETROLEUM & MINERALS

DHAHRAN- 31261, SAUDI ARABIA

DEANSHIP OF GRADUATE STUDIES

This thesis, written by **SAHEED ADEWALE LATEEF** under the direction of his thesis advisor and approved by his thesis committee, has been presented and accepted by the Dean of Graduate Studies, in partial fulfillment of the requirements for the degree of **MASTER OF SCIENCE IN CHEMICAL ENGINEERING**.

Oki Muraza

Dr. Oki Muraza
(Advisor)

Mozzhar Hossain

Dr. Mohammad M. Hossain
(Member)

Dr. Muhammed S. Ba-Shammakh
Department Chairman

Shaikh Abdur Razzak

Dr. Shaikh Abdur-Razzak
(Member)

Dr. Salam A. Zummo
Dean of Graduate Studies

16/5/12

Date

This thesis is dedicated, from the depth of my heart:

To the glory of almighty Allah,

Who has blessed me with everything to succeed in this voyage.

To my parents,

Whose sincere prayers have kept me going since the day I was born.

To my darling wife, Aminah Adebayo-Lateef,

Whose love, understanding, encouragement and endless support,

Have been a source of inspiration to me.

To my in-laws,

For their sincere prayers and unalloyed supports.

And my siblings,

For their understanding and prayers.

ACKNOWLEDGMENTS

All adorations are due to almighty Allaah, the Most benevolent, the Most Merciful for everything HE has done for me.

Utmost gratitude goes to King Fahd University of Petroleum and Minerals and the Kingdom of Saudi Arabia for the opportunity afforded me to undertake my master program.

My deepest appreciation goes to my advisor, Dr Muraza Oki for his guidance on this work. Every discussion with him is always very impactful. My committee members, Dr Mozahar Hossain and Dr Shaikh Abdur Razzaq, are also deeply appreciated for their insightful ideas and contributions towards the success of this project.

I won't forget to appreciate the staff and faculties of the department of chemical engineering led by Dr Muhammed S. Ba-Shammakh. My appreciation will not be complete without appreciating the Director of the great Centre of Nanotechnology (CENT), Dr Zain H. Yamani, all the scientists especially Mr Idris Akolade Bakare, for all their supports throughout the period of this research work.

I am greatly indebted to render my sincere appreciation to my parents, siblings and my wife, for their prayers, unending support and unalloyed encouragement that pushed me to the end of this work. I pray may almighty Allah bless them all with HIS abundant blessings and mercies.

And lastly but not the least, I give many thanks to Nigerian community here in the Kingdom (NCUPM), may Allaah uphold our love. Thanks very much for everything.

TABLE OF CONTENTS

ACKNOWLEDGMENTS ..... **V**

TABLE OF CONTENTS ..... **VI**

LIST OF TABLES ..... **IX**

LIST OF FIGURES ..... **X**

LIST OF ABBREVIATIONS ..... **XII**

ABSTRACT ..... **XIII**

ملخص الرسالة ..... **XV**

CHAPTER 1 INTRODUCTION **1**

1.1 Crucial parameters in designing intergrowth zeolites **1**

1.1.1 Silicon and aluminum content **2**

1.1.2 Structure directing agents **3**

1.1.3 Crystallization time **4**

1.1.4 Synthesis temperature **4**

1.1.5 Type and concentration of alkali used **4**

1.2 Why the intergrowth zeolites? **6**

1.3 Post treatment applied to zeolites **7**

1.3.1 Steaming **7**

1.3.2 Alkali treatment **8**

1.3.3 Chemical leaching **9**

1.3.4 Acid treatment **9**

1.3.5 Incorporation of metal/ metal oxides on zeolites **10**

1.4 Application of zeolites in catalysis 10

1.5 Objectives of the study 12

CHAPTER 2 LITERATURE REVIEW 13

2.1 Methods of producing olefins 14

2.1.1 Thermal cracking 15

2.1.2 Catalytic cracking 16

2.1.3 Cracking mechanisms 18

2.2 Catalytic cracking of hexane 20

2.3 Reaction pathways for cracking of n-hexane over acid catalysts. 20

2.4 SSZ-54 23

CHAPTER 3 EXPERIMENTAL METHODS AND APPARATUS 26

3.1 Synthesis of SSZ-54 zeolite 26

3.1.1 Hydrothermal synthesis method 26

3.1.2 Microwave-assisted synthesis 29

3.1.3 Ion exchange of the samples 30

3.1.4 Production of hierarchical zeolite 30

3.2 Characterization methods 31

3.2.1 X-ray diffraction (XRD) methods 31

3.2.2 Scanning Electron Microscopy (SEM) 32

3.2.3 Nitrogen physisorption (BET method) 32

3.2.4 High Resolution Transmission Electron Microscopy (HRTEM) 32

3.2.5 Cs-corrected STEM 33

3.2.6 Temperature-Programmed Desorption (TPD) 33

3.2.7 Fourier Transform IR (FT-IR) 34

3.3 Catalysts testing 34

CHAPTER 4 RESULTS AND DISCUSSION 35

4.1 Evaluation of the parent samples 35

4.1.1 Characterization of the samples 35

4.1.2 Products analysis 46

4.2 Effects of alkali-acid treatment on catalytic activity 51

4.2.1 Characterization results 51

4.2.2 Products breakdown 55

4.2.3 Evaluation of cracking ability and determination of activation energy 59

4.3 Microwave-assisted SSZ-54 synthesis and its application in hexane cracking. 62

4.3.1 Characterization of the samples 62

4.3.2 Cracking result 68

4.4 Hydrothermal synthesis versus microwave-assisted synthesis: comparison between individual cracking ability. 72

CHAPTER 5 CONCLUSIONS AND RECOMMENDATIONS 73

5.1 Conclusions 73

5.2 Recommendations 74

REFERENCES 79

VITAE 90

LIST OF TABLES

Table 1-1 Intergrowth zeolites and the optimum conditions for their preparation 5
Table 1-2 Intergrowth zeolites and their applications..... 11
Table 2-1 Possible reaction pathways for n-hexane cracking..... 23
Table 2-2 Different structure directing agents for synthesis of SSZ-54 25
Table 3-1 List of equipment and specifications..... 27
Table 3-2 Molar composition of reacting mixtures 28
Table 4-1 FTIR analysis of the samples 42
Table 4-2 Physicochemical properties of the samples (error = ±2%)..... 44
Table 4-3 Activity (conversion and yield of total olefins, %) of SSZ-54 with MTT and TON frameworks at different Si/Al ratios and time on stream..... 51
Table 4-4 FTIR analysis of the samples at adsorption temperature of 150 ^{o}C 54
Table 4-5 Physicochemical properties of the samples (error = ±2%)..... 55
Table 4-6 Conversion and yields of light olefins with other products at 1 h time on stream for SZ-50-DSA. 58
Table 4-7 Rate constant for cracking of hexane over SZ-50-DSA at different temperatures at 1 h TOS. 60
Table 4-8 Textural properties of the samples (error = ±0.5-1.4%)..... 65
Table 4-9 FTIR analysis of the samples (error = ±0.5%) 67
Table 4-10 Conversion and selectivity to C1-C4= at different time on stream (error = ±2%)..... 69

LIST OF FIGURES

Figure 2-1 Cracking reaction pathways Lee *et al* 19
Figure 3-1 Experimental Procedure for SSZ-54 synthesis 29
Figure 3-2 Desilication and mild dealumination of SSZ-54 31
Figure 4-1 XRD patterns of calcined zeolite synthesized with mixed OSDA where different concentrations of isopropylamine [IPA] and 1,6-hexane diamine (DAH) were used. (a) MTT phase was observed (b) Intergrowth formed and (c) TON phase was detected. 36
Figure 4-2 XRD patterns of different modelled phases as revealed by DiFFax. (a) MTT phase (b) SSZ-54 and (c) TON phase. Ref: [1]..... 37
Figure 4-3 XRD patterns of calcined zeolite synthesized with 16% DAH and 84% IPA (a) different synthesis temperatures, (b) different crystallization times and (c) different Si/Al ratios. 38
Figure 4-4 SEM images of separate phases synthesized. The top images; Figure (a) corresponds to MTT phase while fig (c) is the TON phase. The bottom image; fig (b) is the image of SSZ-54 (intergrowth). Ref: [106], [90] 39
Figure 4-5 Cs-corrected STEM-HAADF images of SSZ-54. a) Low-magnification image showing several crystals orientated perpendicular to the pore channels. b) a closer observation of the pore channels. c) High-resolution image of a SSZ-54 crystal partially orientated 40
Figure 4-6 Cs-corrected STEM-HAADF images of SSZ-54. a) A closer observation of the figure 4-5c, where the different domains are marked. b) Enlarged micrograph of the TON region with the model superimposed. c) Similar observation on the MTT zone with the model overlaid. Si and Al atoms appear in blue while oxygen appears in red 41
Figure 4-7 FT-IR spectra of MTT-TON Intergrowth Zeolite (after blank subtraction) showing the bands for Lewis and Brønsted acid sites at adsorption temperature of 150 ^{o}C. 43
Figure 4-8 NH_3-TPD profiles of the parent samples of SSZ-54 44
Figure 4-9 N_2 adsorption plot for SZ-50-P and SZ-100-P. 46
Figure 4-10 (a) Conversion, selectivity and products distribution versus TOS (h) for Z-50 (b) olefin composition and P/E versus TOS (h) 47
Figure 4-11 Conversion, selectivity and products distribution versus TOS (h) for Z-100 (b) olefin composition and P/E versus TOS (h) 49
Figure 4-12 Yield of total olefin produced by SZ-50-P and SZ-100-P versus TOS..... 50
Figure 4-13 XRD spectra of the samples. Upper spectra of both figures represent desilicated-dealuminated samples. (a) Si/Al of 50 (b) Si/Al of 100. 52
Figure 4-14 SEM and TEM images of parent and hierarchical SSZ-54. (a,c) Parent sample while (b,d) represent the image of the samples after

desilicated and mild dealumination. Top images represent SEM micrographs while the bottom images show those of TEM. 53
Figure 4-15 Deconvoluted FTIR spectra of the hierarchical samples 53
Figure 4-16 Conversion of n-hexane at different TOS for SZ-50 samples and SZ-100 samples at 650 ^{o}C. P indicates parent samples while DSA represents desilicated-dealuminated samples. 56
Figure 4-17 Yields of total olefin and paraffin for all the samples at 650 ^{o}C at 1 h time on stream (C2=, C3= and C4= constitute olefin while paraffin is composed of C1-C5) 57
Figure 4-18 Conversion and product selectivity at different temperatures for SZ-50-DSA..... 59
Figure 4-19 Arrhenius plot for SZ-50-DSA at various temperatures. 61
Figure 4-20 XRD spectra of the parent sample and the hierarchical samples 63
Figure 4-21 SEM and TEM images of parent and hierarchical SSZ-54. (a,d) Parent sample (b,e) desilicated sample and (c,f) desilicated-dealuminated sample. Top images represent SEM micrographs while the bottom images show those of TEM 64
Figure 4-22 Surface area measurements of the samples 66
Figure 4-23 Yields of paraffin, olefin and BTX for P-50, DS-50 and DSA-50. (a) Illustrates the parameters at 1 h TOS (b) shows the parameters at 10 h TOS 71
Figure 4-24 Catalytic activity of hydrothermal and microwave-assisted samples at Si/Al = 50 72

LIST OF ABBREVIATIONS

MTT	:	Mobil Twenty-Three
TON	:	Theta One
BET	:	Brunauer Emmett Teller
FAU	:	Faujasite
FESEM	:	Field Emission Scanning Electron Microscope
BTX	:	Benzene Toluene Xylene
MOR	:	Mordenite
MFI	:	Mordenite Framework Inverted
OSDA	:	Organic Structure Directing Agent
P/E	:	Propylene to ethylene ratio
MAZ	:	Mazzite
SSZ	:	Stanley Stacy Zones
ZSM	:	Zeolite Socony Mobil
XRD	:	X-ray Diffraction
TOS	:	Time on stream

ABSTRACT

Full Name : [Saheed Adewale Lateef]

Thesis Title : [Development of SSZ-54 catalysts for catalytic cracking of alkanes for production of light olefins]

Major Field : [Chemical Engineering]

Date of Degree : [May 2017]

A detailed study of the preparation of SSZ-54, an intergrowth of MTT and TON frameworks using a novel mixture of two templates; isopropyl amine (IPA) and 1,6-hexane diamine (DAH), was carried out with hydrothermal and microwave reactors. The characterization of the products done using X-ray diffraction (XRD), scanning electron microscopy (SEM) and aberration-corrected scanning transmission electron microscopy (Cs-corrected STEM) unveil assemblies of needles with spans of about 1 micron and 20-30 nm in thickness, confirms the formation of SSZ-54. The amount of the structure directing agents, synthesis time and temperature were pivotal in the synthesis of SSZ-54 zeolite. Furthermore, we observed that the higher molecular weighted molecule (DAH) has more influence on the control of the metamorphosis of the SSZ-54 phase.

Catalytic evaluation of SSZ-54 zeolite with cracking of n-hexane reveals high activity, good selectivity to olefins and minimal paraffin. Also, SSZ-54 displays better catalytic performance than either of its component frameworks (MTT and TON frameworks) in offering better stability, slower resistance to coking and improved yield to olefins.

Investigation of the effects of alkali (NaOH + TEAOH) and acid (nitric acid) treatments on the properties and catalytic performance of proton-type SSZ-54 zeolite reveals no

structural collapse, improvement in physicochemical properties and ultimately, better catalytic activity, selectivity to olefins with prolonged catalyst life than the parent samples.

Catalytic behavior towards change in reaction temperature reveals considerable drop in activity and overall olefin selectivity as temperature drops. Selectivity data shows increase in ethylene selectivity as temperature increases and more propylene at lower reaction temperatures.

Considering the methods of sample synthesis, microwave-assisted synthesis offers faster route than hydrothermal method. Also, microwave- assisted synthesized samples show better activities than hydrothermally-produced samples because of better structural and acidity characteristics.

In addition, the shape selective property of SZZ-54 zeolite to mainly olefins owing to its unique innate pore structure was demonstrated as the selectivity to BTX on SSZ-54 was minimized to ca. 1 % over 10 h time on stream in all the samples.

ملخص الرسالة

الاسم الكامل: سهيد أديوالي اللطيف

عنوان الرسالة: تطوير SSZ-54 المحفزات لالتكسير التحفيزي من الألكانات لإنتاج الأوليفينات الخفيفة

التخصص: هندسة كيميائية

تاريخ الدرجة العلمية: مايو 2017

دراسة تفصيلية لإعداد إس إس زد-54 (SSZ-54)، وهي محفز زيوليتي مكون من نمو ثنائي لمزيج جديد من اثنين من القوالب الزيوليتيه و هما إم تي تي (MTT) و تي أو إن (TON).بإستخدام خليط نوعين من القوالب الكيميائية العضوية وهما إيزو بروبيل أمين و 1،6 هكسان ديامين، و التي تمت بواسطة الأفران الحرارية وعن طريق المايكرويف التحضيري. توصيف المنتجات المحضرة باستخدام حيود الأشعة السينية (XRD) والمجهر الإلكتروني المجهري (SEM) وتصحيح المسح الضوئي المجهر الإلكتروني (STEM) لكشف النقاب عن تجمعات التركيبية على امتدادات حوالي 1 ميكرون وسمك حوالي 20-30 نانومتر، و لقد لوحظ بأن كمية القوالب العضوية، ووقت التوليف ودرجة الحرارة أثناء التحضير أدوات محورية في تركيب الزيوليت إس إس زد-54 .وعلاوة على ذلك، لاحظنا أن القالب ذات الجزيء الأعلى و الذي هو 1،6 هكسان ديامين له تأثير أكبر على السيطرة على التحول من مرحلة التحضير.
التقييم التحفيزي للزيوليت إس إس زد-54 مع تكسير الهكسان يكشف عن نشاط عالي، انتقائية جيدة للأوليفينات والحد الأدنى من البارافين .أيضا، تبين أن إس إس زد-54 يعرض أفضل أداء حفازي من أي من أطرها المكونة (إم تي تي و كذلك تي أو إن) في تقديم أفضل استقرار، أبطأ مقاومة لتكون الركربون وتحسين العائد على الأوليفينات.

و من خلال التحقيق في آثار القلويات (هيدروكسيد الصوديوم + تيترا إيثايل أمونيوم هايدروكساید) وآثار الحامض (حمض النيتريك) لعلاج و تعديل الخصائص والأداء التحفيزي للبروتون من نوع إ إس زد-54 الزيوليتي و الذي يكشف عن انهيار هيكلي، وتحسين الخصائص الفيزيائية والكيميائية وفي نهاية المطاف، تحسين في النشاط التحفيزي، والانتقائية إلى الأوليفينات مع حياة محفز لفترات طويلة مقارنة بالعينات الأم.السلوك التحفيزي نحو التغيير في درجة حرارة التفاعل يكشف عن انخفاض كبير في النشاط والانتقائية للأوليفين الكلي مع انخفاض درجة الحرارة .وتظهر بيانات الانتقائية زيادة في انتقائية الإيثيلين مع زيادة درجة الحرارة وزيادة البروبيلين عند درجات حرارة تفاعل أقل.
وبالنظر إلى أساليب تحضير العينات، فإن التوليف بمساعدة التسخين بواسطة المايكرويف يوفر طريقا أسرع من طريقة التحضير الحراري. كذلك، تظهر العينات المصنعة بمساعدة المايكرويف أنشطة أفضل من العينات المنتجة بواسطة الفرن الحراري بسبب خصائص هيكلية وحموضة أفضل.
وبالإضافة إلى ذلك، تم إثبات شكل انتقائية الزيوليت إس إس زد-54 إلى الأوليفينات بشكل أساسي بسبب الهيكلة المسامية الفريدة من نوعها بالإضافة لتعديل الإنتقائية لمركبات البنزين و التلوين و الإكزايلين على محفز إس إس زد-54 و التي تم حصرها و تقليلها تصغيرها إلى أقل من 1% على مدار 10 ساعات من التفاعل في جميع العينات.

CHAPTER 1

INTRODUCTION

The framework specification for zeolites is done by considering the crystallographic model [1]. However, the arrangement of atoms in some zeolites lacks definite ideal crystal specifications such that the atomic positions in space and the configurations are not adequately described by any model [1]. This is referred to as faulting and it is consequence of the variations in the ways the "sheets" or "rods" of the atoms are arranged relatively to other sheets or rods in the neighbourhood. Examples of such are RUB-4 [2], beta zeolite [3], [4] MOR/MFI family [5], the MFI/MEL family [6], FAU/EMT family [7], CHA/AEI family [8] etc. They are referred to as intergrowth materials.

This chapter presents the parameters that are considered in the design of intergrowth zeolites and factors affecting them. Also discussed are some vital characteristics of intergrowth materials, post treatment methods applied to zeolites and effects of each of them and finally the specific areas of application of intergrowth zeolites are summarized in Table 1-2.

1.1 Crucial parameters in designing intergrowth zeolites

Intergrowth zeolites are made of two or more similar and closely-related zeolite frameworks synthesized together in the same pot. The specific characteristics, properties and functions of these structures are dependent on the nature of the intergrowths. The way

the framework grow in-between the structure is dependent on some factors which would be highlighted below;

1.1.1 Silicon and aluminum content

For zeolites, among the most important reactants are the water-soluble compounds of silicon and aluminium. This is because of the source of Brønsted and Lewis acid sites that they produce. Besides, the specific shapes being possessed by zeolite frameworks are determined by the silica and alumina content and the way they are arranged. Therefore, to fine-tune the properties of the zeolite to suit desired application, sources of silicon and aluminium need to be properly studied and taken care of.

The control of intergrowth can be achieved by altering the Si/Al ratio [6], [9]. Fransesconi *et al*. [6] reported the transformation of MFI/MEL intergrowth from MFI through the intergrowth to pure MEL as Si/Al changed from 8 through 25. Similar observation was reported by Smith *et al.* [8], in the synthesis of SAPO-34/SAPO-18, otherwise known as CHA/AEI intergrowth. Silicon content in the reactant can be varied and a range of structures can be obtained which can vary from being a pure form of one of the constituents or the intergrowth of the two components [8]. This is evident from their work where they obtained pure SAPO-18 when the silicon was 1% and below and the CHA/AEI intergrowth began to form as soon as the silicon content was being increased (1.7-7%).

Apart from varying the silicon content, the source of silica is also another key factor in the control of intergrowth. Zhang *et al.* [9] posited that the source of silicon used determines and control the intergrowth. This was done in the synthesis of ZSM-5/ZSM-11 intergrowth where colloidal silica, silicic acid, tetraethyl orthosilicate (TEOS), water glass, silica gel

and fumed silica were in-turn used as silica sources. While keeping other synthesis conditions constant, except in TEOS where the ZSM-5 was 50-60%, others were reported to be between 30-40% ZSM-5 [9].

In a similar vein to the above, generally, aluminium source used also influences the behavior of intergrowth [9]. Study using aluminium sulfate and sodium metaaluminate with diethylamine (DEA) and dimethylamine (DMA) used as SDAs revealed the formation of intergrowth of ZSM-23/ZSM-22 only when the molar ratio of DEA to DMA was 1:24 for aluminium sulfate while the molar ratio of DEA to DMA of 1:12 was all it needed for the formation of intergrowth if sodium metaaluminate is used. All other ratios led to formation of either a pure phase of one of the component frameworks or an amorphous phase. All these underscore the role of silicon and aluminum in the intergrowth formation.

1.1.2 Structure directing agents

It is a well –established procedure that zeolite synthesis requires the usage of structure directing agents which are usually organic material [1], [2], [6], [7], [10]–[14], mainly amine and quaternary ammonium ions. These SDAs control structural formation for zeolites. Proper selection and combination of these SDAs will ensure getting the required framework. In some cases, only one SDA is enough to obtain the required intergrowth [1] [2], [15] while mixing OSDAs are necessary in some others [1], [10]. The quantities of these templates can be varied to control the intergrowth behavior. This is evident in the works of Burton *et al.* [1] and Gonzalez *et al*. [10] where varying the quantities of OSDAs influences the intergrowth behaviors.

1.1.3 Crystallization time

Sujuan *et al.* [16] propounded the concept of varying the crystallization time to control intergrowth formation, among other factors. Villaescusa *et al*.[17] supported the report of Sujuan *et al.* with the synthesized STF/SFF intergrowth where 6 days crystallization produced pure STF phase as against intergrowth being produced at 9 days crystallization, all at the same temperature of 150 ^{o}C. This underscores the role of crystallization time in the formation of intergrowth.

1.1.4 Synthesis temperature

Synthesis temperature is one of the most important parameters, not only for the formation of zeolite but also in the control of intergrowth. At the crystallization time of 9 days, Villaescusa *et al.* reported the variation in the composition when the temperature was varied. They obtained 33%STF at 150 ^{o}C and 85%STF was obtained at 170 ^{o}C [17] .

1.1.5 Type and concentration of alkali used

Control of intergrowth is also achieved by adjusting the concentration of the base [18]. For instance, the concentration of sodium hydroxide in the initial solution can be adjusted in order to control the intergrowth of the zeolite synthesis [18]. Type of the alkali used also affects the crystallization time which in turn affects the intergrowth [9]. Sodium ion is known to have positive effect on crystallization time while potassium ion is a retarder of the crystallization [9] and this controls the formation of intergrowth.

The above explanations can also be seen at a glance by the **Table 1-1** which is presented below. It shows the various intergrowth zeolites as well as the optimum conditions of their synthesis.

Table 1-1 Intergrowth zeolites and the optimum conditions for their preparation

Frameworks	Optimum Conditions	Ref.
ZSM-23/ZSM-22	Ratio of DMA to DEA • 1:24 for $Al_2(SO_4)_3$ • 1:12 for sodium metaaluminium DMA =dimethylamine, DEA = diethylamine	[19]
Zeolite Beta	• 300-700nm seeds (OSDA) • $\frac{TBAOH}{NaOH+TBAOH} = 0.4$, 65^0C, 0.5h TBAOH = tetrabutylammonium hydroxide	[20],[21]
CHA/AEI	Si content 0.5-7.0%	[8]
EUO/NES/NON	• $1SiO_2$:1.33TMPOH:$0.34B_2O_3$:$120H_2O$:$2CH_3OH$ • Si/Al = 36.3, Na/Al =5.3 TMPOH = tetramethylphosphonium	[2],[15]
FAU/EMT	• Na_2O/SiO_2= 0.375, OH^-/SiO_2=0.75 • T1/T2 = 0.5, 0.7 • T/Al_2O_3= 0.7, 0.3 T = T1+T2, T1=15-Crown-5, T2=18-Crown-6	[7],[10]
MFI/MEL	Si/Al = 11 and 25	[6]
MOR/MFI	170^0C for 4 days	[5]
MTT/TON	$\frac{N-isopropyl-1,3-propanediamine}{1-methylbutylamine} < 0.25$	[1]
SAPO-34/ZSM-5	Pt-Sn-based Si/Al =60	[22]
ZSM-5/ZSM-11	AlOOH (Boehmite), TEOS(tetraethylorthosilicate), SiO_2/Al_2O_3 = 23-60	[9]
MCM-49/ZSM-35	CHA/HMI= 2.3-3.0, 80^0C for 4hr and then 166^0C CHA=cyclohexamine, HMI= hexamethyleneimine	[16]
Beta/MCM-41	• 110^0C for 48h • 408K, 31h, 40rpm	[23],[24]
MCM41/Beta	• Si/Al = 39, 100^0C, 24h • Si/Al =12.5	[12]
STF/SFF	0.5DECDMP:0.5F:SiO_2:$2H_2O$, 150^0C or 170^0C for 9 days DECDMP= N,N-diethyl-2,5-cis-dimethylpiperidinium	[17]
OFF/ERR	• Sodium aluminate • Glycerol (no N-containing SDA) • 30mins stirring and • Static crystallization at 122^0C	[25]
MAZ/ZSM-5	• $(TMA)_2O$ • $(C_2H_5)_4NBr$ • $(C_4H_9)_4NBr$	[26]
Zeolite X on A	• Tetraethylamine, disodium oxide for 16-28days	[27]

1.2 Why the intergrowth zeolites?

As a result of complex nature of industrial petrochemical reactions, some single-phase catalysts are incapable of handling such complex processes which necessitate the need to produce hybrid materials with better characteristics such as high catalytic activity, good selectivity and shelf life. This improvement in the properties of the intergrowth catalysts is due to synergy that exists between the component phases. Established methods in producing intergrowths are highlighted above and are also reported [28].

Although it is not clear if all the component frameworks contribute to the catalytic performance but some would do. Various ways the phases contribute to the performance of the catalysts could be by acting as a support for the other component, by making the active components stable, by having more than one function and/or by moderating the performance of acid and basic sites among others [28].

The properties embedded in intergrowth zeolites are not peculiar to them. Instead, the existing properties in the single-phased component are improved. Property such as stability, reported by Smith *et al*. for CHA/AEI intergrowth is better than each of the component frameworks [29]. Improvement in catalytic activity was brought about by formation of intergrowth but the correlation for such increase with the structure was not studied [10].

On the other hand, further argument on the activity of intergrowth zeolite was put forward and correlated to change in acidity as a result of defects creation in the intergrowth materials [6]. Also, there is a slight widening in the size of channels intersection in the case of intergrowth than for single-framework zeolite. This change in the dimension and

geometry of cavities is of paramount importance for shape -selective property. This could be responsible for improved activity in the intergrowths [6].

1.3 Post treatment applied to zeolites

Zeolites are very important crystalline materials in the industry. They are used in catalysis, adsorption, ion exchange *et cetera*. They are mostly present in microporous state and their properties can be fine-tuned towards the desired properties. Such desired properties could be hydrophobicity, acid strength, pore architectures and a host of others. Pore sizes in zeolite affect shape selective property in catalysis. However, where there is only micropores present in zeolite, there tends to be a case of diffusion limitation and thus affect the catalytic activities and product selectivity [30]. In order to enhance the catalytic activity by modifying the pore sizes, various research have gone on to report many techniques which majorly involves mesopores creation. This leads to increase in accessibility of active sites [30]. On the other hand, modifying the surface of the zeolite is another fruitful endeavor to improve the activity of the zeolite. Such modification technique could be by incorporating metals into the structure. Some of the methods to achieve the above are highlighted below:

1.3.1 Steaming

Steaming has been identified as one of the most popular ways of creating mesopores in zeolites because of its ability to greatly enhance the movement of both silicon and aluminium species in the framework [31]. This is done by hydrothermal treatment of zeolites in the presence of steam [31] at a temperature of around 500 ^{0}C while the zeolite is in the ammonium or hydrogen form. This causes the Al-O-Si bond to hydrolyze and

subsequently removing the aluminium then causing a vacancy or partial amorphization in the framework [31]. Silicon would fill the spaces left by aluminium atoms and some left-over spaces form the mesopores. Many spaces are filled with amorphized debris and need to be removed by acid treatment [31]. The challenges associated with the steaming is the blockage of the framework by the debris and loss of active site as a result of acid treatment to remove the amorphized substances [31]. Steaming has been applied to many zeolite frameworks such as mazzite [32], ferrierite [33], mordenite [34], ZSM-5 [35] and zeolite Y [36], [37].

1.3.2 Alkali treatment

Treatment of zeolite with a base removes silicon in the framework. Matsukata *et al.* [31] reported desilication procedure where sodium hydroxide was used to treat the crystals of ZSM-5. It was reported that afterwards, some of the crystals of the zeolite dissolved in the base [31]. In addition, increasing the concentration of the base as well as the time of contact between the base and the catalyst resulted in increasing the external surface area and the volume of the mesopores thus created [31]. Also, zeolite Y has also been treated with a base and other frameworks such as ferrierite with alkali aluminates have been reported [31], [38]. However, in any of the cases, acid treatment would be followed to remove the base and other amorphous materials which could reside inside the pores [31], [38], [39].

The process of base treatment has been extended to zeolite beta where sodium hydroxide and a mixture of sodium hydroxide and tetraalkylammonium hydroxide were tested [21] in the controlled desilication process. It was reported that the desilicated catalyst using the chemicals above showed better catalytic conversion and selectivity of gas-oil, n-decane and 1,3,5-triisopropylbenzene cracked to produce diesel and propylene [21]. This study

was also extended to mixture of NaOH and 1-hexadecyltrimethylammonium bromide [cetyltrimethylammonium bromide (CTAB)] in a process termed desilication and re-assembly [40]. In this method, the silicon that was removed by initial treatment with NaOH was later re-inserted in a more coordinated manner into the structure of the zeolite thereby providing better mesopore.

1.3.3 Chemical leaching

Another method of creating mesopore is by removal of aluminium from the framework of the zeolite [30]. This can be done by adding chemical substance other than either base or an acid to the zeolite. Ethylene diamine tetraacetic acid (EDTA) [41], $SiCl_4$ [42] and $(NH_4)_2SiF_6$ [43] have been reported to provide mesopores upon reacting with zeolite though it was also stressed that it usually results into structure collapse especially in the case of EDTA and ammonium complex when the time of reaction is elongated [31].

1.3.4 Acid treatment

This is done by mildly-treating the zeolite with the either mineral acid such as nitric acid (diluted) or an organic acid such as oxalic acid in such a way that the extra framework material created during steaming is dissolved and subsequently removed [31]. Acid treatment provides a guaranteed way of increasing the mesopores formed by steaming by just emptying the pores blocked by the debris during the steaming process [31], [44], [45].

Another method that has been used to create mesopores in zeolite is by harsh treatment with acids without steaming [31] where aluminium is removed. Although, this method is proved to be good but the challenge involved is the destruction of the catalyst because of the strong acid involved. Hence, proper consideration of the judgement between the

method to be used and the type of the zeolite involved is imperative. The method was reportedly applied for mordenite [46], beta zeolite with the latter giving problems in separation between intra-crystalline mesopores and the zeolitic mesopores [47].

The problems associated with direct acid attack, without steaming, on the zeolite is the loss of acid site by increasing the Si/Al ratio which can be taken care of if steaming operation is controlled [31].

1.3.5 Incorporation of metal/ metal oxides on zeolites

Other than the aforementioned approaches to modify the structure of zeolites, there are many other methods being employed to achieve the desired characteristics in the zeolite. Besides, it is not only the single framework zeolites whose structures can be modified, intergrowth materials have also been restructured in the past to achieve kind of properties which depends on application. Some of such methods is the zeolite modification with metals. Mihailova *et al.* modified the surface of zeolite beta (BEA) modified with metals or metal oxides [11] and improve the catalytic performance of BEA. Also, incorporation of PdO on BEA enhanced selective oxidation of chlorinated hydrocarbons [48]. Various reports abound on the incorporation of metal/metal oxide on zeolites [49]–[52].

1.4 Application of zeolites in catalysis

The use of zeolites to speed up the rate of reaction as well as influencing the products of the reaction was dated back to 1960s [53] especially for organic reactions. Since then, various new applications for zeolites has been growing in the petrochemical industry. Processes such as oligomerization, dewaxing, methanol-to-gasoline (MTG) have been among success stories of ZSM-5 [53]. Intergrowth zeolites, because of their exceptional

catalytic activities, have been reported to be excellent in catalysis. Some of the areas include methanol-to-olefin [8], nitration, alkylation and hydroisomerization [20], [21] *etc.*

Table 1-2 shows the various areas of applications of intergrowth zeolites as well as the framework structure of each:

Table 1-2 Intergrowth zeolites and their applications

Frameworks	Applications	Ref
ZSM-23/ZSM-22	Used as adsorbent, ion exchangers and Catalyst	[19]
Zeolite Beta	➢ Used in aromatic alkylation processes such as alkylation of benzene with propylene to produce cumene ➢ Isomerization, alkene hydration, aromatic acylation and Nitration processes.	[20], [21]
CHA/AEI	Methanol to Olefins	[8]
EUO/NES/NON	Hydrogenation	[2],[15]
FAU/EMT	Used as molecular sieves in refining processes	[7],[10]
MFI/MEL	Used in decane cracking process	[6]
MOR/MFI	Used as Adsorbent	[5]
MTT/TON	Hydrogenation	[1]
SAPO-34/ZSM-5	Propane Dehydrogenation	[22]
ZSM-5/ZSM-11	Hydrocracking	[9]
MCM-49/ZSM-35	Alkylation of Benzene with dilute ethylene in FCC catalyst	[16]
Beta/MCM-41	➢ Hydrodearomatization of diesel ➢ Naphthalene hydrogenation	[23], [24]
MCM41/Beta	Palm oil cracking for the production of liquid hydrocarbon	[12]
STF/SFF	Separation, ion exchange and catalytic applications.	[17]
OFF/ERR	• Conversion of methanol to Olefin • Selective catalyst dewaxing • Molecular sieving of n-butenes	[25]
MAZ/ZSM-5	• FCC Gasoline aromatization	[26]

1.5 Objectives of the study

Based on the numerous details explained in the preceding sections of this writing, the general objectives of this research are to synthesize a highly active, highly stable catalyst and evaluate the performance of this catalyst in a fixed bed reactor. This will include a novel mix of the templates and the study of its catalytic activity. The study will also incorporate the contribution of acid and alkaline treatments on improvement or otherwise on textural properties of the catalyst and finally, catalytic ability. In order to accomplish these, the specific objectives are highlighted below:

1. Synthesis of SSZ-54 zeolite, using hydrothermal, as well as microwave-assisted synthesis methods, and study the influence of
    - Concentration of organic structure directing agents
    - Silica to alumina ratios
    - Crystallization time and
    - Crystallization temperature, on the structure of the catalyst.
2. The investigation of the influence of the crystallization method on structural properties and activity of SSZ-54 zeolite.
3. Desilication by alkaline treatment and subsequent dealumination by acid treatment and study their influence on the structural and acidity properties of SSZ-54
4. Catalytic evaluation in a fixed bed reactor with a view to achieving maximum catalytic performance by examining (i) acidity effect on the conversion of hexane and selectivity towards light olefins with disparate Si/Al ratios and (ii) change in reaction condition (reaction temperature) on catalytic conversion of hexane.

CHAPTER 2

LITERATURE REVIEW

This chapter chronicles the major technological processes used to produce light olefins using various hydrocarbons and their sources as raw materials. The increase in world consumption trend of the light olefins (ethylene and propylene), which are driven by the increase in the demand because of widening in applications are also discussed. In addition, detailed explanation of the catalytic cracking mechanism is also highlighted.

There are many petrochemicals being produced in industries using both ethylene and propylene as feedstock [54]. Notable examples are polyolefin, monomers and intermediates manufacturing. This is due to the ability of these chemicals to have their properties fine-tuned for many applications. Besides, some other important petrochemicals are also being produced from them via polymerization, alkylation, aromatization and in synthesis of oxygenated additives for automotive fuel [55]. For instance, petrochemicals derived from ethylene, are high density polyethylene (HDPE), low density polyethylene (LDPE), linear low density polyethylene (LLDPE), ethylbenzene, polystyrene *et cetera* which are used to manufacture, among other uses, many household and industrial equipment like films, gloves, bags, containers, wire and cable insulation, packaging materials, pipes, conduits, containers, insulators *et cetera* [56].

As a result of increase in the volume of end-use commodities, the demand for polypropylene and ethylene has been on the increase. An instance is the World demand of

propylene which was, in 1974, 18% and has now risen to about 59% [56]; the data which is still expected to increase at 4-4.5% per annum for ethylene and 5-6.7% for propylene.

2.1 Methods of producing olefins

The established methods for producing them are; as a by-product by steam cracking of oil gas, naphtha or alkanes [57]. Another method is the Fluidized Catalytic Cracking (FCC). The key purpose of FCC units is to synthesize gasoline while simultaneously propylene is obtained as a by-product just like the case of steam cracking process. A lot of research is currently carried out to maximize the yield of propylene from FCC units due to the rise in the demand for propylene [58]. Another one, though used solely for ethylene is the oxidative coupling of methane [59]. It involves conversion of methane into ethylene without the need for production of syngas which is energy-consuming [60]. One of the drawbacks of this method is the search for stable catalyst with reasonable activity and selectivity [60], [61]. The yield is currently low, hence no commercial production has been reported [62]. Methanol to olefins is another method that has been extensively reported to be a very good way to produce both ethylene and propylene [63]–[65]. Catalytic dehydrogenation process is another process but being faced with the challenge of coke formation and high energy requirement as a result of the endothermic nature of the reaction [66].

Cracking of naphtha by the use of catalyst and/or heat for production of light olefins have been extensively reported [54],[67]–[69]. Thermal cracking is not economically viable because of the enormous amounts of heat it consumes [68] as compared to catalytic cracking which consumes less heat. The consumption of energy for steam cracking

accounts for around 70 % of the overall cost of production and enormous amount of coke is generated which blocks the tube and reduce the heat transfer coefficient of the tube [69]. Apart from that, carburization and decoking are the necessary procedures to remove such coking. These lead to reduction in the level of ethylene and failure of the tube hence shortens its life time [69]. The details of some of the methods are highlighted below:

2.1.1 Thermal cracking

Larger hydrocarbons are broken down into smaller fractions by the application of heat.

Artexte *et al.*, reported production of light olefins by thermal valorization of high density of polyethylene (HDPE). According to them, this reaction is necessary to enable recycling of plastics and turning them to something useful. It was stated that the reaction produced high yield of light olefins at lower temperature and lower time on stream though a highly specialized conical spouted bed reactor is needed to carry out such reaction because of low thermal conductivity of the polyethylene [70]. Increasing space time leads to more olefins production but this can lead to secondary reactions also [70].

Thermal cracking of vegetable oil for light olefins production has been documented. Light olefins are used for production of polyolefins which are important in petrochemical industry. This leads to production of carbon dioxide (CO_2) as by-product [71], [72].

Furthermore, it was shown that long-chained oil which has been deoxygenated with the help of hydrogen is also useful and provide a viable and promising alternative to naphtha which has widely been used for that purpose [73].

2.1.2 Catalytic cracking

Thermal cracking, due to high energy involvement, produces large amount of industrial pollutants such as NO_x and CO_2 from combustion of the fuels [74]. As a result of environmental considerations, producing olefins from less environmentally hazardous sources would be a welcome development. As stated above, nitrogen gases are produced from high temperature cracking, therefore, eliminating this would be by application of a lower temperature-based cracking process. Besides, high temperature implies high energy which culminates into high investment cost. To reduce the cost of investment, a lower energy requirement process is imperative. Going by the above analysis, catalytic cracking has been proved to solve those problems.

Various hydrocarbons have been catalytically cracked by various catalysts in the past and the results have shown yield in short reaction time and comparatively low temperature. This section will review some of the literatures consulted in the study of catalytic cracking.

Acidic ferrierite (H-FER) and H-ZSM-5 and the combination of the two have been used in the cracking of decane [75]. It was shown that H-FER has lower catalytic activity than H-ZSM-5 but ethylene selectivity was small in H-ZSM-5. Proper blending with H-FER which resulted in more yield of both propylene and ethylene [75].

Various acidic zeolites and modified forms have also been reported for catalytic cracking of naphtha [76], [77], decane [77] etc. In the work of Liu *et al.*, adding phosphorus into the H-ZSM-5 was able to increase the hydrothermal stability and selectivity of the zeolite towards ethylene and propylene being produced but however reduced the acid site concentration. It was also reported that steaming made the phosphorus to block the surface

of the zeolite and was later removed by washing, then activity increased further [77]. Copper, silver and phosphorus were applied in the cracking of naphtha using n-heptane as the model compound [76].

The effects of ratio of silica to alumina, modification and treatment of zeolite in alkaline environment in the cracking of vacuum gas oil was also investigated by Awayssa *et al.* [78]. It was reported that increase in silica to alumina ratio increase the yield of the olefins. Moreover, addition of manganese also led to more yield of olefin because of particles of manganese (IV) oxide which reduces the acid concentration of the catalyst. Treatment in alkaline environment which resulted into formation of hierarchical pore framework of the zeolite also led to more yield of the ethylene and propylene [78].

Catalytic cracking was also brought to biological materials through the cracking of micro-alga oil over ZSM-5 zeolite [79]. Findings revealed that the catalytic cracking of the microalga produced much higher yield than thermal cracking of the same organism [79].

Acidified ZSM-5 has shown to be an excellent catalyst in naphtha cracking but comes with the shortfall that coke is usually formed which requires frequent regeneration of the spent catalyst through calcination. However, in order to minimize the cost of regeneration and possible down time of operation, stability of this catalyst was studied by modification with copper [80]. With copper, the steam generated during calcination which resulted in permanent damage to the catalyst is reduced by the addition of the copper in a reducing environment. The addition of copper was able to prolong the life of the catalyst because of its lower Brønsted acid in oxidative environment and high Brønsted acid in a reducing

environment as compared with H-ZSM-5, hence yield of light olefins was improved with the addition of copper by prolonging the life of the catalyst [80].

2.1.3 Cracking mechanisms

Thermal cracking: As it was explained earlier, thermal cracking takes place at elevated temperatures. Its mechanism involves formation of free radicals at elevated temperatures which are, afterwards, propagated and then terminated when the radicals react with each other. This mechanism was proposed by Rice and Herzfeld [81] and later modified by Rice and Kossiakoff [82].

Catalytic cracking: The cracking of alkane comes with proper understanding of the type of acid sites present on the surface of the catalyst. For zeolites, there are two types of surface acidity-Brønsted and Lewis acid sites [83]. For catalytic cracking reactions that take place on Brønsted acid site, the cracking ability is determined by the concentration and strength of the Brønsted acid sites [84]. It was reported that cracking of n-alkanes takes place under two mechanisms. These are classical and monomolecular cracking mechanisms.

Classical cracking: This is otherwise called bimolecular cracking and it involves attack on the alkane product by acid site of the zeolite to form carbenium ion intermediate. Carbenium ion then forms into an alkane by hydride transfer from the feed and converts it to an alkyl carbenium which cracks via β-scission to an alkene and a smaller carbenium ion [85]. The chain reaction can continue in the same way.

Monomolecular mechanism: This mechanism involves direct protonation of alkane to form a high energy transition state looking like a penta-coordinated carbocation which

subsequently dehydrogenates to yield olefins [86]. This is made possible as it occurs at high temperature of around 800 K which enables solid acid catalysts like zeolite to act as super acids thereby releasing protons on the Brønsted acid sites for protonation of paraffin. Termination of this reaction is brought by returning the proton back to the acid site by the carbocation which finally forms olefin.

It needs to be pointed out that the size of the pore of zeolite influences the mechanism of cracking. Medium pore favours monomolecular cracking while large pore zeolites tend to have more paraffin from bimolecular cracking. The concept of cracking mechanism rate (CMR) was explained by Hou *et al.* to support their arguments [87]. A summary of cracking mechanisms given by Lee *et al.*[88] is presented in the figure below;

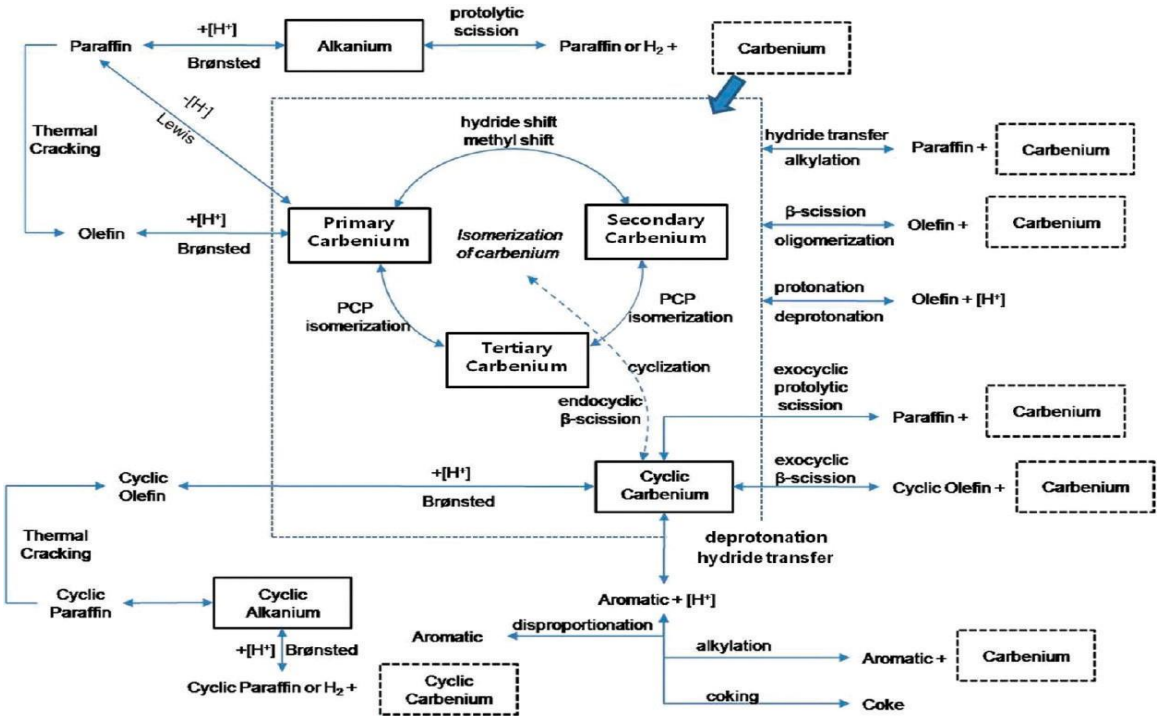

Figure 2-1 Cracking reaction pathways Lee *et al*

2.2 Catalytic cracking of hexane

Hexane is one of the most important member of light naphtha which are broken down (cracked) to produce olefins mainly ethylene, propylene and butylene. These petrochemicals have been harnessed in various petrochemical applications. Hence, cracking hexane is an important process in petrochemical industries. Various catalysts have been deployed to this process but however, our target here is on zeolites.

A great deal of work has been expended in the cracking of n-hexane to produce olefins. Mochizuki *et al*. [89] studied the effect of crystal size and temperature on conversion and products distribution using tubular flow micro-reactor. They found that conversion increases as temperature of reaction increases. Also, small crystal size has higher selectivity to propylene and butane while the large crystal MFI zeolite produced more ethylene and BTX. Suppression of BTX formation in small crystal sized-zeolite is because of stearic hindrance. In addition, selectivity towards ethylene and BTX increases with increasing temperature. Catalyst size was also reported to affect rate of deactivation. Smaller sized-catalysts deactivate slower than large sized-catalysts because of diffusion path length which is shortened in small crystal size. Similar observation was reported by Jamil *et al.* [90] and Oki *et al.* [91] in the TON framework studied and Rownaghi *et al.* [92]. The key reasons offered for this trend of behavior are the larger external surface area for nano-sized zeolite than micron-sized. Also, size reduction reduces the path length thereby prevent coking which ultimately enhances longer life.

2.3 Reaction pathways for cracking of n-hexane over acid catalysts.

Cracking of members of paraffin occurs, on acid catalysts such as zeolites, by chain reaction which involves initiation, propagation and termination steps [87], [93].

Initiation step: This involves attack on the paraffin by the acid sites of the zeolite leading to protonation of C-C/C-H bonds. Decomposition of the formed compound leads to generation of hydrogen or smaller paraffin and carbenium ions. This step is monomolecular cracking.

Propagation step: The chain propagation step could be either by hydride transfer between the carbenium and reactant molecules or β- scission of the carbenium ions. The former gives more paraffin and carbenium ions while the latter produces olefins.

Termination step: Termination of the reaction takes place by deprotonation of the carbenium or carbonium ions which culminates to restoration of acid sites on the zeolite catalysts.

In accordance with the description above, n-hexane cracking over SSZ-54 can be illustrated as follows;

1. Protonation of paraffin yields alkane or hydrogen and carbenium or carbonium intermediates

$$n - C_6H_{14} + HB \overset{P1}{\rightarrow} H_2 + C_6H_{13}^+B^-$$

$$n - C_6H_{14} + HB \overset{P2}{\rightarrow} CH_4 + C_5H_{11}^+B^-$$

$$n - C_6H_{14} + HB \overset{P3}{\rightarrow} C_2H_6 + C_4H_9^+B^-$$

$$n - C_6H_{14} + HB \overset{P4}{\rightarrow} C_3H_8 + C_3H_7^+B^-$$

$$n - C_6H_{14} + HB \overset{P5}{\rightarrow} C_4H_{10} + C_2H_5^+B^-$$

2. Hydride transfer between n-hexane molecule and the generated carbenium ions

$$n - C_6H_{14} + C_6H_{13}^+B^- \overset{T1}{\rightarrow} C_6H_{14} + C_6H_{13}^+B^-$$

$$n - C_6H_{14} + C_5H_{11}^+B^- \overset{T2}{\rightarrow} C_5H_{12} + C_6H_{13}^+B^-$$

$$n - C_6H_{14} + C_4H_9^+B^- \overset{T3}{\rightarrow} C_4H_{10} + C_6H_{13}^+B^-$$

$$n - C_6H_{14} + C_3H_7^+B^- \overset{T4}{\rightarrow} C_3H_8 + C_6H_{13}^+B^-$$

$$n - C_6H_{14} + C_2H_5^+B^- \overset{T5}{\rightarrow} C_2H_6 + C_6H_{13}^+B^-$$

3. Simultaneously, β-scission can take place with the hydride transfer above

$$C_6H_{13}^+B^- \overset{S1}{\rightarrow} C_4H_8 + C_2H_5^+B^-$$

$$C_6H_{13}^+B^- \overset{S2}{\rightarrow} C_3H_6 + C_3H_7^+B^-$$

$$C_5H_{11}^+B^- \overset{S3}{\rightarrow} C_3H_6 + C_2H_5^+B^-$$

$$C_5H_{11}^+B^- \overset{S4}{\rightarrow} C_2H_4 + C_3H_7^+B^-$$

$$C_4H_9^+B^- \overset{S5}{\rightarrow} C_2H_4 + C_2H_5^+B^-$$

4. Deprotonation of the carbenium ions and restoration of acid sites.

$$C_3H_7^+B^- \overset{D1}{\rightarrow} C_3H_6 + HB$$

$$C_2H_5^+B^- \overset{D2}{\rightarrow} C_2H_4 + HB$$

Cracking reactions are not limited to the above as there can be occurrence of some other reactions such as isomerization, cyclization, dehydrogenation, oligomerization, aromatization, *et cetera*. This ultimately leads to further conversion and more/complex products formation.

The relative contribution of the reaction routes dictates the final products [94].

Table 2-1 Possible reaction pathways for n-hexane cracking

Products	Pathways	Products	Pathways
H_2	P1	C_3H_8	P4, T4
CH_4	P2	C_4H_8	S1
C_2H_4	S4, S5, D2	C_4H_{10}	P5, T3
C_2H_6	P3, T5	C_5H_{12}	T2
C_3H_6	S2, S3, D1	C_6H_{14}	T1

2.4 SSZ-54

SSZ-54 is an intergrowth of MTT (1D) and TON (1D) frameworks [1]. MTT framework zeolite is a 10-member ring rod-like material [95]. MTT framework zeolite has been employed in some important industrial reactions such as isomerization of butane, catalytic cracking of alkanes to yield propene and ethene [96] because of its essential tiny structure which is useful in shape-selective applications.

In addition, TON framework is another one-dimensional rod-like zeolite with 10-member ring and a diameter of 0.55nm x 0.45nm [97], [98]. It has also been applied in certain catalytic reactions such as hydrocracking and isomerization of n-paraffin mixtures [99].

Therefore, juxtaposition of the two structures discussed above, it is expected that SSZ-54 would be a one-dimensional structure, having a 10 member rings in rod-like structure. The challenge which can be imposed on using this zeolite for hydrocarbon reactions is coking owing to its long structure and tiny pores. Coking is expected to take place which can cause blockage of zeolite thereby introducing mass transfer limitation of reactants. This will create hindrance for the proper location of active sites by the reactants. In a bid to forestall

this occurrence, tuning of morphology as well as creation of mesopores is adequately needed.

Many reports abound in the fine tuning of the morphology of one dimensional zeolite in open literatures. Such methods as varying the amount of hydroxyl ions present with respect to silica amount, use of co-solvent [100], fraction of silica to water [101] *et cetera* have been reported to be greatly important for modifying the structure of zeolite for better catalytic performance and stability. Other methods reported so far are by purposely changing the synthesis methods. Among the methods employed reported were either hydrothermal synthesis or solvothermal synthesis [1], [2] and [103]. Although these methods have come with challenges of exotic structures and properties and this has called for attention [102]. In a bid to alleviate the challenges, Wang *et al*. reported another method called ionothermal synthesis [102]. This method involves the use of ionic liquid as both the structure directing agent and the solvent [102] and this has made way for the synthesis of novel molecular sieves and to determine the mechanism for such synthesis.

Although, commercial as well as full-bodied laboratory synthesis of SSZ-54 catalyst has not been reported in any open literature prior this period, the inventors of this catalyst thus hypothesized the following SDAs. The summary of all his hypothesis is presented in the following table;

Table 2-2 Different structure directing agents for synthesis of SSZ-54

SDAs	Quantities (g)	T(°C)	Time	Ref.
N-isopylethylenediamine	0.40	170	9 days	[1]
N-isopropyl-1,3-propanediamine and 1-methylbutylamine	0.042 and 0.23	170	12-14 days	[1]
N-isopropyldiethylenetriamine and isobutylamine	0.08 and 0.12	170	12-14 days	[1]
Dimethylamine and diethylamine	2.5 and 0.19	170	50h	[19]

In line with the above, a painstaking study of the synthesis of SSZ-54 using a novel dual template strategy will be reported. In addition, its catalytic prowess would be examined with cracking of n-hexane. Several improvements in the synthesis as well as post-synthesis treatment would be stated in a bid to improve the catalytic performance of SSZ-54.

CHAPTER 3

Experimental methods and apparatus

The details of the experimental procedures taken as well as characterization methods adopted are presented in this chapter and figures are embedded, where necessary.

3.1 Synthesis of SSZ-54 zeolite

The synthesis of SSZ-54 was carried out using hydrothermal synthesis and microwave reactors. The effects of changing the concentrations of the duo of the SDAs used was studied alongside synthesis temperature, Si/Al ratio and time of reaction (crystallization). Diffusion limitation is predicted to hinder the performance of this catalyst because of its length and tiny pores. To forestall that, alkaline desilication and mild dealumination were carried out and proper characterization methods were employed.

3.1.1 Hydrothermal synthesis method

The following reagents were used to synthesize our catalyst of interest. These are; aluminium nitrate nonahydrate [$Al(NO_3)_3.9H_2O$] (Janssen Chimica), colloidal silica (Aldrich, 40%), de-ionized water, isopropylamine [IPA] (Acros,99%), 1,6-hexamethylene diamine [DAH] (Acros, 99%) and potassium hydroxide [KOH] (AppliChem, 85%).

Also, the list of equipment used as well as their specifications are presented in **Table 3-1**;

Table 3-1 List of equipment and specifications

Equipment	Manufacturer	Model number
Weighing balance	Mettler Toledo	ML204/03
Programmable Stirring Hotplate	Torrey Pines Scientific	HS 65
Desktop Centrifuge	Thermo Scientific	---------
Hydrothermal Synthesis Reactor	Hiro Company	KH-02
Oven	Thermo Scientific	HO514

The preparation of SSZ-54 using a dual template technique was done as follows; into a small bottle of about 100 ml is placed 45 g water and 0.74 g of 1N KOH was dissolved in it. The mixture is placed on a hot plate and set to a revolve at 300 rpm at room temperature after which 0.33 g of aluminium nitrate nonahydrate was added. Then, after stirring for 10 min, 8.37 cm^3 of IPA (Aldrich, 98%) was added and followed by addition of 1.887 g of DAH and finally 6.607 g of colloidal silica (Aldrich, 40%) to make a suspension. The molar ratio of the resulting solution was 1 SiO_2: 0.02 $Al(NO_3)_3.9H_2O$: 0.3 KOH: 1.932 isopropyl amine: 62.53 H_2O.

The reaction mixture is then closed, sealed and rotated for 2 h at 300 rpm. The mixture is then transferred into a Teflon cup of Parr 120 ml reactor, heated at 170 ^oC at a stirring speed of 40 rpm tumbling. After 50 h, the mixture is cooled and the product is collected and washed in de-ionized water using a desktop centrifuge.

The cleansed samples are then air dried for 24 h before being dried in an oven at 110 ^oC for 12h. The products are analysed by XRD technique. The product has a SiO_2/Al_2O_3 of 50.

The quantities of each of the constituents are then varied and the procedure above is repeated for each of the experimental runs. Other compositions were prepared and molar ratios are presented as shown in **Table 3-2** below;

Table 3-2 Molar composition of reacting mixtures

S/N	Si/Al ratio	Combining moles
1-12	50	1SiO_2: (0-2.3) DAH: (2.3-0) IPA: 0.02 Al_2O_3 : 0.3 KOH: 62.53 H_2O
5	50	1SiO_2: 0.368 DAH: 1.932 IPA: 0.02 Al_2O_3 : 0.3 KOH : 62.53 H_2O
13	100	1SiO_2: 0.368 DAH: 1.932 IPA: 0.01Al_2O_3 : 0.3 KOH : 62.53 H_2O

Formulation 5 (**Table 3-2**) was repeated and the synthesis temperature was varied. The temperatures used were 150 ^oC, 160 ^oC, 170 ^oC and 180 ^oC to study the effects of temperature on the structure of the zeolite and to find the optimum temperature for MTT/TON intergrowth formation.

Effect of synthesis time was also studied to determine the optimum crystallization time for the MTT/TON intergrowth formation. Synthesis times studied were 16 h, 32 h, 36 h, 40 h and 50 h.

In addition, the effect of the ratio of silica to alumina was investigated. This was done by varying the amounts of alumina in the reacting solution and Si/Al ratios of 50 and 100 were produced. The removal of templates was done by calcination of the as-synthesized samples at 650 ^oC for 12 h with the heating rate of 10 K/min under the flow of air and subsequently, ion exchange followed thereby converting the zeolite to proton form.

The figure below shows the summary of the experimental procedure described above and the subsequent sub-sections describes the ion exchange, desilication and mild dealumination procedures.

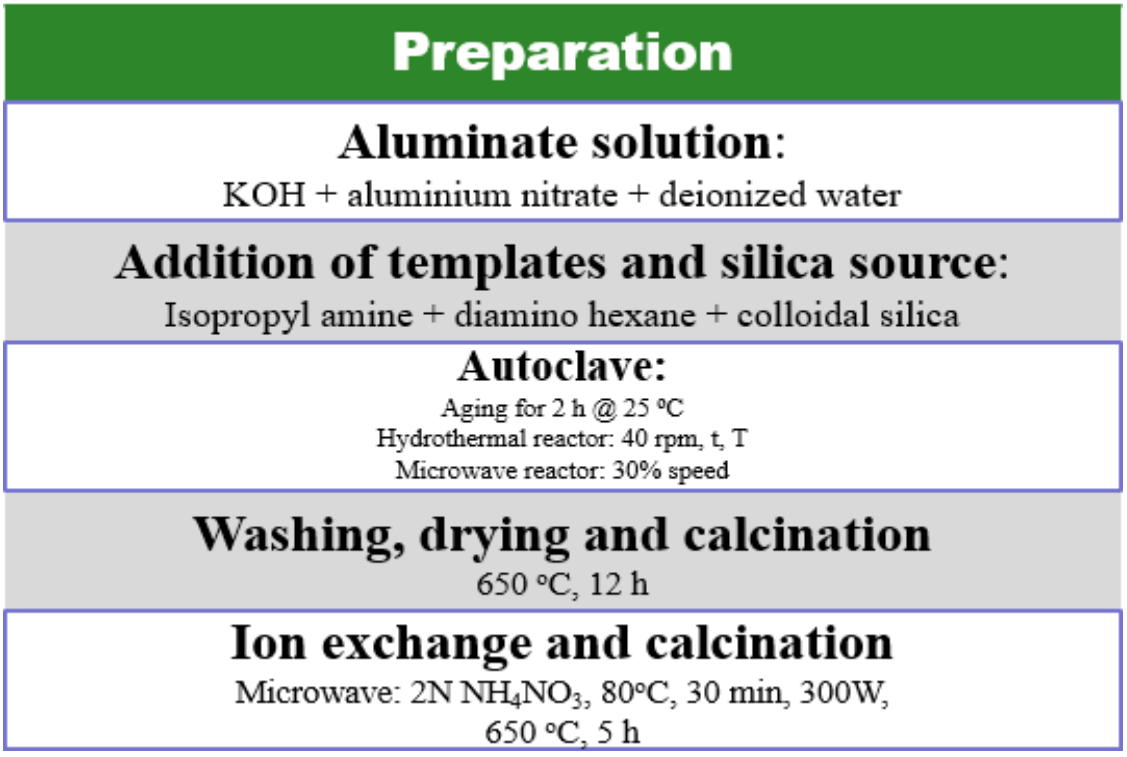

Figure 3-1 Experimental Procedure for SSZ-54 synthesis

3.1.2 Microwave-assisted synthesis

The crystallization of zeolite was controlled using microwave irradiation technique. The synthesis of the SSZ-54 zeolite was performed by mixing 0.617 g of potassium hydroxide (KOH, Aldrich 98%) with 37.847 g of deionized water in a Teflon cup 60 cm^3 capacity, 0.275 g of aluminium nitrate nonahydrate [$Al(NO_3)_3.9H_2O$] (BDH Chemicals, Poole England), was added. An aluminate solution is then formed after agitation for 5 min. Then, 6.978 ml of isopropyl amine (Acros,99%) was added and accompanied by 1.568 g of

hexane diamine (Acros, 99%) after which 5.507 g of colloidal silica (LUDOX TM-40). A white solution is formed. The molar ratio of the resulting solution was 1 SiO_2:0.02 Al_2O_3:0.3 KOH: 1.93 isopropyl amine: 0.368 hexane diamine: 62.54 H_2O. This was left aging for 2 h before being transferred to microwave reactor for crystallization. The as-prepared solution has Si/Al ratio of 50.

The solution that was prepared was heated at 180 ^oC in a microwave reactor (MicroSYNTH, Milestone, 700 W) with synthesis time of 12 h under constant stirring. The collected samples were washed and centrifuged with deionized water and air-dried for about 12 h after being put in oven for 12 h at 110 ^oC. Calcination followed at 600 ^oC to remove the organic materials (templates) inside with ramping rate of 10 ^oC/min for 12 h.

3.1.3 Ion exchange of the samples

The sample was treated with 25 ml of 2M NH_4NO_3 and put into microwave reactor. The sample was heated to 85 ^oC at a ramping speed of 6 ^oC/min. It dwelled at 85 ^oC for 15 min which was then followed by cooling. Then the sample prepared was washed by centrifuge at 3200 rpm.

3.1.4 Production of hierarchical zeolite

Desilication was done using an equal volume of each of 0.2 M TEAOH and 0.2 M NaOH with the ratio of 30 ml of the solution to 1 g of the sample. The solution was heated to 80 ^oC and the sample was added and allowed to dwell inside for 30 min. The product was washed and dried as above. Calcination took place at 550 ^oC for 5 h.

Dealumination was carried out with 3M HNO_3. 1 g of the sample was treated in 25 ml of the acid using microwave at a temperature of 85 ^oC using a ramping rate of 10 ^oC per minute. It was allowed to dwell at that temperature for 10 min and cooled to room temperature, washed and dried at 140 ^oC for 5 h and calcined at 550 ^oC for 5 h [95]. Then finally product was dried.

The summary of the above description is provided in Figure 3-2 below;

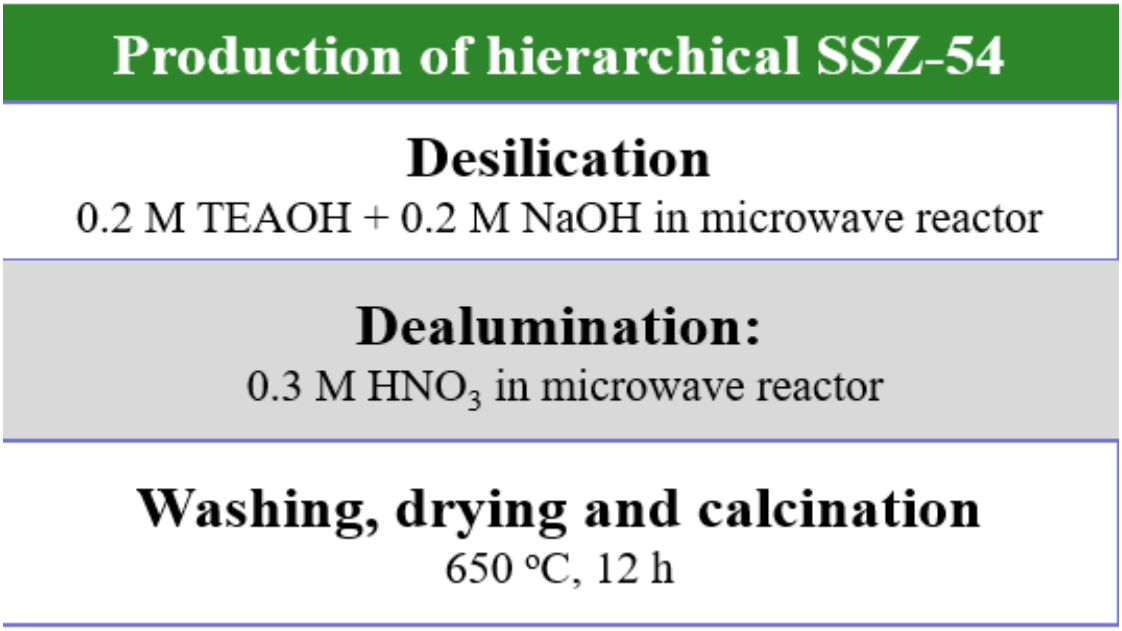

Figure 3-2 Desilication and mild dealumination of SSZ-54

3.2 Characterization methods

3.2.1 X-ray diffraction (XRD) methods

Identification of product phase and crystallinity was carried out with the aid of XRD analyzer. The patterns were recorded on Rikagu made Miniflex II Desktop X-ray Diffractometer using Ni filtered Cu Kα radiation with the wavelength of 1.5406Å. A 30kV voltage and 15mA current copper tube is embedded in the machine together with a detector

for position, a scintillation counter and the sample holder. Angle range of 5-50^{o} 2Ɵ, scan speed of 3^{o}/min and step width of 0.03^{o} were all used.

3.2.2 Scanning Electron Microscopy (SEM)

Morphology of the samples was studied with the SEM. The crystals were suspended in ethanol and was then dropped on the carbon film sample cell. 25kV acceleration was used for proper magnification of the images.

3.2.3 Nitrogen physisorption (BET method)

The measurement of the surface area and pore properties of the samples were carried out by measuring adsorption vs desorption characteristics of the sample with N_2 at 77 K. This was carried out with the adsorption analyzer from micromeritics. Pre-treatment of the sample was carried out which consists of degassing the sample at 80 ^{o}C for 1 h and was followed by 300 ^{o}C for 4 h at about 5mmHg. The aim of the treatment was to remove some elements of moisture and organic substances which might have probably been physisorbed on the catalyst surface. Then the mesopore volume and the pore size distribution were determined by Barrett-Joyner-Halender (BJH) model while micropore volume was determined with t-plot method.

3.2.4 High Resolution Transmission Electron Microscopy (HRTEM)

High Resolution Transmission Electron Microscope (HRTEM) was done with Philips FEI TecnaiF30 instrument and the data were recorded at an operating voltage of 200 kV. This is to investigate the crystal size and structure of the crystals.

It is done by grinding the specimen, in powdered form and spreading it on a carbon film which has a Cu grid support. Heating of the sample under Tungsten filament was done and the sample was finally transferred to the sample chamber. Very high magnifications such as x24k to x49k were used.

3.2.5 Cs-corrected STEM

Atomic-resolution images were obtained in a FEI TITAN XFEG transmission electron microscope operated at 300 kV an equipped with a spherical aberration corrector for the electron probe. The samples were crushed using mortar and pestle and dispersed in ethanol. Few drops of the suspension were placed on carbon coated copper microgrids.

3.2.6 Temperature-Programmed Desorption (TPD)

Distribution, density and the strength of the acid sites were determined by ammonia temperature programmed desorption (NH_3-TPD). This is carried out by feeding the wider opening of the quartz U-shaped microreactor with about 0.10 g of the sample after a 'ball' of about 9mm diameter of quartz wool has been put in first. The tube is inserted into the AutoChem II 2920 analyser by micromeritics. Helium gas was used for degassing at 26 ml/min, 600 ^{o}C and allowed at that temperature for 30 min. The temperature was reduced gradually to 100 ^{o}C and flushed with ammonia at the flow of 50 ml/min for 30 mins followed by replacement with helium at the same rate for 1 h after which the temperature is increased to 650 ^{o}C. During this time, the ammonia is desorbed as the temperature is rising and the data were collected after the experiment and recorded on thermal conductivity detector (TCD).

3.2.7 Fourier Transform IR (FT-IR)

Fourier transform IR was done with pyridine as probe molecule on a VERTE70 FTIR spectrometer (Thermo Scientific) with 4 cm^{-1} as the resolution used. The samples were prepared in powdered form and pressed into a self-supported wafer of ca. 10 mg/cm^2 of about 1.3 cm diameter and mounted onto the diaphragm of the spectrometer equipment. The samples were pretreated at 673 K and vacuum of 0.001 Pa for 1 h and cooling to room temperature followed.

Subsequently, adsorption of pyridine proceeded at 150 ^oC for 20 min. Outgassing was carried out in vacuum for 25 min at 150 ^oC, 250 ^oC and 350 ^oC to remove excess pyridine with IR spectrum being recorded following each heating period.

3.3 Catalysts testing

Catalytic activities of SSZ-54 was examined by cracking of light naphtha using n-hexane (97% assay, Sigma) as the model compound. The reaction was carried out in a packed bed reactor of ID: 5 mm. The catalyst samples were sieved to particle size range of 100-300 nm and then pelletized. The volumetric flow rate of the carrier gas used was 20 ml/min and the pressure was maintained at 0.2 bar throughout the period of the experiment. The weight of the catalyst used will be described in relevant section under the next chapter. The analysis of the reaction products was done with online gas chromatograph (Agilent Technologies, GC-7890A) equipped with double detectors.

The set-up for catalytic evaluation in a fixed-bed reactor is shown as **Fig.S6**, Appendix B.

CHAPTER 4

RESULTS AND DISCUSSION

4.1 Evaluation of the parent samples

Details of reaction conditions.

Volumetric flow rate of n-hexane = 0.02 ml

Weight of the catalyst = 0.3 g

Temperature of the reaction = 650 ^{o}C

The naming system adopted is SZ-x-y where x represents Si/Al and y represents the condition whether parent, P or treated DSA. For example, SZ-100-P represents the parent sample of SSZ-54 synthesized with Si/Al of 100.

4.1.1 Characterization of the samples

Effects of variation in the proportion of templates

Variation of the proportion of IPA and DAH in the reaction mixture was done and a series of intergrowth behavior was observed. **Table 3-2** above shows the composition of reactants in the mixture and the XRD of the as-synthesized samples are revealed in **Fig. 4-1**. Therein, we observed a phase transformation from pure MTT phase (0 % DAH) [see **Fig. 4-1** and **4-2**] through intergrowth (16-25% DAH) with the rest dedicated to TON.

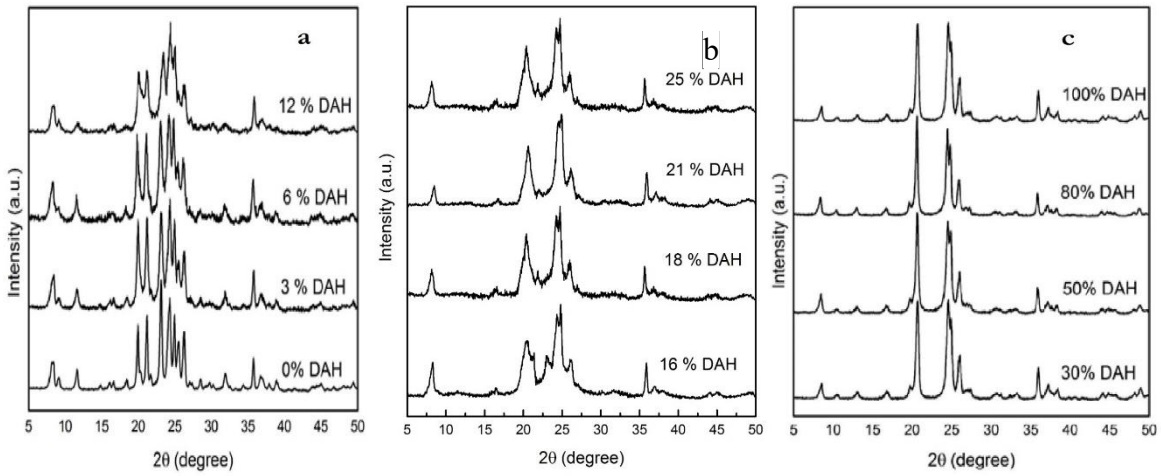

Figure 4-1 XRD patterns of calcined zeolite synthesized with mixed OSDA where different concentrations of isopropylamine [IPA] and 1,6-hexane diamine (DAH) were used. (a) MTT phase was observed (b) Intergrowth formed and (c) TON phase was detected.

Deductions from these results are that MTT structure forms when there is enough IPA to fill the pores of the sample (% of DAH < 16%). However, as the ratio of IPA/DAH is being reduced, it creates insufficiency in the amount of IPA to fill those pores, this results in the formation of SSZ-54 intergrowth. Furthermore, after 25 % DAH composition, the result changes to spectra dedicated to pure TON. Although there are few variations in the peaks obtained after changing the compositional amounts (for SSZ-54), these do not constitute phase change in the structures, as such, the structures are identified as SSZ-54. We then observed that relative amounts of OSDAs in the reaction mixture is relevant as far as the behavior of intergrowth is concerned. Our basis of comparison was in the works of Burton *et al.* [1] and Wang *et al.* [19] though, in both cases a different OSDA systems were used, our results are consistent. In addition, DIFFaX simulation of standard SSZ-54 patterns reported by Burton *et al.* [1] revealed that our sample consists of 70% MTT and 30% TON (at 16 % DAH) and 60% MTT and 40% TON for 16-25 %. Hence, we have synthesized

MTT/TON intergrowths reported by both Burton *et al.* (40 % MTT) and Wang *et al.* (60 % MTT) from variation in the quantity of templates.

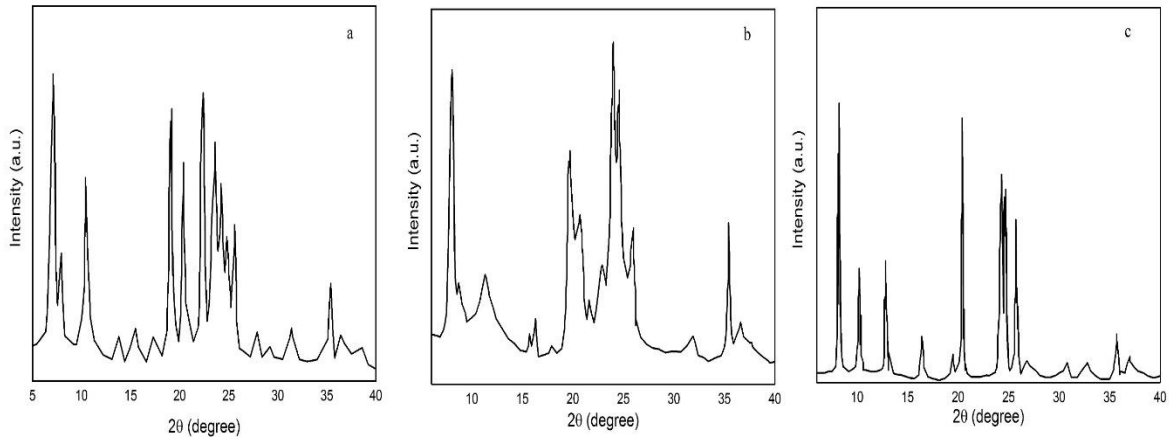

Figure 4-2 XRD patterns of different modelled phases as revealed by DiFFax. (a) MTT phase (b) SSZ-54 and (c) TON phase. Ref: [1]

Effect of synthesis temperature

Formulation **5** from the **Table 3-2** was repeated for temperature variation. The temperatures adopted were 150 ^{o}C to 180 ^{o}C at 50 h for each sample. Spectra of the as-synthesized XRD patterns are shown in **Fig. 4-3a**. Considering the synthesis at 150 ^{o}C, there exists some noticeable amount of impurities especially the peak at 23° identified as crystoballite. Temperatures of 160 ^{o}C and 170 ^{o}C proved to be the required temperatures for intergrowth formation though 170 ^{o}C synthesis temperature showed to be the optimum temperature in terms of crystallinity of the sample. Meanwhile, increasing the synthesis temperature to 180 ^{o}C was detrimental as the SSZ-54 phase produced had several impurity phases.

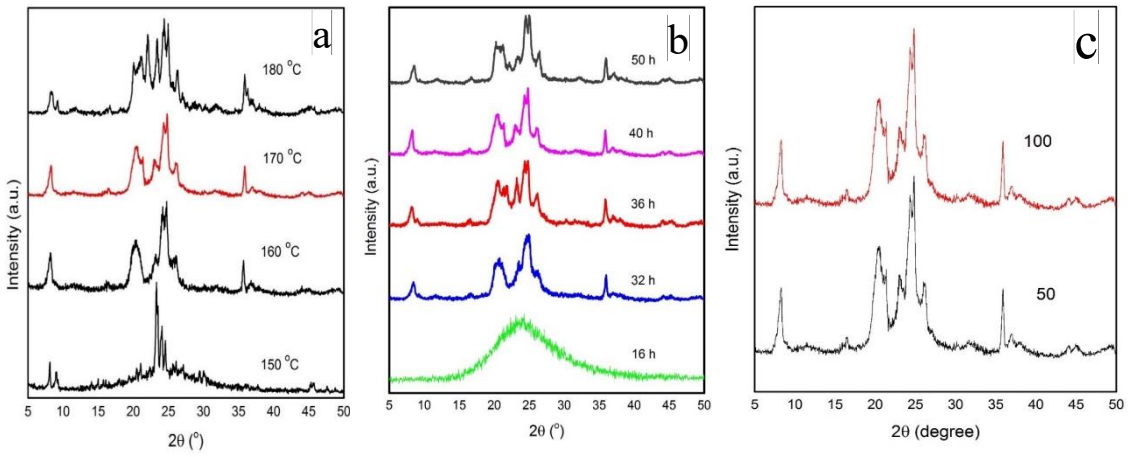

Figure 4-3 XRD patterns of calcined zeolite synthesized with 16% DAH and 84% IPA (a) different synthesis temperatures, (b) different crystallization times and (c) different Si/Al ratios.

Effect of synthesis time

Regarding the synthesis of the MTT/TON intergrowth at 170 ^{o}C , a minimal synthesis time of nine days was reported in the work of Burton *et al.* [1] while 50 h was reported in the work of Wang *et al.*[19]. In our voyage, we considered synthesis times of 16 h, 32 h, 36 h, 40 h and 50 h. After the XRD analysis, the results are presented in **Fig. 4-3b**. We observed intergrowth formation at 32 h. The result obtained at 16 h showed the formation of an amorphous substance. Variation in the degree of crystallinity is what differentiated the samples formed 32 up to 50 h as all gave good and consistent results. Interestingly, our results have proven the possibility of producing SSZ-54 intergrowth at obviously lower synthesis times than the ones reported earlier which were 9 d and 50 h reported by Burton *et al.* [1] and Wang *et al.* [19] .

Effect of silica to alumina (Si/Al) ratio

In a view to producing hydrophobic SSZ-54 and to improve its stability, we varied the ratio of silica to alumina. From the **Fig. 4-3c**, the phases are preserved and for the first time, we were able to produce SSZ-54 samples with disparate Si/Al ratios.

Field Emission Scanning Electron Microscopy (FE-SEM)

Ability to produce clear and unblemished image has made FE-SEM a very efficient method for morphological studies of materials. Morphology of the samples are presented in **Fig. 4-4** and those of MTT and TON are shown alongside for proper comparison. The morphologies of MTT, TON and SSZ-54 (**Fig. 4-4a, b and c)** disclosed that the samples are made of assembled needle-like structures. MTT structure has been reported by Bakare *et al*., [105] and TON by Anas *et al.*, [106]. From what we have in Fig. 4-4c, SSZ-54 morphology looks exactly like the constituting frameworks of MTT and TON.

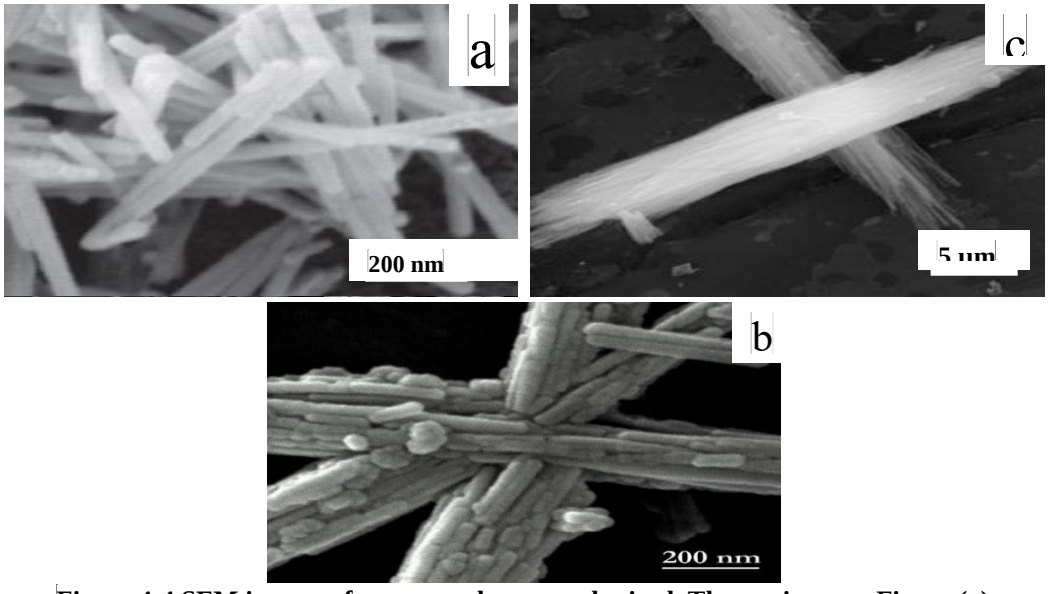

Figure 4-4 SEM images of separate phases synthesized. The top images; Figure (a) corresponds to MTT phase while fig (c) is the TON phase. The bottom image; fig (b) is the image of SSZ-54 (intergrowth). Ref: [95]**,** [90]

Cs-corrected STEM

In recent years, spherical aberration corrected (C_s-corrected) Scanning Transmission Electron Microscopy has been proved to be an extremely powerful technique for the observation with unprecedented resolution beam for sensitive materials such as zeolites and zeotypes [107]–[109]. And in particular it is of paramount importance dealing with the analysis of structural defects[110] .

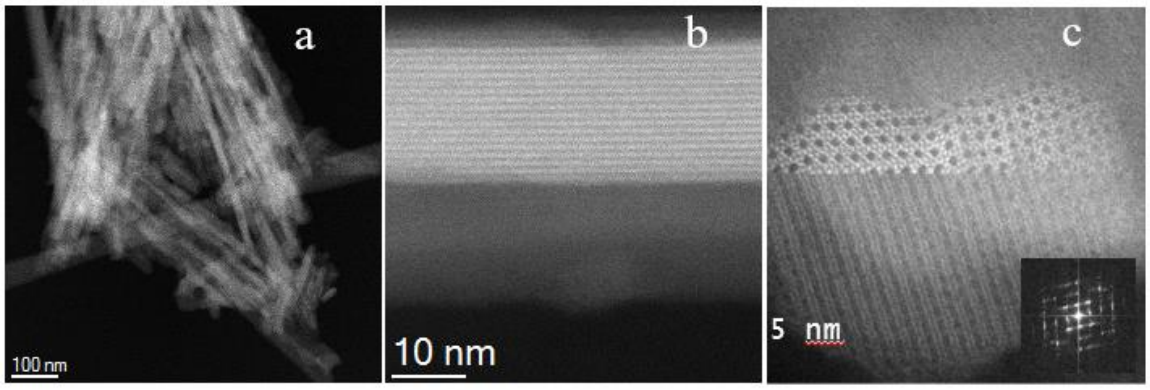

Figure 4-5 Cs-corrected STEM-HAADF images of SSZ-54. a) Low-magnification image showing several crystals orientated perpendicular to the pore channels. b) a closer observation of the pore channels. c) High-resolution image of a SSZ-54 crystal partially orientated

C_s-corrected STEM images using a high angle annular dark field detector (HAADF) of the synthesized SSZ-54 are shown by the **Fig. 4-5**. **Figure 4-5a** displays a low magnification image, revealing the needle-like morphology where the length of the zeolitic crystals reached up over a micron; while the thickness was around 20 to 30 nm. **Figure 4-5b** shows a closer observation perpendicular to the channel direction (needles) where the microstructure can be also elucidated with a distance between layers of 10.83 Å. By tilting the crystals, a 90 degrees image was possible to be recorded corroborating the good crystallinity of the materials, which allow the observation of the pore arrangement and the

stacking disorder between both structures. **Figure 4-5c** depicts a crystal slightly tilted but that clearly allows the observation of the pores together with the intergrowths; the FFT, inset, presents streaking instead of single spots (which would correspond to a single crystal structure) corroborates the stacking in the structure. A closer look, **Fig. 4-6a**, allows the identification of the building units and differentiates both materials. To fully corroborate this assumption, the superimposed is presented in **Figures 4-6b and 4-6c** for TON and MTT respectively, observing a clear agreement between the theoretical model and the experimental data.

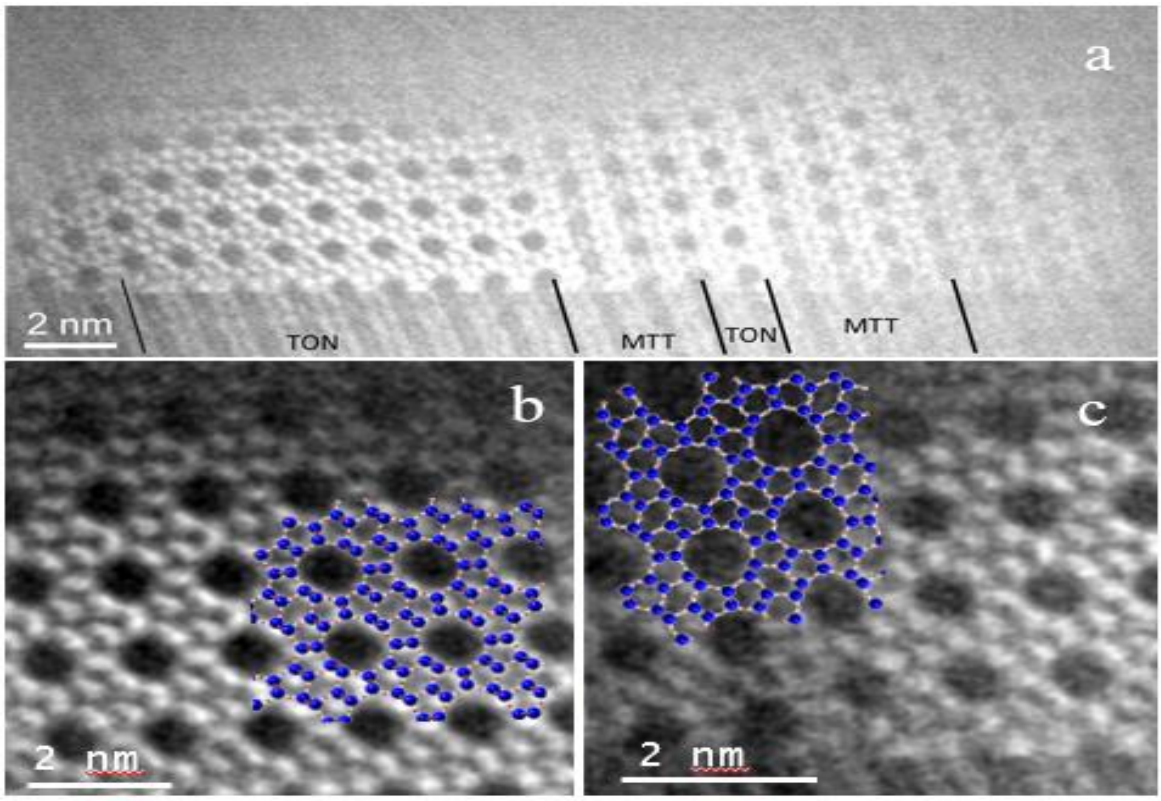

Figure 4-6 Cs-corrected STEM-HAADF images of SSZ-54. a) A closer observation of the figure 4-5c, where the different domains are marked. b) Enlarged micrograph of the TON region with the model superimposed. c) Similar observation on the MTT zone with the model overlaid. Si and Al atoms appear in blue while oxygen appears in red

Fourier Transform IR

Pyridine-adsorbed FTIR spectra of SZ-50-P and SZ-100-P at 150 ^{o}C is presented in Fig. **4-7** while the data at 150 ^{o}C, 250 ^{o}C and 350 ^{o}C adsorption temperatures are shown in **Table 4-1**. The presence of the acid sites, represented by the vibration bands at ca. 1454 cm^{-1}, 1490 cm^{-1} and 1546 cm^{-1} corresponds to bounded pyridine with Lewis (L), incompletely-formed Lewis and Brønsted sites (L+B) sites and Brønsted (B) acid sites respectively [111] and as such, are used to identify the presence of Lewis and Bronsted acid sites. **Table 4-1** shows the quantification of the areas of each acid sites as fitted from the IR spectra at different temperatures from the consideration extinction coefficient [112]. The amount of Brønsted acid sites in SZ-50-P is considerably greater than Lewis sites and this is attributed to insufficient Al for ion exchange in SZ-100-P thus resulting in reduction in Brønsted acidity as Si/Al increases [113]. However, Lewis acid site is by far more than Brønsted in SZ-100-P as seen from the areas calculated from the spectra (see **Table 4-1)**

Table 4-1 FTIR analysis of the samples

Sample code	**From calculation**			
	B[a]	L[a]	B/L	Temperature
SZ-50-P	130.0452	52.2921	2.49	150 ^{o}C
	97.4360	27.0102	3.61	250 ^{o}C
	74.1677	18.6158	3.98	350 ^{o}C
SZ-100-P	29.1246	206.6023	0.14	150 ^{o}C
	27.4761	20.9210	1.31	250 ^{o}C
	25.8962	14.8569	1.74	250 ^{o}C

a: From the calculation using extinction coefficient (μmol/g).

Moreover, as the temperature is increasing, both Brønsted and Lewis acid sites got reduced though at different rates. For instance, in SZ-50-P, Brønsted acid site reduced by 25% (150 ^{o}C - 250 ^{o}C) and 24 % (250 - 350 ^{o}C) with corresponding reduction in Lewis acid site by 48 % and 31 % respectively. Increase in B/L factor in **Table 4-1** as the temperature got increased from 150 ^{o}C through 350 ^{o}C in SZ-50-P and SZ-100-P corroborates this finding. By this, it can be inferred that while Lewis is present, the strength is considerably weak and it can possibly have effect on the reaction.

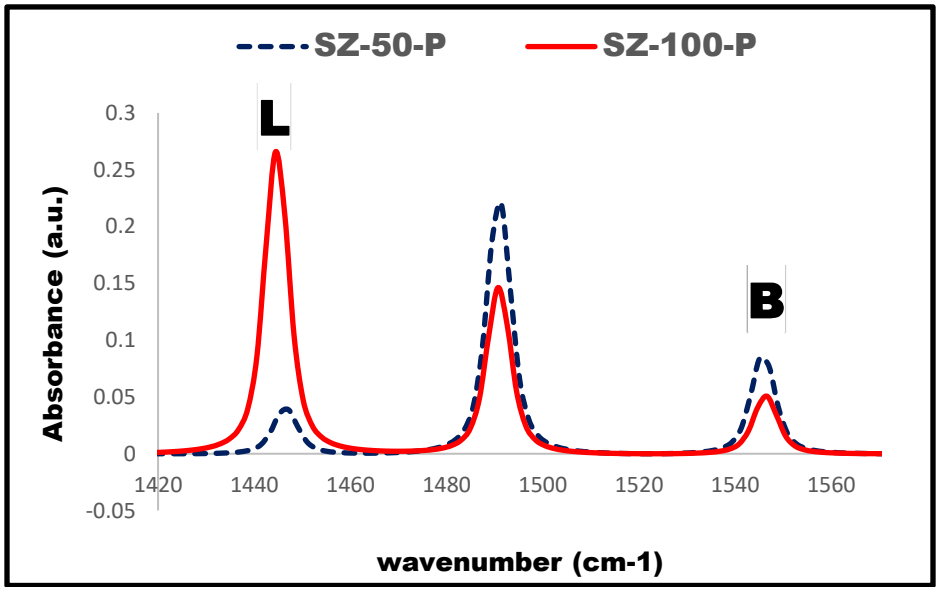

Figure 4-7 FT-IR spectra of MTT-TON Intergrowth Zeolite (after blank subtraction) showing the bands for Lewis and Brønsted acid sites at adsorption temperature of 150 ^{o}C.

Temperature-programmed desorption (TPD)

The acid sites in the samples are identified by NH_3-TPD. Two peaks are observed which correspond to high temperature and low temperature peaks. The low temperature peak, obtained at 215-220 ^{o}C and high temperature peak, at 450-500 ^{o}C correspond to weak and strong acid sites respectively. The position of the peaks in the low temperature region for

both samples is relatively the same while the high-temperature peak vanished in the SZ-100-P.

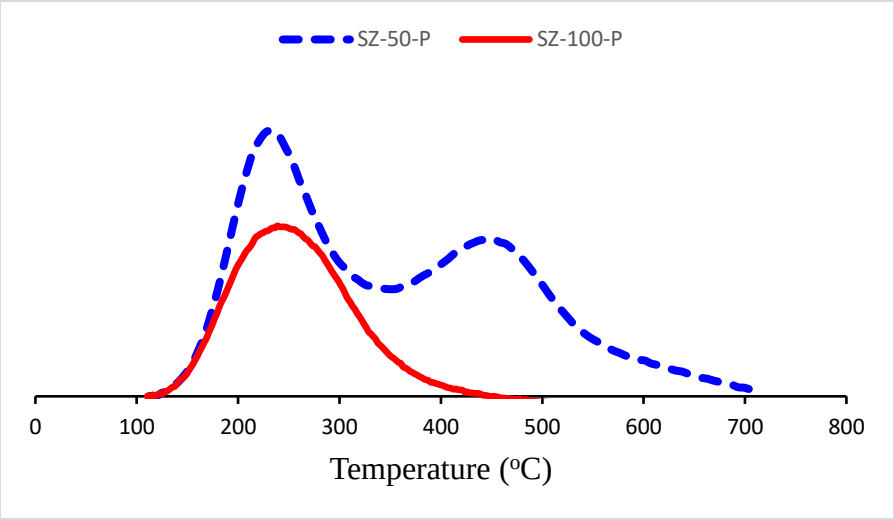

Figure 4-8 NH3-TPD profiles of the parent samples of SSZ-54

The distribution is given in part of **Table 4.2** below. It is worth mentioning that the absence of strong acid site in SZ-100-P, indicated by non-appearance of *h-peak*, confirms relative lower quantity of aluminium in the framework of SZ-100-P which drastically reduces the strength of Si-O-Al bond due to paucity of framework aluminium [114]. In totality, SZ-50-P possesses high quantity of acid sites (both strong and weak) than SZ-100-P.

Table 4-2 Physicochemical properties of the samples (error = ±2%)

Sample code	S_{BET} [a]	S_{micro} [b]	S_{meso} [c]	V_{total} [d]	V_{micro} [e]	Average pore size [f]	TSA [g]
SZ-50-P	231	176	55	0.183	0.073	31.73	37.91
SZ-100-P	162	98	65	0.179	0.042	44.09	21.47

a: m^2/g, measured by BET method

b: m^2/g, measured by t-plot method

c: m^2/g, $S_{BET} - S_{micro}$

d: cm^3/g, volume adsorbed at p/po= 0.97

e: cm^3/g, measured by t-plot method

f: Å, measured from N_2 physisorption

g: total surface acidity, µmol, measured by NH_3-TPD

Nitrogen adsorption

Nitrogen physisorption result is shown in **Fig. 4-9**. The samples showed a low uptake of N_2 at $p/p_o < 0.4$ with no distinct hysteresis loop which is indicative of highly microporous material. The nitrogen uptake increased between $p/p_o = 0.4$-1 with substantial increase in uptake took place between $p/p_o = 0.9$-1 indicating few amounts of mesopores in the structure. Both BET surface area and pore volumes are higher in SZ-50-P than in SZ-100-P. The factor that might be responsible for the reduction in surface area in SZ-100-P as compared to SZ-50-P are lower relative crystallinity and relative weaker silane bond in the SZ-100-P sample [115].

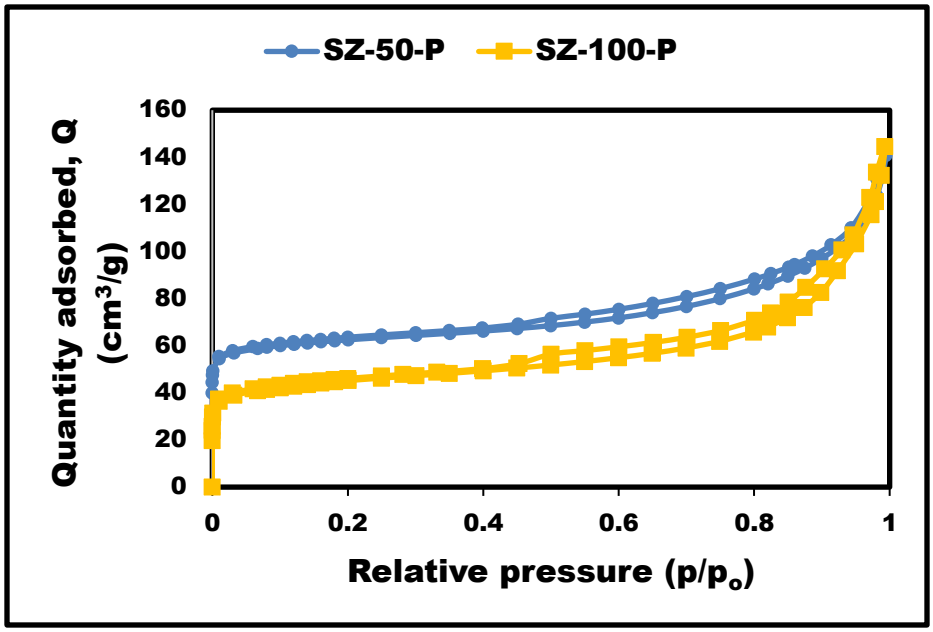

Figure 4-9 N2 adsorption plot for SZ-50-P and SZ-100-P.

Although, both samples preserve the phases of SSZ-54 regardless of the Si/Al, emphasis must be placed that, quantitatively, SZ-50-P is more crystalline than SZ-100-P. Higher uptake in SZ-50-P is consistent with larger pore volume. The identically steep slope of both samples indicates their comparable mesoporosity. The summary of the data is provided in **Table 4-2** also.

4.1.2 Products analysis

The conversion of the n-hexane and distribution of products obtained after cracking at 650 ^{o}C were presented in **Fig. 4-10 and 4-11**. We observed high selectivity to light olefins perhaps because of prevalence of monomolecular cracking over other reaction routes. This leads to formation of carbonium ions which are then decomposed to give rise to alkanes, olefins and carbenium ion [116]. The composition of olefin is majorly propylene. In fact, the proportion of propylene in the total olefins composition obtained from both samples

during the reaction was, at least, 55 % (**Fig. S1 in appendix**). However, overall conversion in SZ-100-P was lower than that in SZ-50-P throughout the 10 h during which the investigation was carried out. The lower conversion observed in SZ-100-P can be rationalized to its lower total surface and micropore areas and total pore volume than its counterpart (**Fig. 4-10, 4-11** and **Table 4-2)**. It is also important to assert that higher conversion as shown in SZ-50-P is not only determined by the higher surface area but also by more Brønsted acid sites as the quantity of Bronsted acidity determines, among other factors, the cracking ability of a zeolitic material [117]. Conversion falls sharply at the start of the reaction but becomes moderate as the reaction proceeds especially in SZ-100-P. The nature of the curves implies that the rate of deactivation in SZ-100-P is not as rapid as in SZ-50-P and could be ascribed to larger average pore diameter of the crystals which allows easy passage of products and thus reduces pore blockage. Another reason could be because of lower surface acidity as high acidity is reported to engender hydrogen transfer and poses difficulty in olefin desorption from the active sites which promotes coke formation, blocking of pores and deactivation of active sites [118], [50].

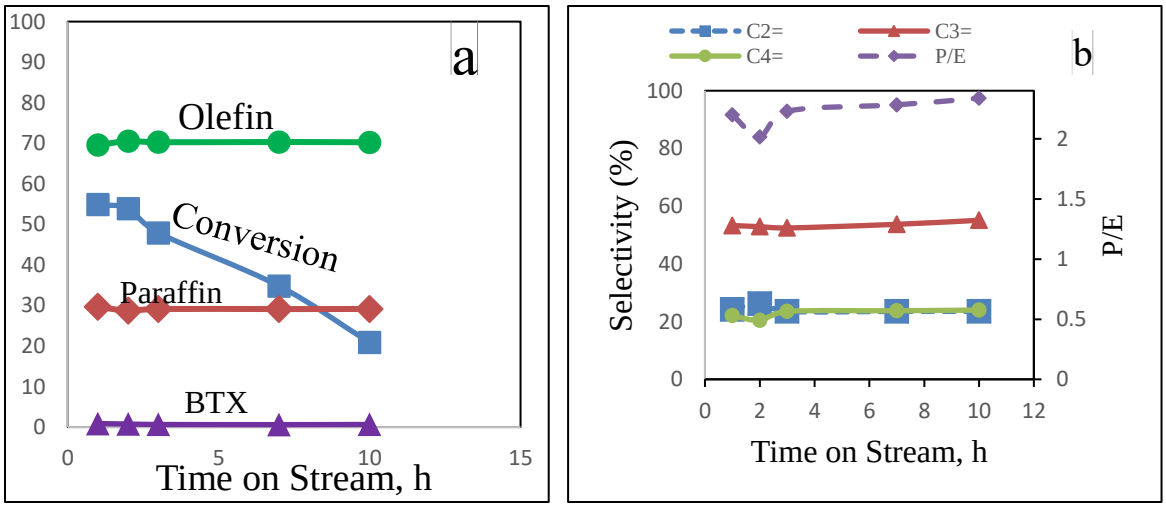

Figure 4-10 (a) Conversion, selectivity and products distribution versus TOS (h) for Z-50 (b) olefin composition and P/E versus TOS (h)

Similar high catalytic ability has been reported for MTT [119] and TON [90] in hexane cracking for light olefin production but the major drawback was in rapid deactivation. However, SSZ-54 has shown to be a more stable catalyst (in terms of conversion and olefin selectivity) without jeopardizing high catalytic activity as well as good selectivity to light olefins, majorly propylene, minimal paraffin production and negligible BTX selectivity.

In general, the combined selectivity of propylene and ethylene are quite high in both samples but higher in SZ-50-P than in SZ-100-P because of higher density of Brønsted acid as it favours light olefin formation [113]. In addition, the ratio of propylene to ethylene obtained is quite high with higher ratios in SZ-50-P. About 2.4 was obtained in SZ-50-P while approximately 1.5 was obtained in SZ-100-P (**Fig. 4-10 b and 4-11 b**). This high ratio is maintained throughout the duration of the experiment. The lower P/E ratio observed in SZ-100-P could be because of the relatively smaller total volume of the pores which hinders seamless passage of propylene in the channels of the catalyst. However, the overall high P/E observed in SSZ-54 zeolite is due to suppression of bimolecular cracking which is propylene consumer [120] and does not take place in 1D pore zeolite; fortunately SSZ-54 falls under that category. Considering paraffin formation during the reaction, the selectivity to paraffin is higher in Z-100 than in Z-50 and it is because of higher Lewis in the former which favours hydride transfer which ultimately leads to paraffin formation [117].

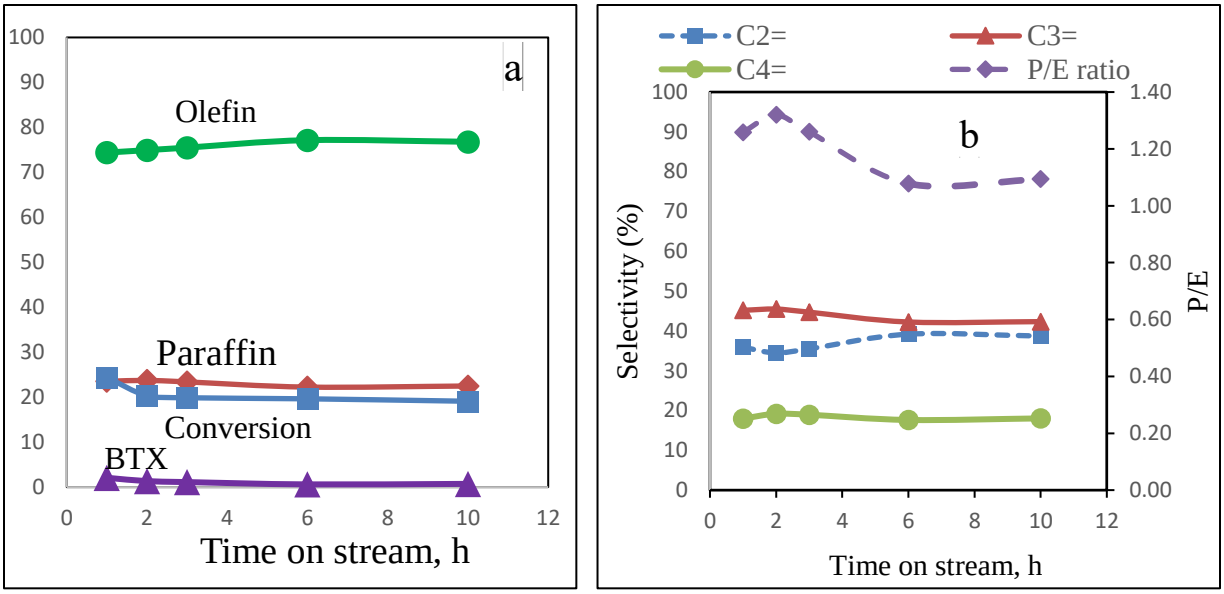

Figure 4-11 Conversion, selectivity and products distribution versus TOS (h) for Z-100 (b) olefin composition and P/E versus TOS (h)

The total yield of olefin was as high as 30% (**Figure 4-12**) with propylene always higher than ethylene. The yield of BTX was kept as low as <0.5 % throughout the period of the reaction in both samples (**Figure 4-12)**. This is advantageous as the need to install BTX separation equipment would not be necessary. Although the selectivity to olefin was always high, the n-hexane conversion kept reducing. The reason for this is because of deposition of carbonaceous materials which blocked the pore of the catalyst thus offer diffusion limitation. Also, as shown in **Table 4-2**, smaller pore diameter of Z-50 in responsible for its faster deactivation [121]. By and large, the high P/E makes it apt for SSZ-54 to be used as a selective catalyst for n-hexane cracking or as an additive to more stable zeolites such as ZSM-5 or USY to boost yield of propylene.

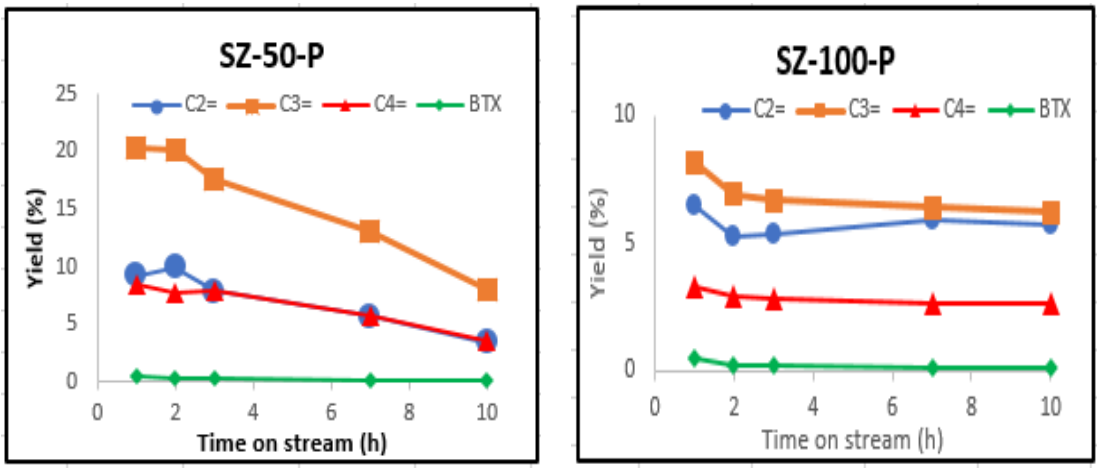

Figure 4-12 Yield of total olefin produced by SZ-50-P and SZ-100-P versus TOS

In order to properly verify our hypothesis of combining two variant structures to produce a hybrid zeolite with better characteristics, we evaluated the activities of MTT and TON frameworks for the same Si/Al ratios as SSZ-54 samples and at the same time-on-stream. The result presented in **Table 4-3** depicted initial activities of SZZ-54 which was sandwiched between those of MTT and TON frameworks at Si/Al ratios of 50 and 100 as well as yield of total olefins. The activity of SSZ-54 was later kept almost stable as the time-on-stream progresses while the activities of MTT and TON dropped rapidly. As such, there is a significant improvement offered by SSZ-54 over the two parent frameworks and the improvement brought was largely in the slower rate of deactivation for SSZ-54 and higher yield to olefins than both of its component frameworks. This improved catalytic activity exhibited by SSZ-54 can be best described using synergy between the activities of both constituted phases. By, we can infer a better catalytic performance by combining two frameworks in the system we studied here.

Table 4-3 Activity (conversion and yield of total olefins, %) of SSZ-54 with MTT and TON frameworks at different Si/Al ratios and time on stream.

		Time on stream (h)									
		Conversion (%)					Yield (%)				
Sample code	Si/Al	1	2	3	7	10	1	2	3	4	5
M-50	50	50.0	44.6	35.2	26.0	17.3	19.9	22.3	10.1	5.3	6.7
T-50	50	57.4	35.6	32.4	19.3	14.1	39.1	24.1	21.7	8.8	5.7
Z-50	50	54.9	53.9	47.9	34.8	20.8	38.5	38.1	33.7	24.8	15.1
M-100	100	16.3	17.0	15.7	14.0	12.9	10.9	11.4	10.5	9.4	8.7
T-100	100	24.7	23.3	20.6	14.3	8.70	16.8	15.9	13.8	6.8	3.9
Z-100	100	24.4	20.3	19.9	19.6	19.1	18.1	15.2	14.1	15.2	14.7

4.2 Effects of alkali-acid treatment on catalytic activity

4.2.1 Characterization results

The XRD spectra of both the parent and hierarchical samples are contained in **Figure 4-13**. By glancing through the Fig. 4-13, we observed that all the peaks dedicated to SSZ-54 zeolite are also present in our synthesized samples [1]. Also, the spectra of the desilicated and dealuminated samples are well aligned with those of the parents for each SSZ-54 samples. However, we observed a slight change in the diffraction peaks after acid and alkaline treatments, hence, degree of crystallinity changed. The degree of the crystallinity of the samples (degree of crystallinity = 100% × [(integrated intensity)$_{DSA}$/(integrated intensity)$_{P}$]) was calculated as 102 and 99 respectively for SZ-50 and SZ-100 sample where DSA represents desilicated-dealuminated sample and P stands for parent sample which was used as the standard. Hence, we infer that desilication and mild dealumination

have little effect on the crystallinity of the samples. However, we did not notice any destruction in the framework of the samples.

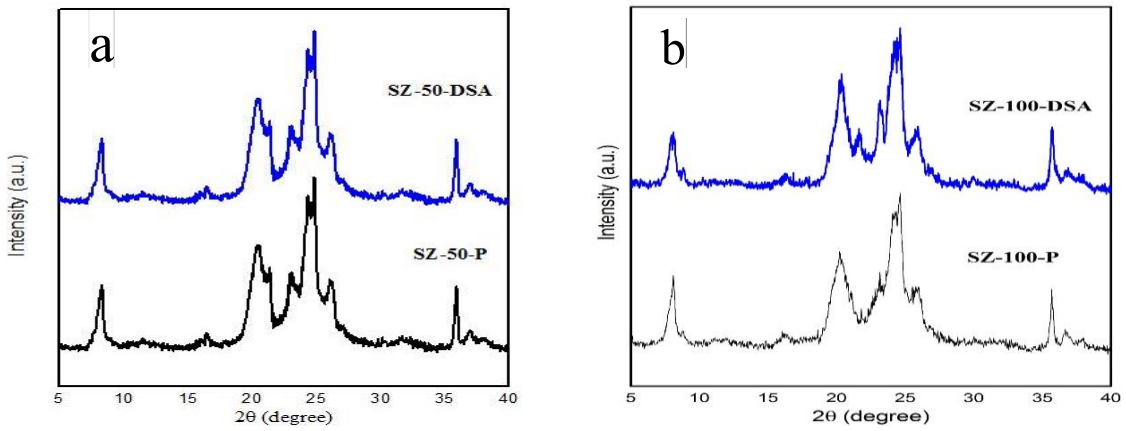

Figure 4-13 XRD spectra of the samples. Upper spectra of both figures represent desilicated-dealuminated samples. (a) Si/Al of 50 (b) Si/Al of 100.

The FE-SEM micrographs of both samples of parent and desilicated-dealuminated SSZ-54 samples are shown in **Figure 4-14**. Therein, the morphology of the samples displayed contains some assemblage of rods and needles which are segregated after desilication and dealumination. This is suggested from the strands displayed in **Fig. 4-14b**. In addition, TEM analysis (also **Fig. 4-14**) also showed the needle-like structures (in parent and desilicated-dealuminated SSZ-54 samples) which is a corroboration to what was observed in FE-SEM characterization discussed above. Also, revealed on the TEM micrograph was void created between the individual rods after desilication and dealumination (Fig. 4-14d).

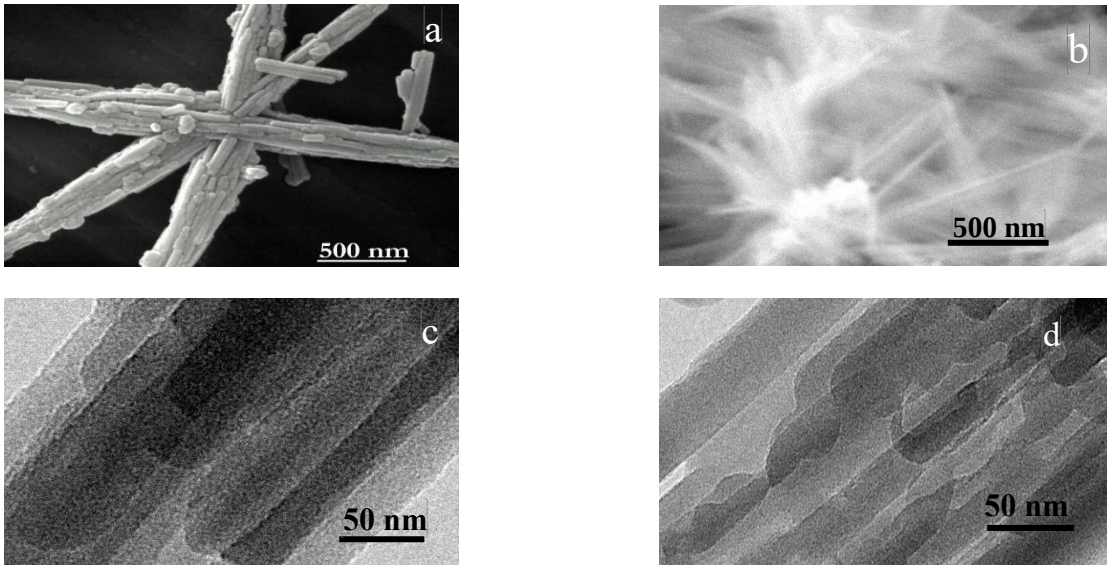

Figure 4-14 SEM and TEM images of parent and hierarchical SSZ-54. (a,c) Parent sample while (b,d) represent the image of the samples after desilicated and mild dealumination. Top images represent SEM micrographs while the bottom images show those of TEM.

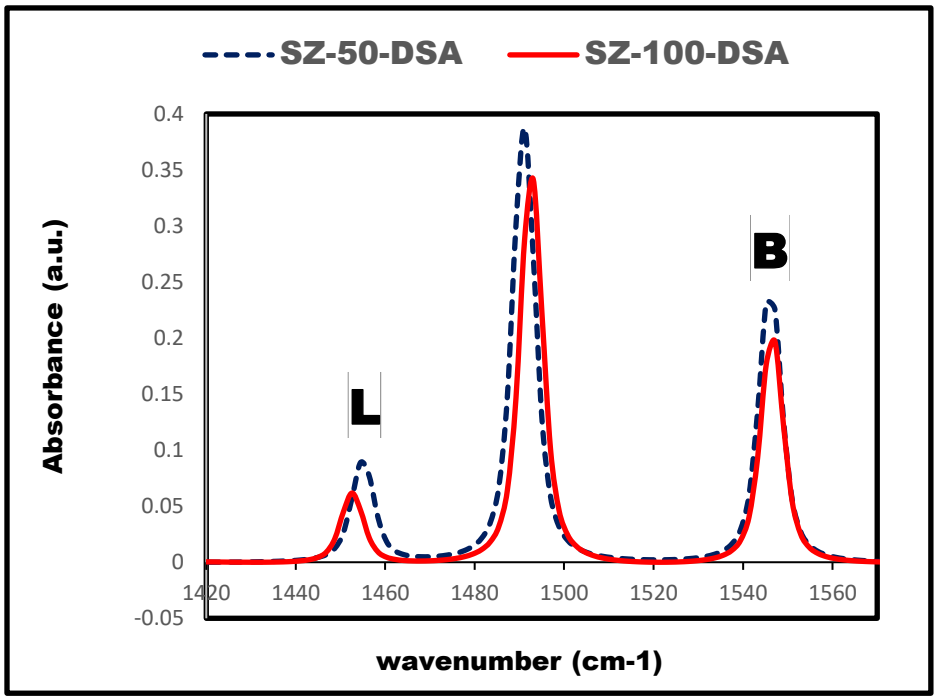

Figure 4-15 Deconvoluted FTIR spectra of the hierarchical samples

Pyridine adsorption spectra of each catalyst sample at adsorption temperature of 150 ^{o}C is shown in **Fig. 4-15**. We observed reduction in the amount of the Brønsted acidity as we increased Si/Al from 50 to 100 (vide supra).

Furthermore, we observed a drastic change in acidic property of the samples after desilication and mild dealumination. Such changes as significant increase in Brønsted and Lewis acidity (see **Table 4-4**). The data are presented in **Table 4-4**.

Table 4-4 FTIR analysis of the samples at adsorption temperature of 150 ^{o}C

	B	**L**	**B[a]**	**L[a]**	**B/L[a]**
SZ-50-P	2.33	1.06	130.05	52.29	2.49
SZ-100-P	0.42	3.41	29.12	206.60	0.14
SZ-50-DSA	3.54	1.05	166.32	43.55	2.20
SZ-100-DSA	2.85	1.08	131.89	43.89	0.12

a: From the calculation using extinction coefficient (μmol/g)

Textural properties of the parent and treated SSZ-54 samples are shown in **Table 4-5**. In general, we recorded improvement in the textural properties after treatment with alkali and acid. Taking the specific group individually, we observed decrease in micropore area as well as micropore volume as we increased Si/Al ratio from 50 to 100. However, after treatment, BET surface area and total pore volume increased remarkably after modification. Acid and base treatment has more effect on increasing micropore volume in SZ-100-P than SZ-50-P and might due to greater crystallinity in the latter than former which makes the channels to be more opened after the treatment. The hysteresis loop shown in **Fig. S3**, reveals that at small relative pressure up to 0.5 for both parent samples, the

isotherm displays no distinct hysteresis and look like a type II isotherm which is a characteristic of largely microporous sample. There is a remarkable adsorption at higher relative pressure in all the samples. Ostensibly, for all the range of relative pressures, desilicated-dealuminated samples show higher uptake which is an indication of increase in porosity. Towards p/po = 1, the less steep nature of the curves in the modified SSZ-54 indicates increase in pore volume than in the parent SSZ-54 samples.

Table 4-5 Physicochemical properties of the samples (error = ±2%)

Sample code	S_{BET} [a]	S_{mic} [b]	S_{meso} [c]	V_{total} [d]	V_{mic} [e]	HF [f]
SZ-50-P	231	176	55	0.183	0.0731	0.095
SZ-100-P	162	98	65	0.179	0.0422	0.094
SZ-50-DSA	268	158	110	0.2685	0.0790	0.121
SZ-100-DSA	295	143	152	0.3483	0.0718	0.106

a,b, c, d, and e are as in **Table 4-2**

f: Hierarchical factor, $(S_{meso}/S_{BET}) * (V_{mic}/V_{total})$

4.2.2 Products breakdown

The catalytic activity of the parent and desilicated-dealuminated SSZ-54 samples with Si/Al ratios of 50 and 100 is displayed in **Fig.4-16**. The explanation for the catalytic activity of the parent SSZ-54 samples has been given in section 4.1.2. From the Fig. 4-16, we

observed considerable increase in overall conversion from the parent SSZ-54 samples to the desilicated-dealuminated samples irrespective of the Si/Al ratio.

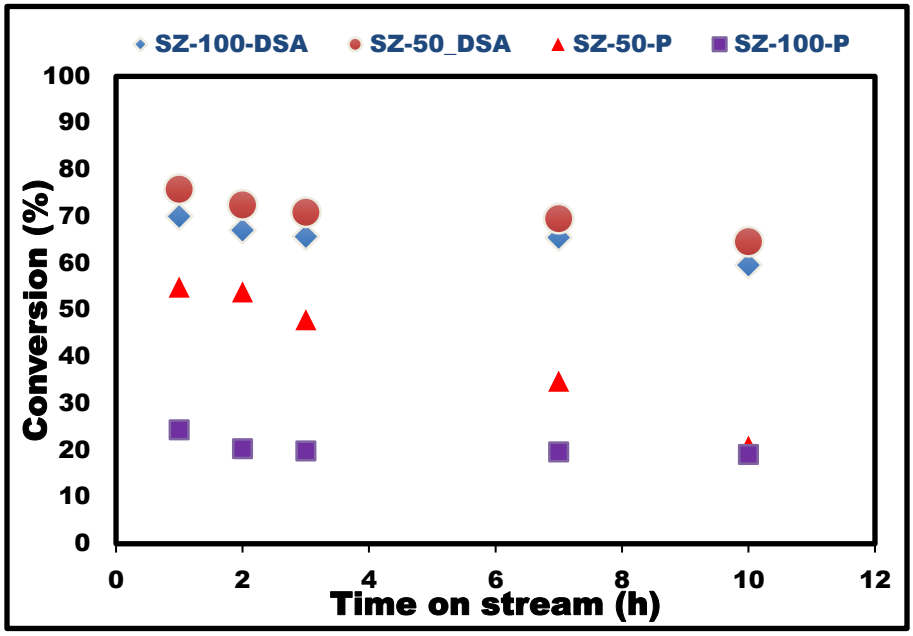

Figure 4-16 Conversion of n-hexane at different TOS for SZ-50 samples and SZ-100 samples at 650 °C. P indicates parent samples while DSA represents desilicated-dealuminated samples.

Considering the desilicated-delauminated samples, SSZ-50-DSA showed higher catalytic conversion than SZ-100-DSA. Although, SZ-100-DSA has higher surface area than SZ-50-DSA, the higher conversion ability exhibited by the latter is credited to higher micropore area where the acid sites needed for the reaction are located. The influence of micropores in zeolitic materials is also expressed by hierarchical factor (HF) which illustrates the degree of access to the active sites [122]. And from **Table 4-5**, SZ-50-DSA clearly has higher HF than SZ-100-DSA, hence, it displayed higher catalytic conversion. Besides, compared to the parent samples, treated SSZ-54 samples have displayed higher catalytic stability. This is illustrated from the flat-shaped activity curves of both SZ-50-DSA and SZ-100-DSA as seen in **Fig. 4-16**. The rational is because of the increase in

mesoporosity owing to influence of acid and alkaline treatments which enhances easy passage of products after the reaction and reduces coke formation.

We also observed very high total yield of olefins (**Fig. 4-17**) in all the samples though the yield decreases in the order SZ-50-DSA> SZ-100-DSA > SZ-50-P > SZ-100-P. The reason for this order observed is because increased Brønsted acidity favours production of more olefin [113]. High yield of olefin recorded in all the SSZ-54 samples (as compared to other reportedly active zeolites) is due to prevalence of monomolecular cracking over classical cracking [87]. However, the yield of olefins as well as that of paraffin, irrespective of the samples considered kept reducing with prolonged time on stream. This is summarized in Fig. S4, and can be ascribed to dependence of selectivity on conversion which kept reducing with time through coke formation and blocking of acid sites.

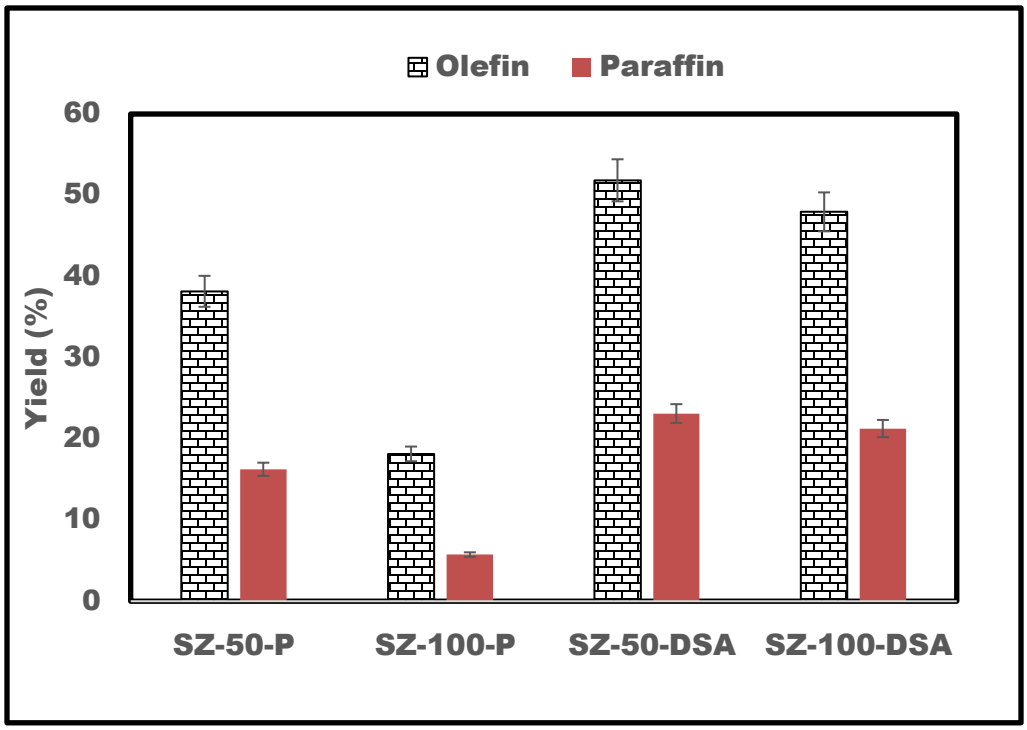

Figure 4-17 Yields of total olefin and paraffin for all the samples at 650 ºC at 1 h time on stream (C2=, C3= and C4= constitute olefin while paraffin is composed of C1-C5)

The yield recorded in these SSZ-54 zeolites is on the high side when compared with other highly reported zeolite such as ZSM-5. The instance is the report by Mochizuki *et al.* [89], the highest yield of all the olefins combined is about 55 % (our SSZ-54 has 51%) at 923 K with Si/Al of 50. It is worthy to note that nano-crystals and almost 10-fold of our W/F were used before they could achieve that.

From the results presented in **Fig. 4-17** above, SZ-50-DSA shows the best result taking yield and conversion into cognizance. Hence, we sought to study the effect of temperature on the cracking of n-hexane over SZ-50-DSA sample. **Figure 4-18** shows the result of cracking of n-hexane over SZ-50-DSA at different temperatures range between 500-650 ^{o}C and **Table 4-6** shows the products distribution alongside temperature of reaction, at 1 h time on stream. We observed noticeable increase in the conversion of n-hexane with increase in temperature of reaction. For instance, at 1 h time on stream, the conversion recorded were 11.86%, 35.38%, 58.72% and 75.87% respectively for 500, 550, 600 and 650 ^{o}C. This observed trend was noticed irrespective of time of the reaction considered (see Fig. S5).

Table 4-6 Conversion and yields of light olefins with other products at 1 h time on stream for SZ-50-DSA.

T (^{o}C)	**Conversion (%)**	**Light olefins yield (%)**			**Total Olefins (%)**	**BTX**	**Paraffins yield (%)**	**P/E**
		C2=	C3=	C4=				
500	11.86	0.41	4.17	2.92	7.50	0.10	4.26	10.17
550	35.38	2.00	12.8	6.24	21.04	3.69	10.64	6.40
600	58.72	5.81	23.62	9.40	38.83	0.45	19.44	4.06
650	75.87	12.51	31.93	7.22	51.66	1.10	23.11	2.55

T = temperature of reaction, C2= ethylene, C3= propylene and C4= butylene, P/E= C3=/C2=

Furthermore, though there is an increase in selectivity of both ethene and propylene with increase in temperature (Fig.4-18), ethene selectivity increased at a faster rate than that of propylene. These findings illustrates that ethene is readily formed via energetically unfavourable primary carbenium ions which forms at high temperature [117]. The formation of this primary carbenium ions at elevated temperatures that gives rise to ethene formation is independent of the mechanism of the reaction. Therefore, it can be said that formation of ethylene is not only limited to cracking reaction but also by successive reaction of other hydrocarbon fractions from C4 and above. This, then results in increase in selectivity of ethene as conversion increases. Hence, we observed decrease in P/E as the temperature of the reaction increased (Fig. 4-18).

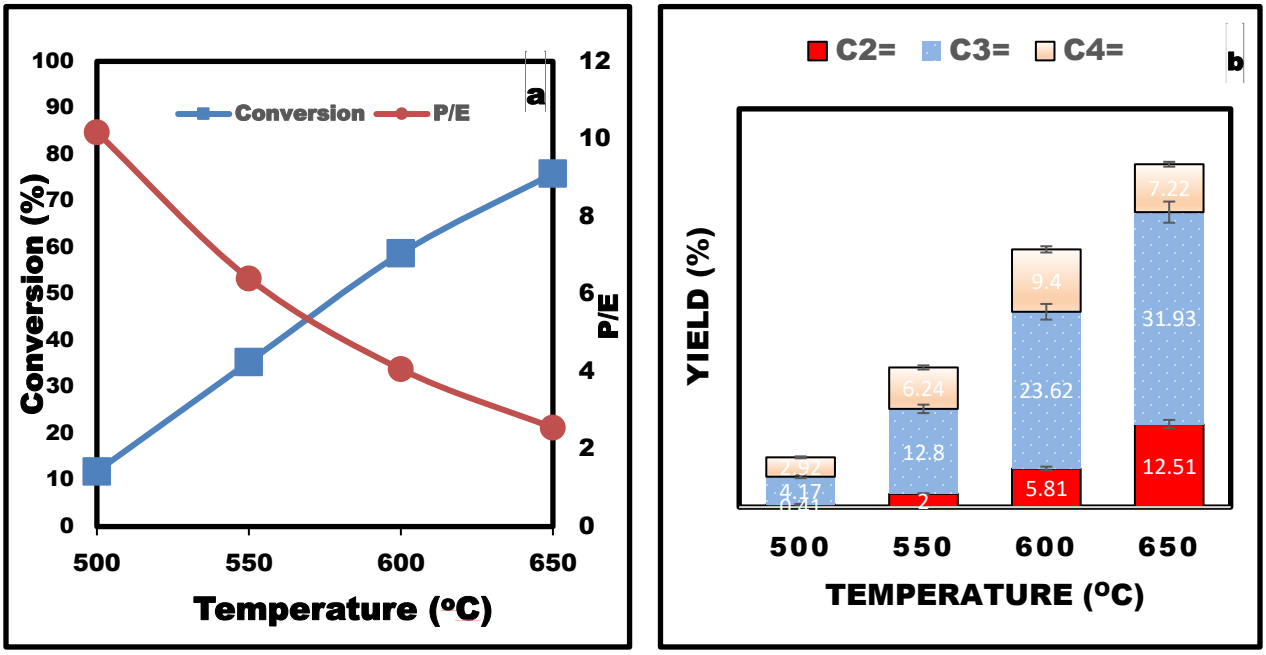

Figure 4-18 Conversion and product selectivity at different temperatures for SZ-50-DSA.

4.2.3 Evaluation of cracking ability and determination of activation energy

Cracking of hexane has been reported to be a first order reaction, hence we evaluated the cracking ability of SZ-50-DSA by the determination of reaction rate constant, k(s^{-1}) using

$$k = f * In(1-\varepsilon) * \frac{d}{m\ x\ 60} - - - - - - - - - - - - - - - - (4)$$

With the variables f, ε, d, and m stand for volumetric flow rate (cm^3/min), conversion, bulk density (0.55 g/cm^3 for n-hexane) and mass of the catalyst (g), respectively [84]. The reaction rate constant was used in the determination of activation energy using the Arrhenius equation in equation (5);

$$In\ k = -\frac{Ea}{RT} + In\ A - - - - - - - - - - - - (5)$$

Table 4-7 Rate constant for cracking of hexane over SZ-50-DSA at different temperatures at 1 h TOS.

T (ºC)	1/T (K^{-1})	ε	K	ln k
500	0.001294	0.1186	1.90944E-06	-13.1687
550	0.001215	0.3538	6.60427E-06	-11.9278
600	0.001145	0.5872	1.33825E-05	-11.2216
650	0.001083	0.75867	2.15015E-05	-10.7474

The rate constants for the cracking of n-hexane were measured over temperature ranges from 500-650 ºC and the result is presented in **Table 4-7**.

The measurement for each temperature considered was done with a fresh catalyst in a bid to eliminate distortion in the results due to ageing effect. Ageing effect is discussed elsewhere and it is not part of our objectives here [84]. **Figure 4-19** shows the Arrhenius plot of SZ-50-DSA over the range of temperature considered. Therein, from the extraction done using the slope of the graph, the activation energy was calculated to be 95.43 kJ/mol.

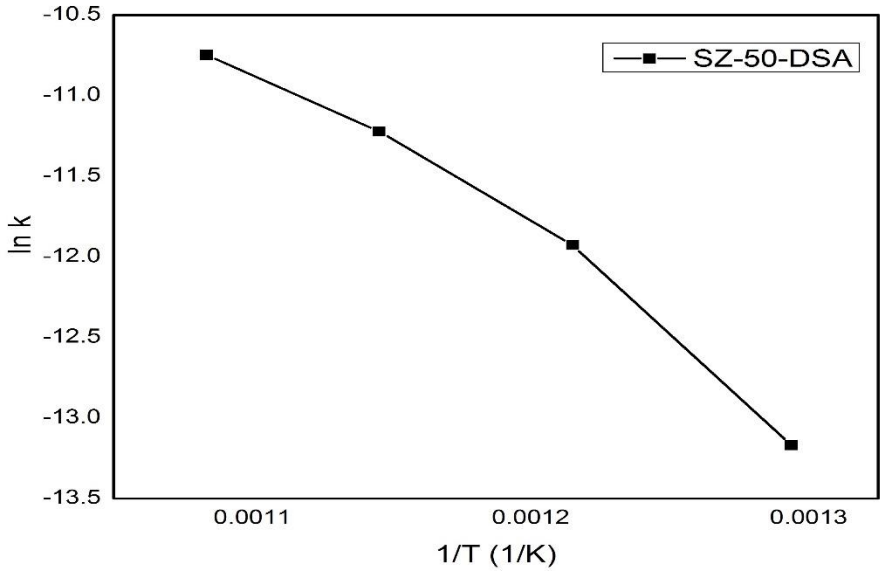

Figure 4-19 Arrhenius plot for SZ-50-DSA at various temperatures.

By comparison, higher activation energies between 108-121 kJ/mol were reported from cracking of hexane over modified ZSM-5 catalysts even though similar range of temperature was used. The lower activation energy obtained with SSZ-54 zeolite is as a result of higher acidity than that of ZSM-5 samples reported by Liu *et al.*[84] and it underscores the relative performance of both catalyst with hexane cracking. This lower activation energy should translate to high energy efficiency using SSZ-54 in an industrial set up and represent lower energy investment which is desirable.

4.3 Microwave-assisted SSZ-54 synthesis and its application in hexane cracking.

Details of reaction conditions and reagents.

Volumetric flow rate of n-hexane = 0.02 ml

Weight of the catalyst = 0.2 g

Temperature of the reaction = 650 ^{o}C

The naming system adopted is x-y where x represents Si/Al and y represents the condition whether parent, P, desilicated DS and DSA stands for desilicated-dealuminated. For example, 100-P represents the parent sample of SSZ-54 synthesized with Si/Al of 100.

4.3.1 Characterization of the samples

The identification of the sample phase was determined with XRD. From **Fig. 4-20**, the peaks obtained are consistent with the SSZ-54 peaks reported by Burton *et al.* [1]. After both the alkaline and acid treatments, all the peaks assigned to SSZ-54 were still intact. The intensities of the peaks also confirmed that crystallinity of the samples was not destroyed by the acid and alkaline treatments. Even, the intensity of the SSZ-54 peaks in the three samples showed that crystallinity increased after treatment in the order DSA-50>

DS-50>P-50. This invariably indicates that structural collapse did not take place by the treatments.

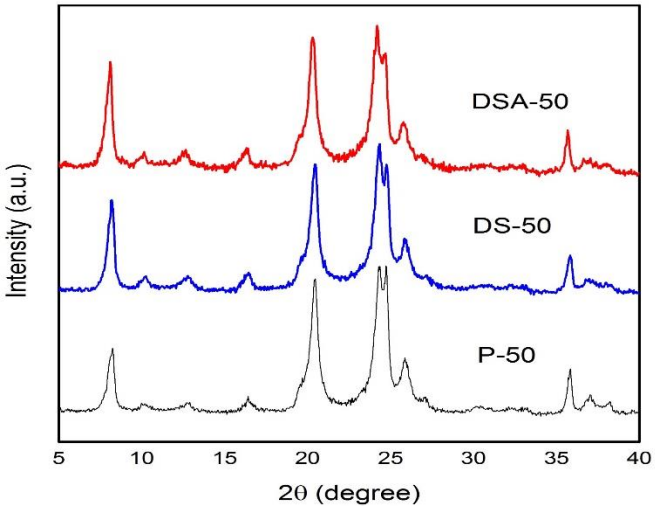

Figure 4-20 XRD spectra of the parent sample and the hierarchical samples

Scanning electron microscopy reveals that the sample is made of needle-like structures (**Fig. 4-21 a and d**), [vide supra]

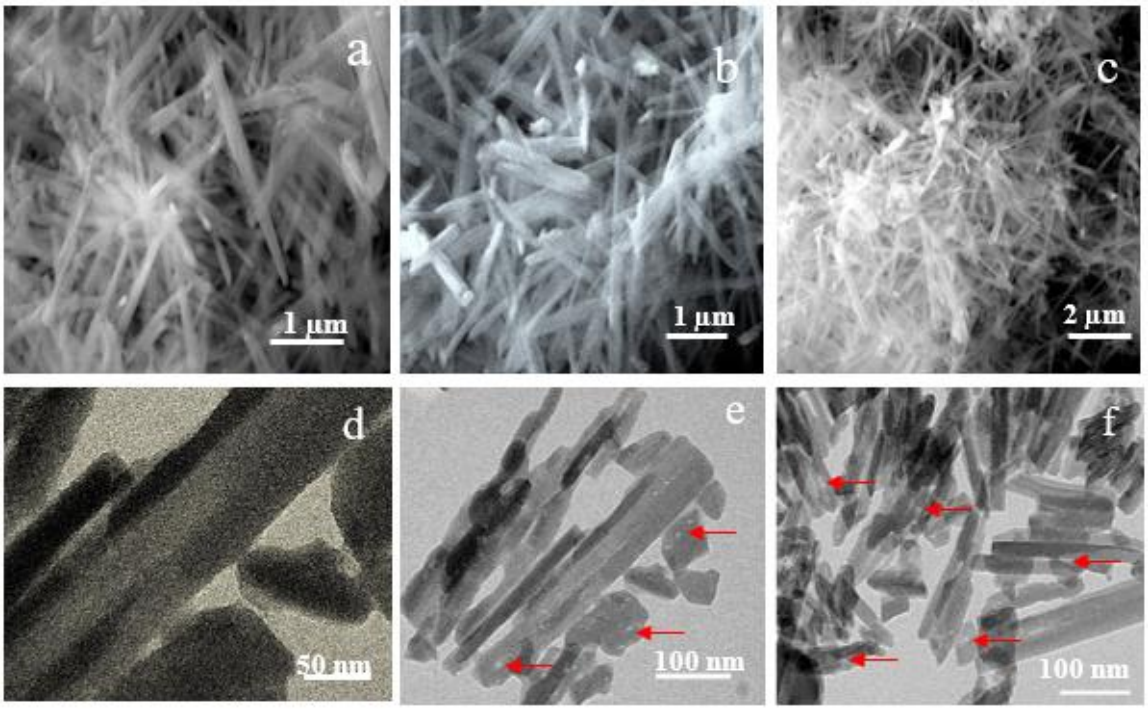

Figure 4-21 SEM and TEM images of parent and hierarchical SSZ-54. (a,d) Parent sample (b,e) desilicated sample and (c,f) desilicated-dealuminated sample. Top images represent SEM micrographs while the bottom images show those of TEM

However, there is little morphological change after desilication and dealumination in that the external surface of the rods are now coarser (Fig. 4-21 b and c). This underscores the role of the alkaline chemicals in removing loose and amorphous particles on the surface of the catalyst. In addition, the presence of mesoporosity is clearly seen by the creation of spherical pores made after desilication (Fig. 4-21 e). These are further procreated by acidic treatment in mild dealumination process (Fig. 4-21 f). Besides, the acid and alkaline treatments were also successful in disengaging the aggregates which might probably improve the surface area of the samples.

Nitrogen isotherm shown in **Fig. 4-22** displays low uptake at low relative pressure, p/po < 0.55, for the parent SSZ-54, which is an indication of microporosity typical of MTT and TON frameworks [106], [119]. At medium to high relative pressures, the uptake increases as shown by the hysteresis loop in **Fig. 4-22** which is illustrative of intercrystallite void in the aggregated rods [115] . Upon alkaline treatment in TEAOH and NaOH, DS-50 shows an enhanced uptake which illustrates an increase in mesoporosity. This happens without loss of microporosity (**Table 4-8**).

Table 4-8 Textural properties of the samples (error = ±0.5-1.4%)

Sample code	S_{BET} [a]	S_{micro} [b]	S_{meso} [c]	V_{total} [d]	V_{micro} [e]	Average pore size[f]
P-50	224	162	62	0.190	0.068	33.94
DS-50	246	166	80	0.241	0.070	39.08
DA-50	274	176	98	0.249	0.073	36.34

In fact, mesopore volume increased by approx. 29 %. Same can be said about micropore volume and total pore volume as it is seen from **Fig. 4-22** where the uptake in DS-50 is higher than that in P-50. This increase in textural properties by desilication can be ascribed to regular arrangement of silicon in the framework. In a similar vein to P-50, at low relative of range 0< p/po<0.4, there is no distinct hysteresis in the curve shown. This observation takes place at earlier relative pressures than in the parent sample. The same trend was also observed in the DSA-50 where the uptake at middle to high relative pressure increased by almost one-half of the parent sample. Considering the surface area, both mesopore and micropore areas got improved by alkaline and acid treatments. The mesopore area increased by 28 % from 62 m^2/g (P) to 80 m^2/g (DS) and finally by approx. 23 % to 98 m^2/g (DSA) (see Table 4-8).

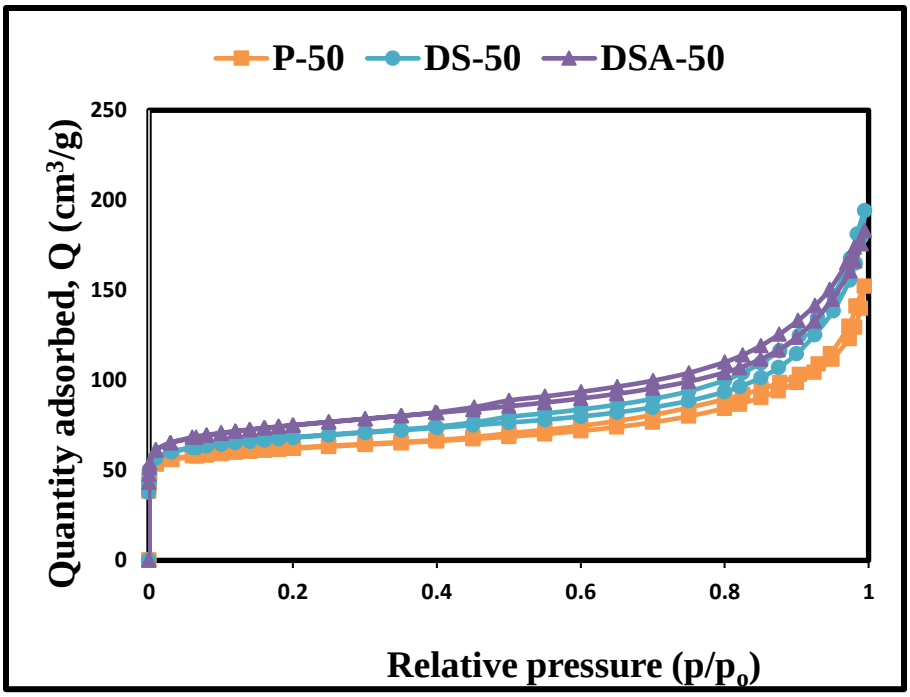

Figure 4-22 Surface area measurements of the samples

FT-IR spectra of adsorbed pyridine onto the parent (untreated) SSZ-54 sample (P-50) together with that of alkaline and acid treated samples (DS-50 and DSA-50, respectively) are measured at different temperatures of 150 ^{o}C, 250 ^{o}C and 350 ^{o}C and the summary is given in **Table 4-9.**

Considering each sample discretely, using the calculated areas of each intensity from consideration of extinction coefficient saw reduction in the number of both Brønsted and Lewis acid sites as the temperature increases though Brønsted acid sites got reduced more than Lewis acid sites. This indicates the presence of stronger Lewis acid sites than Brønsted. Alkaline treatment brought about an increase in number of Lewis acid sites to almost two-folds at all the temperatures of adsorption considered. Brønsted acid site also increased.

Table 4-9 FTIR analysis of the samples (error = ±0.5%)

	B[a]	L[a]	B+L	B/L	T[b]
P-50	124.18	37.22	161.40	3.34	150 ^{o}C
	85.56	28.34	113.90	3.02	250 ^{o}C
	71.72	24.03	95.75	2.98	350 ^{o}C
DS-50	188.46	69.96	258.42	2.69	150 ^{o}C
	138.17	59.22	197.39	2.33	250 ^{o}C
	96.33	44.93	141.26	2.14	350 ^{o}C
DSA-50	180.54	40.97	221.51	4.41	150 ^{o}C
	124.22	31.94	156.17	3.89	250 ^{o}C
	91.45	26.90	118.35	3.40	350 ^{o}C

a: From the calculation using extinction coefficient.

b: Temperature of adsorption

These led to increase in total amount of acid sites. This is consistent with the observation that the number of residual surface aluminium increases as silicon is selectively removed from a siliceous sample resulting in decreasing Si/Al [83]. Also, there are stacked faults in intergrowth materials which might pose hindrance to accessibility of acid sites, these blockades are opened when silicon is selectively removed, access to more acid sites is thus increased. Hence, total acid site increases. Dealumination by acid treatment reduced both Brønsted and Lewis acid sites as well as total acid sites. This is rationalized to be reduction in strong acid sites as extra surface aluminium got removed.

4.3.2 Cracking result

A temperature of 923 K was adopted in the cracking of n-hexane. The results are presented in **Table 4-10** for conversion of n-hexane, selectivity to olefins, paraffin and BTX.

From Table 4-10, conversion obtained in each of the sample decreased with increasing time on stream. This is resulted from deposition of coking materials on the pore and along the channels of the samples. This takes place as reaction progresses. However, generally, conversion decreases in the order DSA-50 > DS-50 > P-50 for all the time on stream. This trend recorded is related to the textural properties of each sample. DSA possessed the best textural properties among the three samples- highest surface area, mesopore area, micropore area and total pore volume. All these made the accessibility to acid sites easiest in DSA-50 sample and hence cracking ability improves.

It is also important to state that the lowest conversion exhibited by P-50 is not only because of lowest surface area but also small quantity of Brønsted acid sites (**Table 4-9 above)** [117]. Moreover, in samples P-50 and DS-50, conversion drops progressively during the reaction while we observed stable conversion during the early hours of reaction before gradual reduction, in the case of DSA-50 (Fig. S6). This depicts slow rate of deactivation in DSA-50 and could be because of large mesopore volume which reduces pore blockage by offering lower diffusion resistance.

Table 4-10 Conversion and selectivity to C1-C4= at different time on stream (error = ±2%).

Sample code	TOS (h)	Conversion (%)	C2=	C3=	C4=	Total paraffin (%)	BTX
P-50	1	72.32	24.24	37.59	7.28	27.12	3.64
	3	65.08	18.57	38.29	13.52	29.62	2.96
	7	49.24	16.15	38.35	13.52	29.38	2.36
	10	39.22	15.82	37.83	15.35	28.87	1.81
DS-50	1	76.58	22.83	36.96	7.58	28.94	3.55
	3	73.50	19.27	37.36	9.46	30.68	3.11
	7	61.80	17.31	37.37	9.27	32.88	3.05
	10	52.96	16.91	37.54	9.25	33.12	3.05
DSA-50	1	90.25	20.74	40.30	9.12	28.36	1.38
	3	89.35	19.73	40.08	9.45	28.81	1.81
	7	82.89	17.71	39.89	11.12	29.40	1.76
	10	70.40	14.06	39.64	13.73	30.91	1.48

Total olefin = C1-C4.

The observed selectivity to paraffin in all the samples tested are approximately less than 30% while the selectivity to BTX was kept to as low as 3%. It should be stressed that DSA-50 produced lowest selectivity to BTX. This is because of the highest ratio of B/L observed in DSA-50 as more Brønsted to Lewis ratio suppresses paraffin formation [117]. In addition, all the samples showed high selectivity to light olefins to almost 2.5 times the selectivity to paraffin. This is due to prevalence of monomolecular cracking over bimolecular cracking [87].

Specifically, DSA-50 showed highest olefin selectivity throughout the 10 h time on stream considered due to its possession of the highest amount of Brønsted acid site in all the samples tested. This is due to increased olefin selectivity with Bronsted acidity. We also observed that in each of the samples, the selectivity to light olefins decreased with simultaneous increase in paraffin selectivity with increasing time on stream. The observed decrease could be ascribed to a reduction in the available acid sites for alkanes-to-olefins conversion because of production and deposition of coking materials on the acid sites.

In addition, increasing time on stream favours the production of more paraffin as it is a more stable group than olefin during cracking reaction [123]. DS-50 also showed the highest selectivity to paraffin while P-50 displayed the lowest. This is related to the amount of Lewis acid site in DS-50 which promotes hydride transfer and ultimately alkane formation [117]. In addition, pore diameter of the crystals (in this case DS-50 has the largest) is a great contributor to the favourable formation of alkanes [87]. The breakdown of each of the light olefins and paraffin selectivity at different time on stream is presented in **Table 4-10 above.**

Although ZSM-5 is one of the most active zeolites going by its high activity. Interestingly to our study, its olefin selectivity is not quite satisfactory and this makes our study on SSZ-54 a worthy endeavour. SSZ-54 being studied, under the same reaction condition, all the samples have shown higher olefin selectivity and most importantly, greater P/E ratio when compared with ZSM-5 reported elsewhere [124] though the Si/Al ratios are not the same in all samples. A very important reason for this observation is because of suppression of bimolecular cracking in SSZ-54 which is dominant in 3D zeolites [120].

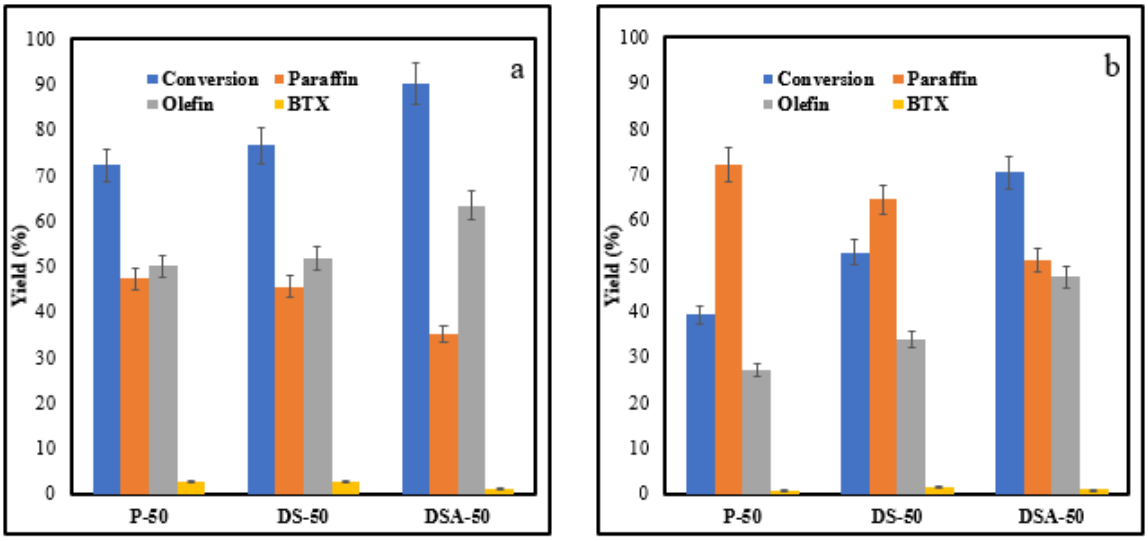

Figure 4-23 Yields of paraffin, olefin and BTX for P-50, DS-50 and DSA-50. (a) Illustrates the parameters at 1 h TOS (b) shows the parameters at 10 h TOS

Considering the yield of the products, during the first hour of reaction, total yields of the olefins were 50%, 51% and 73% for P-50, DS-50 and DSA-50 respectively (**Fig. 4-23**). These kept reducing with prolong exposure in the reaction and it is because of production and deposition of coking materials which blocks the pore of the zeolite and prevents proper desorption of the products from the zeolite channels. Even though the conversion in our SSZ-54 is not as high as reported in ZSM-5, it has impeccable quality of being a viable challenger when its study is fully established.

4.4 Hydrothermal synthesis versus microwave-assisted synthesis: comparison between individual cracking ability.

The cracking ability of the samples synthesized using conventional hydrothermal oven and microwave reactor is presented in Fig. 4-24 below for samples with Si/Al of 50.

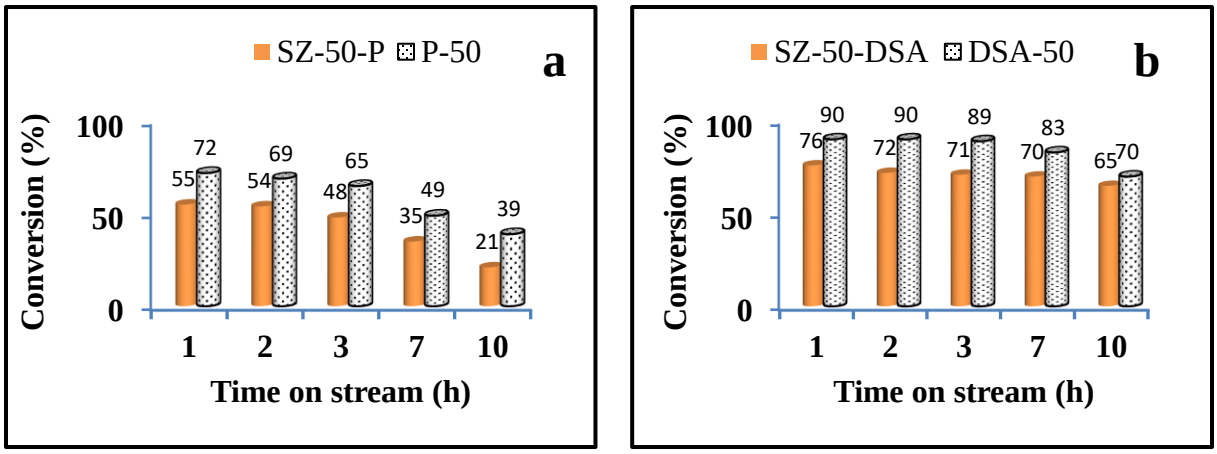

Figure 4-24 Catalytic activity of hydrothermal and microwave-assisted samples at Si/Al = 50

From the results presented, irrespective of the nature of the samples (parent or hierarchical), samples synthesized using microwave displayed catalytic activity than those from hydrothermal oven. This is connected to better physicochemical properties of the former as explained in the earlier sections. In addition, alkali-acid treatment improves the activity of the sample thereby leading to higher catalytic conversion which translates to better yield of olefins.

In summary, within the limits of our systems of studies here, microwave-assisted procedure offers some better desirable qualities over conventional hydrothermal method both in the ease and time of synthesis of the catalysts, morphological and physicochemical properties and the catalytic performance of the samples.

CHAPTER 5

CONCLUSIONS AND RECOMMENDATIONS

5.1 Conclusions

The present investigation aims at synthesizing a highly active, highly stable hybrid zeolite (SSZ-54) catalyst with the best morphology and surface acidity for n-hexane cracking. It was envisioned that this could be achieved by proper combination of OSDAs and apt selection of acid and alkali for post treatment process. Also, studies show that moderate acidity is needed for this reaction, hence we varied Si/Al ratio of the catalysts. In line with this, it became necessary to be able to characterize the catalyst with XRD, SEM, FTIR (pyridine), TEM and ammonia TPD and to evaluate the performance in a fixed bed reactor. And from the results obtained and reported in this thesis, the following are the conclusions drawn:

1. SSZ-54 proved to be a better catalyst than its component frameworks (MTT and TON) in terms of catalytic activity and olefins selectivity.
2. Microwave-synthesized samples showed better crystallinity and physicochemical properties than the samples synthesized with hydrothermal reactor.
3. Physicochemical and sorption properties of the samples were improved by alkali-acid treatment and ultimately improved catalytic performance.

5.2 Recommendations

The study of the synthesis and catalytic performance of SSZ-54 zeolite are still in infant stage and from the results reported here in this thesis, the following recommendations are offered for future studies in this area:

1. To test various sources of aluminum or silicon and proper combination of the OSDAs to obtain the optimum combination of synthesis parameters to achieve morphologically-best SSZ-54 zeolite.
2. Hierarchical SSZ-54 should be produced with top-down approach to preserve the original Si/Al of the zeolite.
3. Other range of Si/Al ratios should be produced to have proper understanding of the acidity of SSZ-54 and thus increases the conversion of hexane.
4. Incorporation of SSZ-54 with surface promoters such as various metals with a view of having enhanced selectivity to light olefins.
5. To conduct catalytic reaction with SSZ-54 under wide variations of reaction parameters such temperature and W/F values.
6. To propose a detailed kinetic model that will take care of every reaction to be able to simulate large reactors.
7. Application of SSZ-54 in other catalytic areas should be explored.

Appendices

Appendix A

The conversion of hexane (C), selectivity and yield to any of the products, given respectively as S_i and Y_i are shown in the equations (1)-(3) below;

$$C = \frac{moles\ of\ hexane\ reacted}{moles\ of\ hexane\ fed} * 100\% \quad (1)$$

$$S_i = \frac{moles\ of\ product\ i}{moles\ of\ hexane\ reacted} * 100\% \quad (2)$$

$$Y_i. = (C * S_i) \quad (3)$$

Reaction rate constant was calculated using equation (4) and equation (5) gave the activation energy

$$k = f * In(1 - \varepsilon) * \frac{d}{m\ x\ 60} \quad (4)$$

$$In\ k = -\frac{Ea}{RT} + In\ A \quad (5)$$

Where f, ε, d, and m stand for volumetric flow rate (cm^3/min), conversion, bulk density (0.55 g/cm^3 for n-hexane) and mass of the catalyst (g), respectively. Also, in equation (5), k = reaction rates constant 9 (s^{-1}), E_a = activation energy (kJ/mol), T = temperature (K) and R= gas constant (J/mol.K).

Appendix B

Supporting Information

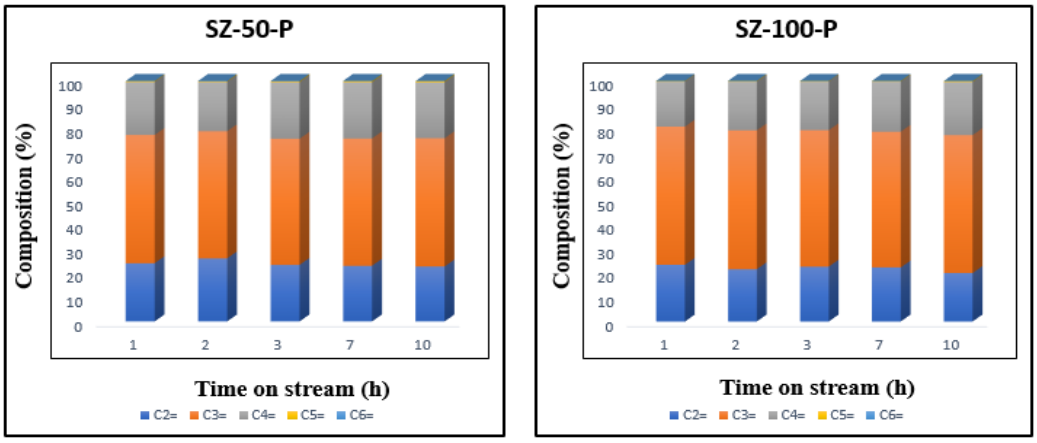

Fig. S1: Olefin composition for Z-50 and Z-100.

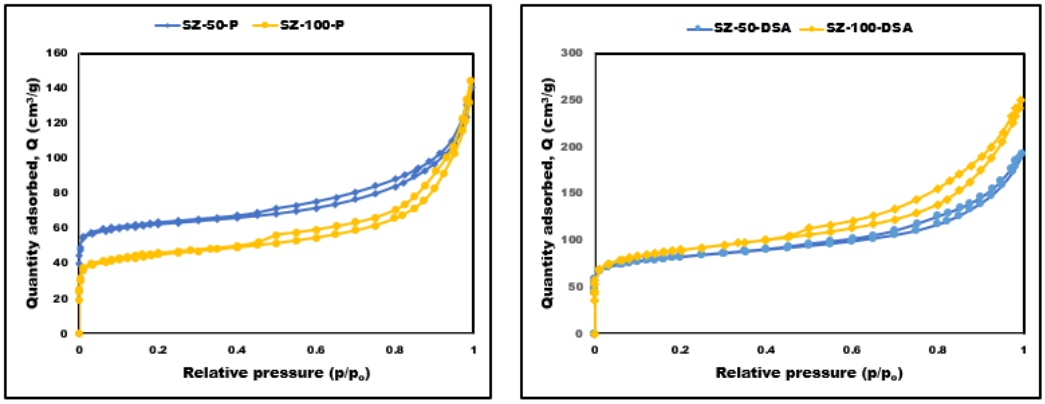

Figure S2: Surface area measurement of the parent and hierarchical samples.

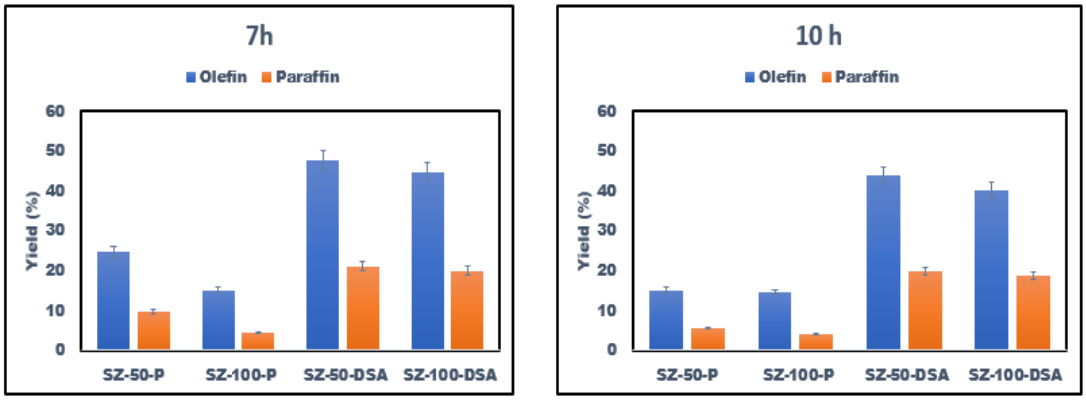

Figure S3: Total yields of olefin and paraffin for n-hexane cracking at 923 K for 7h and 10 h time on stream. Yield of olefins and paraffin decreased with increasing TOS. (C2=, C3= and C4= constitute olefin while paraffin is composed of C1-C5)

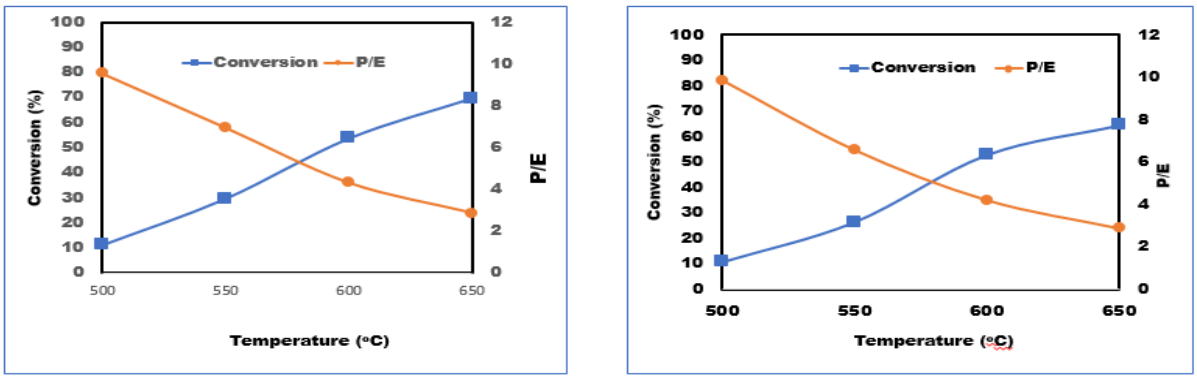

Fig S4 : Conversion of n-hexane and P/E versus temperature of reaction at 7 h and 10 h TOS for SZ-50-DSA. Decrease in temperature, apparently, decreases the conversion of hexane and increases P/E.

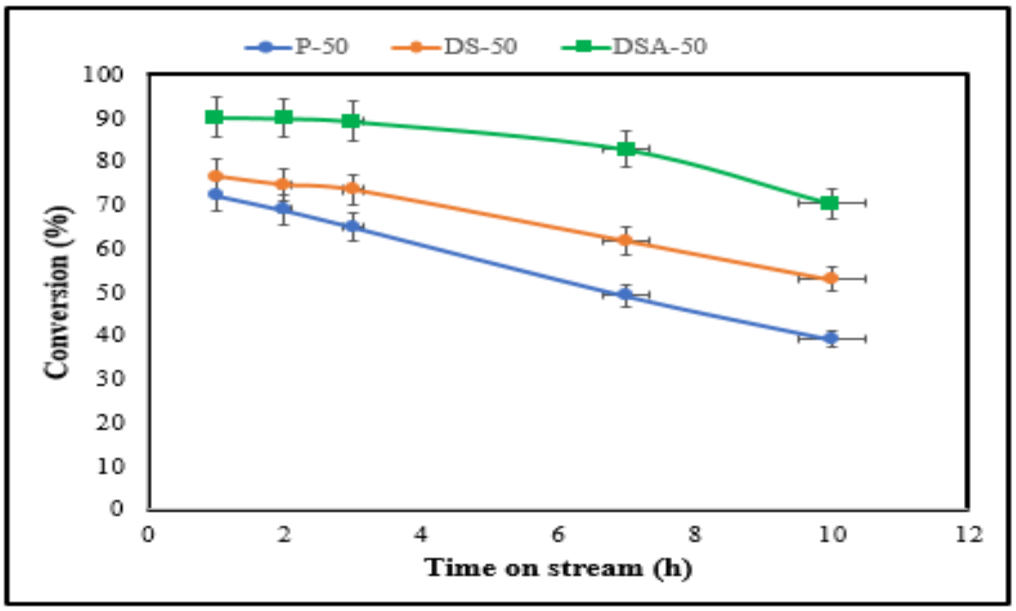

Fig S5: Comparison of conversion for P-50, DS-50 and DSA-50 at different time on stream (h). DSA-50 is the most stable catalyst of the three samples. The parent sample, ostensibly, deactivates faster than others.

Catalytic Evaluation in a fixed bed reactor

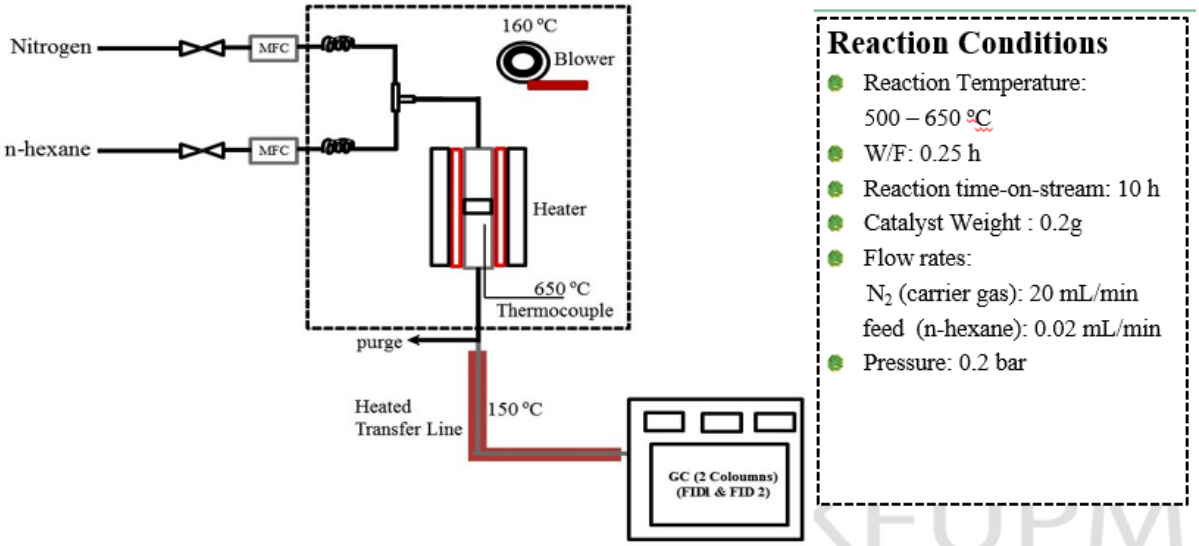

Fig. S6: Fixed bed reactor set up

References

[1] A. W. Burton, S. I. Zones, T. Rea, and I. Y. Chan, "Preparation and characterization of SSZ-54: A family of MTT/TON intergrowth materials," *Microporous Mesoporous Mater.*, vol. 132, no. 1–2, pp. 54–59, 2010.

[2] B. Marler, P. Daniels, and J. Sañé i Muné, "Synthesis and structure of RUB-35, a disordered material of the EUO-NES-NON family," *Microporous Mesoporous Mater.*, vol. 64, no. 1–3, pp. 185–201, 2003.

[3] J. a. Lawton, S. L. Lawton, M. E. Leonowicz, and M. K. Rubin, "The framework topology of zeolite MCM-22," *Stud. Surf. Sci. Catal.*, vol. 98, no. C, pp. 250–251, 1995.

[4] J. M. Newsam, M. M. J. Treacy, W. T. Koetsier, and C. B. D. Gruyter, "Structural Characterization of Zeolite Beta," *Proc. R. Soc. A Math. Phys. Eng. Sci.*, vol. 420, no. 1859, pp. 375–405, 1988.

[5] Y. Bouizi, L. Rouleau, and V. P. Valtchev, "Bi-phase MOR/MFI-type zeolite core–shell composite," *Microporous Mesoporous Mater.*, vol. 91, no. 1–3, pp. 70–77, 2006.

[6] M. S. Francesconi, Z. E. López, D. Uzcátegui, G. González, J. C. Hernández, A. Uzcátegui, A. Loaiza, and F. E. Imbert, "MFI/MEL intergrowth and its effect on n-decane cracking," *Catal. Today*, vol. 107–108, pp. 809–815, 2005.

[7] A. M. Goossens, B. H. Wouters, P. J. Grobet, V. Buschmann, L. Fiermans, and J. A. Martens, "Synthesis and Characterization of Epitaxial FAU-on-EMT Zeolite Overgrowth Materials," 2001.

[8] R. L. Smith, S. Svelle, P. del Campo, T. Fuglerud, B. Arstad, A. Lind, S. Chavan, M. P. Attfield, D. Akporiaye, and M. W. Anderson, "CHA/AEI intergrowth materials as catalysts for the Methanol-to-Olefins process," *Appl. Catal. A Gen.*, vol. 505, pp. 1–7, 2015.

[9] L. Zhang, S. Liu, S. Xie, and L. Xu, "Organic template-free synthesis of ZSM-5/ZSM-11 co-crystalline zeolite," *Microporous Mesoporous Mater.*, vol. 147, no. 1, pp. 117–126, 2012.

[10] G. González, C. S. González, W. Stracke, R. Reichelt, and L. García, "New zeolite topologies based on intergrowths of FAU/EMT systems," *Microporous Mesoporous Mater.*, vol. 101, no. 1–2, pp. 30–42, 2007.

[11] B. Mihailova, V. Valtchev, S. Mintova, a-C. Faust, N. Petkov, and T. Bein, "Interlayer stacking disorder in zeolite beta family: a Raman spectroscopic study.," *Phys. Chem. Chem. Phys.*, vol. 7, no. 14, pp. 2756–2763, 2005.

[12] Y.-S. Ooi, R. Zakaria, A. R. Mohamed, and S. Bhatia, “Synthesis of composite material MCM-41/Beta and its catalytic performance in waste used palm oil cracking,” *Appl. Catal. A Gen.*, vol. 274, no. 1–2, pp. 15–23, 2004.

[13] S. I. Zones and S. J. Hwang, “Synthesis of high silica zeolites using a mixed quaternary ammonium cation, amine approach: Discovery of zeolite SSZ-47,” *Chem. Mater.*, vol. 14, no. 1, pp. 313–320, 2002.

[14] S. Elomari and S. Zones, “Zeolite SSZ-57 composition of matter and synthesis thereof,” *US Pat. 6,544,495*, vol. 2, no. 12, pp. 1–9, 2003.

[15] S. Zanardi, R. Millini, F. Frigerio, A. Belloni, G. Cruciani, G. Bellussi, A. Carati, C. Rizzo, and E. Montanari, “ERS-18: A new member of the NON–EUO–NES zeolite family,” *Microporous Mesoporous Mater.*, vol. 143, no. 1, pp. 6–13, 2011.

[16] S. Xie, S. Liu, Y. Liu, X. Li, W. Zhang, and L. Xu, “Synthesis and characterization of MCM-49/ZSM-35 composite zeolites in the hexamethyleneimine and cyclohexamine system,” *Microporous Mesoporous Mater.*, vol. 121, no. 1–3, pp. 166–172, 2009.

[17] L. a Villaescusa, W. Zhou, R. E. Morris, and P. a Barrett, “Synthesis{,} characterization and control of faulting in STF/SFF topologies{,} a new family of intergrowth zeolites,” *J. Mater. Chem.*, vol. 14, no. 13, pp. 1982–1987, 2004.

[18] L. Hu, S. Xie, Q. Wang, S. Liu, and L. Xu, “Phase selection controlled by sodium ions in the synthesis of FAU/LTA composite zeolite,” *Sci. Technol. Adv. Mater.*, vol. 10, no. 1, p. 15001, 2009.

[19] B. Wang, Z. Tian, P. Li, L. Wang, Y. Xu, W. Qu, H. Ma, Z. Xu, and L. Lin, “Synthesis of ZSM-23/ZSM-22 intergrowth zeolite with a novel dual-template strategy,” *Mater. Res. Bull.*, vol. 44, no. 12, pp. 2258–2261, 2009.

[20] B. Zheng, Y. Wan, W. Yang, F. Ling, H. Xie, X. Fang, and H. Guo, “Mechanism of seeding in hydrothermal synthesis of zeolite Beta with organic structure-directing agent-free gel,” *Chinese J. Catal.*, vol. 35, no. 11, pp. 1800–1810, 2014.

[21] K. Tarach, K. Góra-Marek, J. Tekla, K. Brylewska, J. Datka, K. Mlekodaj, W. Makowski, M. C. Igualada López, J. Martínez Triguero, and F. Rey, “Catalytic cracking performance of alkaline-treated zeolite Beta in the terms of acid sites properties and their accessibility,” *J. Catal.*, vol. 312, pp. 46–57, 2014.

[22] M. Razavian and S. Fatemi, “Synthesis and application of ZSM-5/SAPO-34 and SAPO-34/ZSM-5 composite systems for propylene yield enhancement in propane dehydrogenation process,” *Microporous Mesoporous Mater.*, vol. 201, pp. 176–189, 2015.

[23] H. Zhang and Y. Li, “Preparation and characterization of Beta/MCM-41composite zeolite with a stepwise-distributed pore structure,” *Powder Technol.*, vol. 183, no. 1, pp. 73–78, 2008.

[24] H. Xu, J. Guan, S. Wu, and Q. Kan, “Synthesis of Beta/MCM-41 composite molecular sieve with high hydrothermal stability in static and stirred condition,” *J. Colloid Interface Sci.*, vol. 329, no. 2, pp. 346–350, 2009.

[25] S. Yang and N. P. Evmiridis, “Synthesis and characterization of an offretite/erionite type zeolite,” *Microporous Mater.*, vol. 6, pp. 19–26, 1996.

[26] P. Wang, B. Shen, and J. Gao, “Synthesis of MAZ/ZSM-5 composite from expanded perlite and its catalytic performance in FCC gasoline aromatization,” *Catal. Today*, vol. 125, no. 3–4, pp. 155–162, 2007.

[27] E. de Vos Burchart, J. C. Jansen, and H. van Bekkum, “Ordered overgrowth of zeolite X onto crystals of zeolite A,” *Zeolites*, vol. 9, no. 5, pp. 432–435, 1989.

[28] Z. Xie, Z. Liu, Y. Wang, Q. Yang, L. Xu, and W. Ding, “An overview of recent development in composite catalysts from porous materials for various reactions and processes,” *Int. J. Mol. Sci.*, vol. 11, no. 5, pp. 2152–2187, 2010.

[29] R. L. Smith, W. a. Sławiński, A. Lind, D. S. Wragg, J. H. Cavka, B. Arstad, H. Fjellvåg, M. P. Attfield, D. Akporiaye, and M. W. Anderson, “Nanoporous Intergrowths: How Crystal Growth Dictates Phase Composition and Hierarchical Structure in the CHA/AEI System,” *Chem. Mater.*, vol. 27, no. 12, pp. 4205–4215, 2015.

[30] P. N. R. Vennestrøm, M. Grill, M. Kustova, K. Egeblad, L. F. Lundegaard, F. Joensen, C. H. Christensen, and P. Beato, “Hierarchical ZSM-5 prepared by guanidinium base treatment: Understanding microstructural characteristics and impact on MTG and NH3-SCR catalytic reactions,” *Catal. Today*, vol. 168, no. 1, pp. 71–79, 2011.

[31] S. van Donk, A. H. Janssen, J. H. Bitter, and K. P. de Jong, “Generation, Characterization, and Impact of Mesopores in Zeolite Catalysts,” *Catal. Rev.*, vol. 45, no. 2, pp. 297–319, 2003.

[32] R. Dutartre, L. C. de Ménorval, F. Di Renzo, D. McQueen, F. Fajula, and P. Schulz, “Mesopore formation during steam dealumination of zeolites: influence of initial aluminum content and crystal size,” *Microporous Mater.*, vol. 6, no. 5–6, pp. 311–320, Jul. 1996.

[33] R. J. Pellet, D. G. Casey, H. M. Huang, R. V. Kessler, E. J. Kuhlman, C. L. Oyoung, R. A. Sawicki, and J. R. Ugolini, “Isomerization of n-Butene to Isobutene by Ferrierite and Modified Ferrierite Catalysts,” *J. Catal.*, vol. 157, no. 2, pp. 423–435, Dec. 1995.

[34] K.-H. Lee and B.-H. Ha, “Characterization of mordenites treated by HCl/steam or HF,” *Microporous Mesoporous Mater.*, vol. 23, no. 3–4, pp. 211–219, Aug. 1998.

[35] R. M. Lago, W. O. Haag, R. J. Mikovsky, D. H. Olson, S. D. Hellring, K. D. Schmitt, and G. T. Kerr, “The Nature of the Catalytic Sites in HZSM-5- Activity

Enhancement," 1986, pp. 677–684.

[36] C. Choifeng, J. B. Hall, B. J. Huggins, and R. A. Beyerlein, "Electron Microscope Investigation of Mesopore Formation and Aluminum Migration in USY Catalysts," *J. Catal.*, vol. 140, no. 2, pp. 395–405, Apr. 1993.

[37] Y. Sasaki, T. Suzuki, Y. Takamura, A. Saji, and H. Saka, "Structure Analysis of the Mesopore in Dealuminated Zeolite Y by High Resolution TEM Observation with Slow Scan CCD Camera," *J. Catal.*, vol. 178, no. 1, pp. 94–100, Aug. 1998.

[38] M. Ogura, S. Y. Shinomiya, J. Tateno, Y. Nara, M. Nomura, E. Kikuchi, and M. Matsukata, "Alkali-treatment technique - New method for modification of structural and acid-catalytic properties of ZSM-5 zeolites," *Appl. Catal. A Gen.*, vol. 219, no. 1–2, pp. 33–43, 2001.

[39] G. Nasser, T. Kurniawan, K. Miyake, A. Galadima, Y. Hirota, N. Nishiyama, and O. Muraza, "Dimethyl ether to olefins over dealuminated mordenite (MOR) zeolites derived from natural minerals," *J. Nat. Gas Sci. Eng.*, vol. 28, pp. 566–571, 2016.

[40] T. Biemelt, C. Selzer, F. Schmidt, G. Mondin, A. Seifert, K. Pinkert, S. Spange, T. Gemming, and S. Kaskel, "Hierarchical porous zeolite ZSM-58 derived by desilication and desilication re-assembly," *Microporous Mesoporous Mater.*, vol. 187, pp. 114–124, 2014.

[41] A. Corma, M. J. Díaz-Cabañas, J. Martínez-Triguero, F. Rey, and J. Rius, "A large-cavity zeolite with wide pore windows and potential as an oil refining catalyst.," *Nature*, vol. 418, no. 6897, pp. 514–517, 2002.

[42] D. Goyvaerts, J. A. Martens, P. J. Grobet, and P. A. Jacobs, "Factors Affecting the Formation of Extra-Framework Species and Mesopores During Dealumination of Zeolite Y," 1991, pp. 381–395.

[43] C. S. Triantafillidis, A. G. Vlessidis, and N. P. Evmiridis, "Dealuminated H−Y Zeolites: Influence of the Degree and the Type of Dealumination Method on the Structural and Acidic Characteristics of H−Y Zeolites," *Ind. Eng. Chem. Res.*, vol. 39, no. 2, pp. 307–319, Feb. 2000.

[44] S. Morin, P. Ayrault, N. S. Gnep, and M. Guisnet, "Influence of the framework composition of commerical HFAU zeolites on their activity and selectivity in m-xylene transformation," *Appl. Catal. A Gen.*, vol. 166, no. 2, pp. 281–292, Jan. 1998.

[45] J. Lynch, F. Raatz, and P. Dufresne, "Characterization of the textural properties of dealuminated HY forms," *Zeolites*, vol. 7, no. 4, pp. 333–340, Jul. 1987.

[46] M. Tromp, J. A. van Bokhoven, M. T. Garriga Oostenbrink, J. H. Bitter, K. P. de Jong, and D. C. Koningsberger, "Influence of the Generation of Mesopores on the Hydroisomerization Activity and Selectivity of n-Hexane over Pt/Mordenite," *J. Catal.*, vol. 190, no. 2, pp. 209–214, Mar. 2000.

[47] H. Ajot, J. F. Joly, J. Lynch, F. Raatz, and P. Caullet, “Formation of Secondary Pores in Zeolites During Dealumination: Influence of TheCrystallographic Structure and Of the Si/Al RATIO,” 1991, pp. 583–590.

[48] R. López-Fonseca, J. . Gutiérrez-Ortiz, and J. . González-Velasco, “Catalytic combustion of chlorinated hydrocarbons over H-BETA and PdO/H-BETA zeolite catalysts,” *Appl. Catal. A Gen.*, vol. 271, no. 1–2, pp. 39–46, Sep. 2004.

[49] T. Jiang, J. Song, M. Huo, N. Yang, J. Liu, J. Zhang, Y. Sun, and Y. Zhu, “La $_2$ O $_3$ catalysts with diverse spatial dimensionality for oxidative coupling of methane to produce ethylene and ethane,” *RSC Adv.*, vol. 6, no. 41, pp. 34872–34876, 2016.

[50] N. Rahimi, D. Moradi, M. Sheibak, E. Moosavi, and R. Karimzadeh, “The influence of modification methods on the catalytic cracking of LPG over lanthanum and phosphorus modified HZSM-5 catalysts,” *Microporous Mesoporous Mater.*, vol. 234, pp. 215–223, 2016.

[51] R. Ding, C. Li, L. Wang, and R. Hu, “Biphasic intergrowth effects of La2MnNiO6-MgO composite oxide for methane catalytic combustion,” *Appl. Catal. A Gen.*, vol. 464–465, pp. 261–268, 2013.

[52] T. Li, J. Cheng, R. Huang, J. Zhou, and K. Cen, “Conversion of waste cooking oil to jet biofuel with nickel-based mesoporous zeolite Y catalyst,” *Bioresour. Technol.*, vol. 197, pp. 289–294, 2015.

[53] C. B. Dartt and M. E. Davis, “Applications of zeolites to fine chemicals synthesis,” *Zeolites*, vol. 19, pp. 151–186, 1994.

[54] N. Taghipour, J. Towfighi, A. Mohamadalizadeh, L. Shirazi, and S. Sheibani, “The effect of key factors on thermal catalytic cracking of naphtha over Ce-La/SAPO-34 catalyst by statistical design of experiments,” *J. Anal. Appl. Pyrolysis*, vol. 99, pp. 184–190, 2013.

[55] D. Mier, A. T. Aguayo, A. G. Gayubo, M. Olazar, and J. Bilbao, “Catalyst discrimination for olefin production by coupled methanol/n-butane cracking,” *Appl. Catal. A Gen.*, vol. 383, no. 1–2, pp. 202–210, 2010.

[56] A. S. Dughaither, “Conversion Of Dimethyl-Ether to Olefins Over HZSM-5 : Reactivity and Kinetic Modeling,” no. October, 2014.

[57] S. Hodoshima, A. Motomiya, S. Wakamatsu, R. Kanai, and F. Yagi, “Catalytic cracking of light-naphtha over MFI-zeolite/metal-oxide composites for efficient propylene production,” *Res. Chem. Intermed.*, pp. 3–13, 2015.

[58] G. Wang, C. Xu, and J. Gao, “Study of cracking FCC naphtha in a secondary riser of the FCC unit for maximum propylene production,” *Fuel Process. Technol.*, vol. 89, no. 9, pp. 864–873, 2008.

[59] V. I. Alexiadis, M. Chaar, A. van Veen, M. Muhler, J. W. Thybaut, and G. B. Marin, “Quantitative screening of an extended oxidative coupling of methane catalyst

library," *Appl. Catal. B Environ.*, vol. 199, pp. 252–259, 2016.

[60] N. Hiyoshi and K. Sato, "Oxidative coupling of methane over Mn-Na2WO4/SiO2 catalyst with continuous supply of alkali chloride vapor," *Fuel Process. Technol.*, vol. 151, pp. 148–154, 2016.

[61] V. Fleischer, P. Littlewood, S. Parishan, and R. Schom??cker, "Chemical looping as reactor concept for the oxidative coupling of methane over a Na2WO4/Mn/SiO2 catalyst," *Chem. Eng. J.*, vol. 306, pp. 646–654, 2016.

[62] M. G. Colmenares, U. Simon, M. Yildiz, S. Arndt, R. Schomaecker, A. Thomas, F. Rosowski, A. Gurlo, and O. Goerke, "Oxidative coupling of methane on the Na2WO4-MnxOy catalyst: COK-12 as an inexpensive alternative to SBA-15," *Catal. Commun.*, vol. 85, pp. 75–78, 2016.

[63] M. Westgård Erichsen, S. Svelle, and U. Olsbye, "H-SAPO-5 as methanol-to-olefins (MTO) model catalyst: Towards elucidating the effects of acid strength," *J. Catal.*, vol. 298, pp. 94–101, 2013.

[64] M. Sedighi and J. Towfighi, "Methanol conversion over SAPO-34 catalysts; Systematic study of temperature, space–time, and initial gel composition on product distribution and stability," *Fuel*, vol. 153, pp. 382–392, 2015.

[65] Z. Li, J. Martínez-Triguero, J. Yu, and A. Corma, "Conversion of methanol to olefins: Stabilization of nanosized SAPO-34 by hydrothermal treatment," *J. Catal.*, vol. 329, pp. 379–388, 2015.

[66] S. a Al-Ghamdi, "Thesis: Oxygen-Free Propane Oxidative Dehydrogenation Over Vanadium Oxide Catalysts: Reactivity and Kinetic Modelling," no. December, 2013.

[67] D. C. Longstaff, "Development of a comprehensive naphtha catalytic cracking kinetic model," *Energy and Fuels*, vol. 26, no. 2, pp. 801–809, 2012.

[68] J. H. Lee, S. Kang, Y. Kim, and S. Park, "New approach for kinetic modeling of catalytic cracking of paraffinic naphtha," *Ind. Eng. Chem. Res.*, vol. 50, no. 8, pp. 4264–4279, 2011.

[69] W. Zhiyuan, X. Hong, L. Xiaojian, H. Feng, and Z. Jianxin, "Effect of Potassium Acetate on Coke Growth during Light Naphtha Thermal Cracking," *Ind. Eng. Chem. Res.*, vol. 50, no. 17, pp. 10292–10297, 2011.

[70] M. Artetxe, G. Lopez, M. Amutio, G. Elordi, J. Bilbao, and M. Olazar, "Light olefins from HDPE cracking in a two-step thermal and catalytic process," *Chem. Eng. J.*, vol. 207–208, pp. 27–34, 2012.

[71] S. a. P. da Mota, a. a. Mancio, D. E. L. Lhamas, D. H. de Abreu, M. S. da Silva, W. G. dos Santos, D. a. R. de Castro, R. M. de Oliveira, M. E. Araújo, L. E. P. Borges, and N. T. Machado, "Production of green diesel by thermal catalytic cracking of crude palm oil (Elaeis guineensis Jacq) in a pilot plant," *J. Anal. Appl. Pyrolysis*,

vol. 110, pp. 1–11, 2014.

[72] P. Zámostný, Z. Bělohlav, and J. Šmidrkal, “Production of olefins via steam cracking of vegetable oils,” *Resour. Conserv. Recycl.*, vol. 59, pp. 47–51, 2012.

[73] S. P. Pyl, T. Dijkmans, J. M. Antonykutty, M.-F. Reyniers, A. Harlin, K. M. Van Geem, and G. B. Marin, “Wood-derived olefins by steam cracking of hydrodeoxygenated tall oils.,” *Bioresour. Technol.*, vol. 126, pp. 48–55, 2012.

[74] S. M. Sadrameli and a. E. S. Green, “Systematics of renewable olefins from thermal cracking of canola oil,” *J. Anal. Appl. Pyrolysis*, vol. 78, no. 2, pp. 445–451, 2007.

[75] R. Bastiani, Y. Lau, C. Assumpção, and V. Teixeira, “Application of ferrierite zeolite in high-olefin catalytic cracking,” *Fuel*, vol. 107, pp. 680–687, 2013.

[76] K. Kubo, H. Iida, S. Namba, and A. Igarashi, “Comparison of Steaming Stabilty of Cu-ZSM-5 with those of Ag-ZSM-5, P/H-ZSM-5 and H-ZSM-5 zeolites as naphtha cracking catalyst to produce light olefins at high temperatures.,” *Appl. Catal. A Gen.*, vol. 29, pp. 272–279, 2015.

[77] D. Liu, W. C. Choi, C. W. Lee, N. Y. Kang, Y. J. Lee, C. H. Shin, and Y. K. Park, “Steaming and washing effect of P/HZSM-5 in catalytic cracking of naphtha,” *Catal. Today*, vol. 164, no. 1, pp. 154–157, 2011.

[78] O. Awayssa, N. Al-Yassir, a. Aitani, and S. Al-Khattaf, “Modified HZSM-5 as FCC additive for enhancing light olefins yield from catalytic cracking of VGO,” *Appl. Catal. A Gen.*, vol. 477, pp. 172–183, 2014.

[79] X. Dong, S. Xue, J. Zhang, W. Huang, J. Zhou, Z. Chen, D. Yuan, Y. Xu, and Z. Liu, “The production of light olefins by catalytic cracking of the microalga Isochrysis zhanjiangensis over a modified ZSM-5 catalyst,” *Chinese J. Catal.*, vol. 35, no. 5, pp. 684–691, 2014.

[80] K. Kubo, H. Iida, S. Namba, and A. Igarashi, “Ultra-high steaming stability of Cu-ZSM-5 zeolite as naphtha cracking catalyst to produce light olefin,” *Catal. Commun.*, vol. 29, pp. 162–165, 2012.

[81] F. O. Rice and K. F. Herzfeld, “The Thermal Decomposition of Organic Compounds from the Standpoint of Free Radicals. VI. The Mechanism of Some Chain Reactions,” *J. Am. Chem. Soc.*, vol. 56, no. 2, pp. 284–289, Feb. 1934.

[82] A. Kossiakoff and F. O. Rice, “Thermal Decomposition of Hydrocarbons, Resonance Stabilization and Isomerization of Free Radicals 1,” *J. Am. Chem. Soc.*, vol. 65, no. 4, pp. 590–595, Apr. 1943.

[83] L. Zhao, J. Gao, C. Xu, and B. Shen, “Alkali-treatment of ZSM-5 zeolites with different SiO2/Al 2O3 ratios and light olefin production by heavy oil cracking,” *Fuel Process. Technol.*, vol. 92, no. 3, pp. 414–420, 2011.

[84] H. Liu, G. H. Kuehl, I. Halasz, and D. H. Olson, “Quantifying the n-hexane cracking

activity of Fe- and Al-based acid sites in H-ZSM-5," *J. Catal.*, vol. 218, no. 1, pp. 155–162, 2003.

[85] D. S. Santilli, "Mechanism of hexane cracking in ZSM-5," *Appl. Catal.*, vol. 60, no. 1, pp. 137–141, 1990.

[86] K. Kubo, H. Iida, S. Namba, and A. Igarashi, "Selective formation of light olefin by n-heptane cracking over HZSM-5 at high temperatures," *Microporous Mesoporous Mater.*, vol. 149, no. 1, pp. 126–133, 2012.

[87] X. Hou, Y. Qiu, X. Zhang, and G. Liu, "Analysis of reaction pathways for n-pentane cracking over zeolites to produce light olefins," *Chem. Eng. J.*, vol. 307, pp. 372–381, 2017.

[88] J. H. Lee, S. Kang, Y. Kim, and S. Park, "New approach for kinetic modeling of catalytic cracking of paraffinic naphtha," *Ind. Eng. Chem. Res.*, vol. 50, no. 8, pp. 4264–4279, 2011.

[89] H. Mochizuki, T. Yokoi, H. Imai, R. Watanabe, S. Namba, J. N. Kondo, and T. Tatsumi, "Facile control of crystallite size of ZSM-5 catalyst for cracking of hexane," *Microporous Mesoporous Mater.*, vol. 145, no. 1–3, pp. 165–171, 2011.

[90] A. K. Jamil, O. Muraza, M. Sanhoob, T. Tago, H. Konno, Y. Nakasaka, and T. Masuda, "Controlling naphtha cracking using nanosized TON zeolite synthesized in the presence of polyoxyethylene surfactant," *J. Anal. Appl. Pyrolysis*, vol. 110, pp. 338–345, Nov. 2014.

[91] O. Muraza, A. Abdul-lateef, T. Tago, A. B. D. Nandiyanto, H. Konno, Y. Nakasaka, Z. H. Yamani, and T. Masuda, "Microwave-assisted hydrothermal synthesis of submicron ZSM-22 zeolites and their applications in light olefin production," *Microporous Mesoporous Mater.*, vol. 206, pp. 136–143, 2015.

[92] A. A. Rownaghi, F. Rezaei, and J. Hedlund, "Selective formation of light olefin by n-hexane cracking over HZSM-5: Influence of crystal size and acid sites of nano- and micrometer-sized crystals," *Chem. Eng. J.*, vol. 191, pp. 528–533, May 2012.

[93] A. Corma and A. V. Orchillés, "Current views on the mechanism of catalytic cracking," *Microporous Mesoporous Mater.*, vol. 35–36, pp. 21–30, Apr. 2000.

[94] B. . Williams, W. Ji, J. . Miller, R. . Snurr, and H. . Kung, "Evidence of different reaction mechanisms during the cracking of n-hexane on H-USY zeolite," *Appl. Catal. A Gen.*, vol. 203, no. 2, pp. 179–190, Oct. 2000.

[95] O. Muraza, I. a. Bakare, T. Tago, H. Konno, A. L. Adedigba, A. M. Al-Amer, Z. H. Yamani, and T. Masuda, "Controlled and rapid growth of MTT zeolite crystals with low-aspect-ratio in a microwave reactor," *Chem. Eng. J.*, vol. 226, pp. 367–376, 2013.

[96] B. Wang, Z. Tian, P. Li, L. Wang, Y. Xu, W. Qu, Y. He, H. Ma, Z. Xu, and L. Lin, "A novel approach to synthesize ZSM-23 zeolite involving N,N-

dimethylformamide," *Microporous Mesoporous Mater.*, vol. 134, no. 1–3, pp. 203–209, 2010.

[97] G. T. Kokotailo, J. L. Schlenker, F. G. Dwyer, and E. W. Valyocsik, "The framework topology of ZSM-22: A high silica zeolite," *Zeolites*, vol. 5, no. 6, pp. 349–351, 1985.

[98] B. Marler, "Silica-ZSM-22: synthesis and single crystal structure refinement," *Zeolites*, vol. 7, no. 5, pp. 393–397, 1987.

[99] J. A. M. Arroyo, G. G. Martens, G. F. Froment, G. B. Marin, P. A. Jacobs, and J. A. Martens, "Hydrocracking and isomerization of n-paraffin mixtures and a hydrotreated gasoil on Pt/ZSM-22: confirmation of pore mouth and key–lock catalysis in liquid phase," *Appl. Catal. A Gen.*, vol. 192, no. 1, pp. 9–22, 2000.

[100] A. G. Gomez, G. de Silveira, H. Doan, and C.-H. Cheng, "A facile method to tune zeolite L crystals with low aspect ratio," *Chem. Commun.*, vol. 47, no. 20, p. 5876, 2011.

[101] T. Tago, H. Konno, M. Sakamoto, Y. Nakasaka, and T. Masuda, "Selective synthesis for light olefins from acetone over ZSM-5 zeolites with nano- and macro-crystal sizes," *Appl. Catal. A Gen.*, vol. 403, no. 1–2, pp. 183–191, 2011.

[102] Y. Wang, Y. Xu, Z. Tian, and L. Lin, "Research progress in ionothermal synthesis of molecular sieves," *Cuihua Xuebao/Chinese J. Catal.*, vol. 33, no. 1, pp. 39–50, 2012.

[103] C. S. Cundy and P. a. Cox, "The hydrothermal synthesis of zeolites: History and development from the earliest days to the present time," *Chem. Rev.*, vol. 103, no. 3, pp. 663–701, 2003.

[104] M. E. Davis, "Ordered porous materials for emerging applications.," *Nature*, vol. 417, no. 6891, pp. 813–821, 2002.

[105] I. A. Bakare, O. Muraza, T. Kurniawan, Z. H. Yamani, E. N. Shafei, A. K. Punetha, K.-H. Choi, and T. Yokoi, "Hydrothermal stability of MTT zeolite in hot water: The role of La and Ce," *Microporous Mesoporous Mater.*, vol. 233, pp. 93–101, Oct. 2016.

[106] A. K. Jamil, O. Muraza, M. Yoshioka, A. M. Al-amer, Z. H. Yamani, and T. Yokoi, "Selective Production of Propylene from Methanol Conversion over Nanosized ZSM-22 Zeolites," *Ind. Eng. Chem. Res.*, vol. 53, no. 50, pp. 19498–19505, 2014.

[107] A. Mayoral, R. Arenal, V. Gascón, C. Márquez-Álvarez, R. M. Blanco, and I. Díaz, "Designing Functionalized Mesoporous Materials for Enzyme Immobilization: Locating Enzymes by Using Advanced TEM Techniques," *ChemCatChem*, vol. 5, no. 4, pp. 903–909, Apr. 2013.

[108] A. Mayoral, J. E. Readman, and P. A. Anderson, "Aberration-corrected STEM analysis of a cubic Cd array encapsulated in zeolite A," *J. Phys. Chem. C*, vol. 117,

no. 46, pp. 24485–24489, 2013.

[109] C. D. Weber, C. Bradley, and M. C. Lonergan, "Solution phase n-doping of C60 and PCBM using tetrabutylammonium fluoride," *J. Mater. Chem.*, vol. 2, no. 2, p. 303, 2014.

[110] A. Mayoral, J. Coronas, C. Casado, C. Tellez, and I. Díaz, "Atomic Resolution Analysis of Microporous Titanosilicate ETS-10 through Aberration Corrected STEM Imaging," *ChemCatChem*, vol. 5, no. 9, pp. 2595–2598, Sep. 2013.

[111] J. Hao, Y. Wang, G. Liu, J. Zhang, G. Li, and X. Ma, "Synthesis of ITQ-2 zeolites and catalytic performance in n-dodecane cracking," *Chinese J. Chem. Eng.*, vol. 22, no. 8, pp. 869–874, 2014.

[112] P. Djomgoue and D. Njopwouo, "FT-IR Spectroscopy Applied for Surface Clays," vol. 2013, no. October, pp. 275–282, 2013.

[113] N. Rahimi and R. Karimzadeh, "Catalytic cracking of hydrocarbons over modified ZSM-5 zeolites to produce light olefins: A review," *Appl. Catal. A Gen.*, vol. 398, no. 1–2, pp. 1–17, 2011.

[114] J. Xing, L. Song, C. Zhang, M. Zhou, L. Yue, and X. Li, "Effect of acidity and porosity of alkali-treated ZSM-5 zeolite on eugenol hydrodeoxygenation," *Catal. Today*, vol. 258, pp. 90–95, 2015.

[115] D. Verboekend, M. Chabaneix, K. Thomas, J. Gilson, and P. Javier, "CrystEngComm Mesoporous ZSM-22 zeolite obtained by desilication : peculiarities associated with crystal morphology and aluminium distribution †," pp. 3408–3416, 2011.

[116] S. Jolly, J. Saussey, M. M. Bettahar, J. C. Lavalley, and E. Benazzi, "Reaction mechanisms and kinetics in the n-hexane cracking over zeolites," *Appl. Catal. a-General*, vol. 156, no. 1, pp. 71–96, 1997.

[117] H. Mochizuki, T. Yokoi, H. Imai, S. Namba, J. N. Kondo, and T. Tatsumi, "Effect of desilication of H-ZSM-5 by alkali treatment on catalytic performance in hexane cracking," *Appl. Catal. A Gen.*, vol. 449, pp. 188–197, 2012.

[118] D. Gao, A. Duan, X. Zhang, Z. Zhao, H. E, Y. Qin, and C. Xu, "Synthesis of CoMo catalysts supported on EMT/FAU intergrowth zeolites with different morphologies and their hydro-upgrading performances for FCC gasoline," *Chem. Eng. J.*, vol. 270, no. 0, pp. 176–186, 2015.

[119] O. Muraza, I. a. Bakare, T. Tago, H. Konno, T. Taniguchi, A. M. Al-Amer, Z. H. Yamani, Y. Nakasaka, and T. Masuda, "Selective catalytic cracking of n-hexane to propylene over hierarchical MTT zeolite," *Fuel*, vol. 135, pp. 105–111, 2014.

[120] H. Abrevaya, *Cracking of naphtha range alkanes and naphthenes over zeolites*, vol. 170, no. B. Elsevier B.V., 2007.

[121] Y. Nakasaka, J. Nishimura, T. Tago, and T. Masuda, “Deactivation mechanism of MFI-type zeolites by coke formation during n-hexane cracking,” *Chem. Eng. J.*, vol. 278, pp. 159–165, Oct. 2015.

[122] D. Verboekend and J. Pérez-Ramírez, “Design of hierarchical zeolite catalysts by desilication,” *Catal. Sci. Technol.*, vol. 1, no. 6, pp. 879–890, 2011.

[123] A. Corma, P. J. Miguel, and A. V. Orchillés, “Product selectivity effects during cracking of alkanes at very short and longer times on stream,” *Appl. Catal. A Gen.*, vol. 138, no. 1, pp. 57–73, 1996.

[124] Y. N. Hiroki Konno, Teruoki Tago* and J. N. and T. M. Ryota Ohnaka, “Effectiveness of Nano-scale ZSM-5 Zeolite and its Deactivation Mechanism on Catalytic Cracking of Representative Hydrocarbons of Naphtha,” *Environment*, 2012.

Vitae

Name	:Saheed Adewale Lateef
Nationality	:Nigerian
Date of Birth	:7/2/1988
Email	:aaslateef2012@gmail.com, lateefsaheed0207@gmail.com
Address	:BC 30, Kola Rufai street, Ilobu, Osun state, Nigeria
Academic Background	:Bachelor of Engineering, Federal University of Technology, Minna, Nigeria. (2008-2012)